ESA 6th Advanced Training Course on Radar Polarimetry

POLARIMETRIC SAR TOMOGRAPHY

Spectral Analysis (Specan) techniques

Laurent Ferro-Famil

Université de Rennes 1, Centre d'Etudes Spatiales de la Biosphère

Stefano Tebaldini

Politecnico di Milano

- *From 3-D SAR Imaging to the Beamformer*
- *PolTomSAR imaging using 1D Specan techniques*
- *Advanced PolTomSAR imaging using Specan*
- *Polarimetric TomoSAR tomography*

  Full-Rank specan & and SKP decomposition
- *Spaceborne 3-D imaging using correlation SAR tomography*

From 3-D Synthetic Aperture Imaging To the Beamformer

2-D SAR impulse response

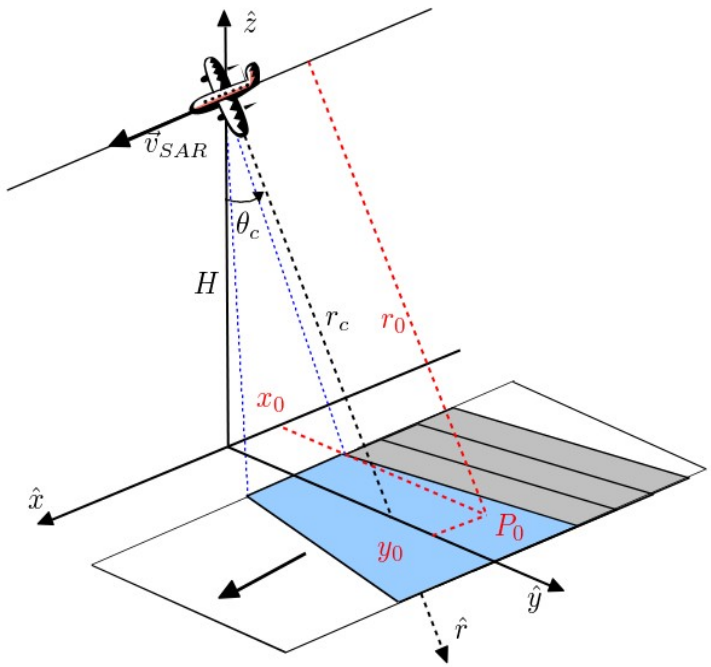

2-D focused signal (x-r domain)

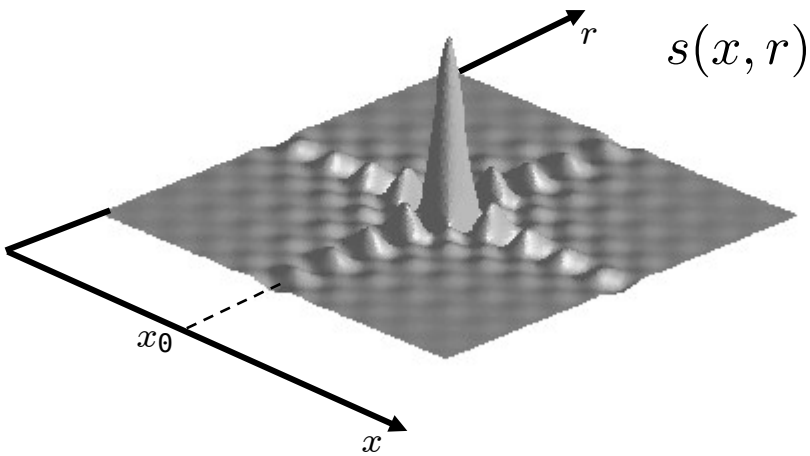

$$s(x,r) = \begin{array}{ll} a_c & \rightarrow \textbf{complex reflection coefficient} \\ h_r(d - r_0) & \rightarrow \text{delayed range impulse response} \\ h_a(x - x_0) & \rightarrow \text{delayed azimuth impulse response} \\ \exp(-j\frac{4\pi}{\lambda_c} r_0) & \rightarrow \textbf{two-way propagation phase} \end{array}$$

2-D SAR imaging

SAR imaging: coherent integration of a reflectivity density

$$s(x,r) = \int a_c(x',r',\nu') h(x'-x, r'-r)\, \mathrm{e}^{-j\frac{4\pi}{\lambda_c} d(x'-x, r'-r)}\, \mathrm{d}x' \mathrm{d}r' \mathrm{d}\nu$$

$$s(x,r) \approx \int_{\mathcal{C}} a_c(x,r,\nu)\, \mathrm{e}^{-jk_c r(\nu)}\, \mathrm{d}\nu$$

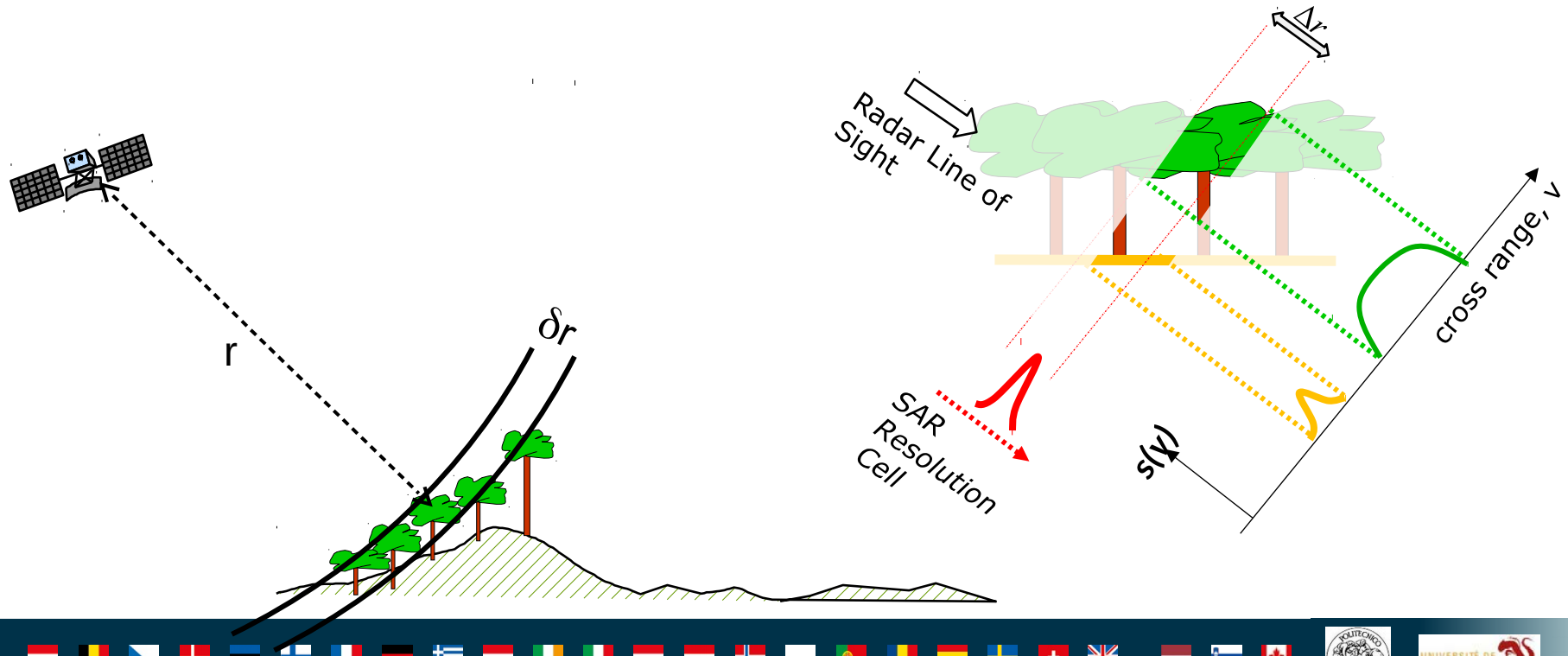

3-D SAR imaging

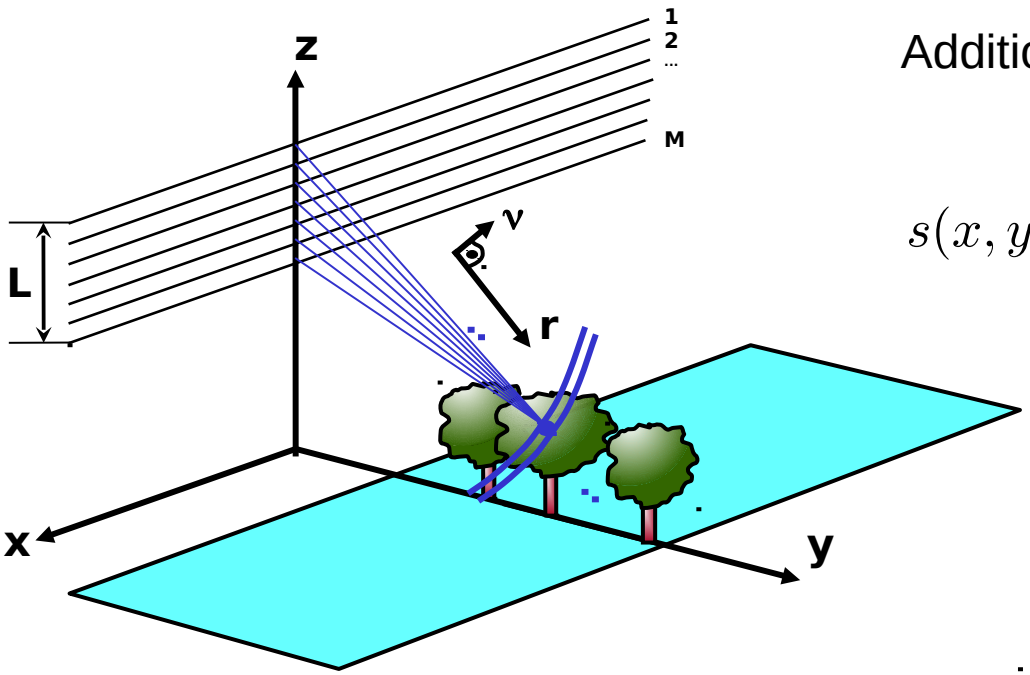

Additional aperture in elevation:
2-D → 3-D focusing

$$s(x,y,z) = \sum_{i=1}^{M} s_i(x, r(y,z))\, \mathrm{e}^{jk_c r(y,z)}$$

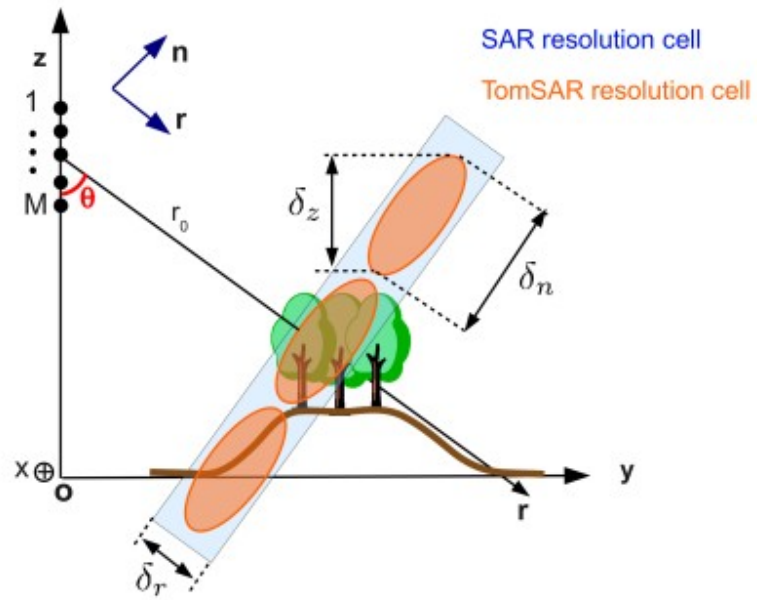

Vertical aperture : L_{tomo}

Resolution : $\delta_z = \delta_n \sin\theta$ with $\delta_n = \frac{\lambda R_0}{2L_{tomo}}$

3-D SAR imaging

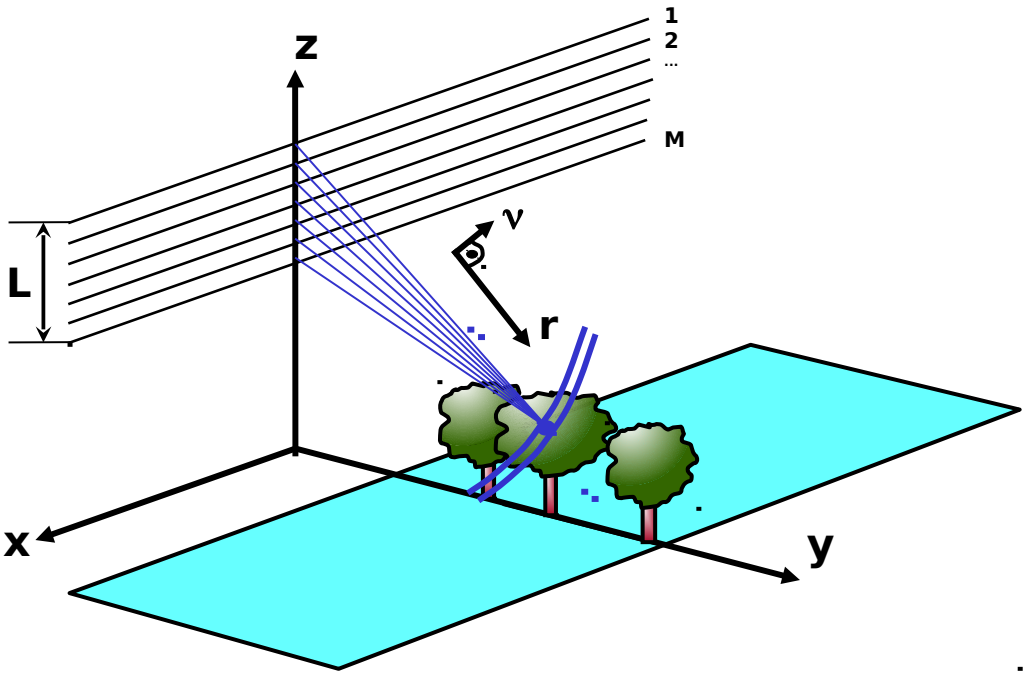

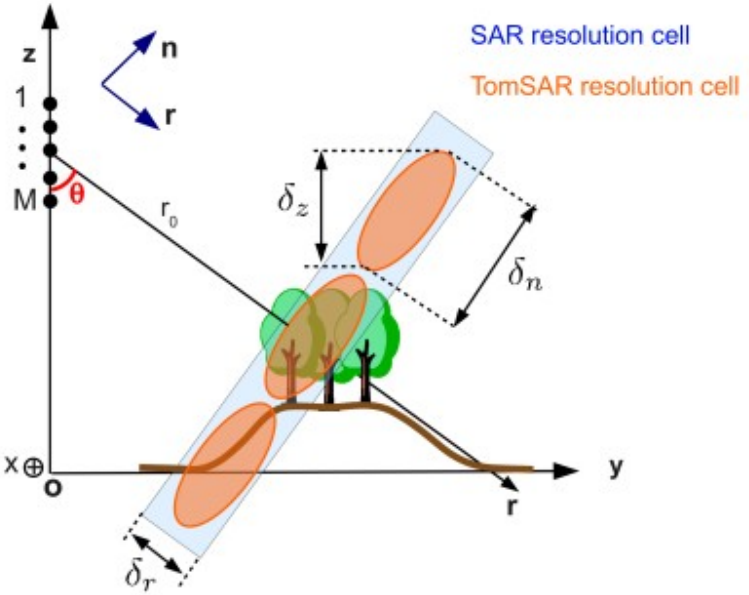

$$s(x,y,z) = \sum_{i=1}^{M} s_i(x, r(y,z))\, \mathrm{e}^{jk_c r(y,z)}$$

Interpolation

HF term

3-D SAR imaging

Co-registration on a reference plane

Valid for $z \in z_{ref} \pm \Delta z_{val}/2$

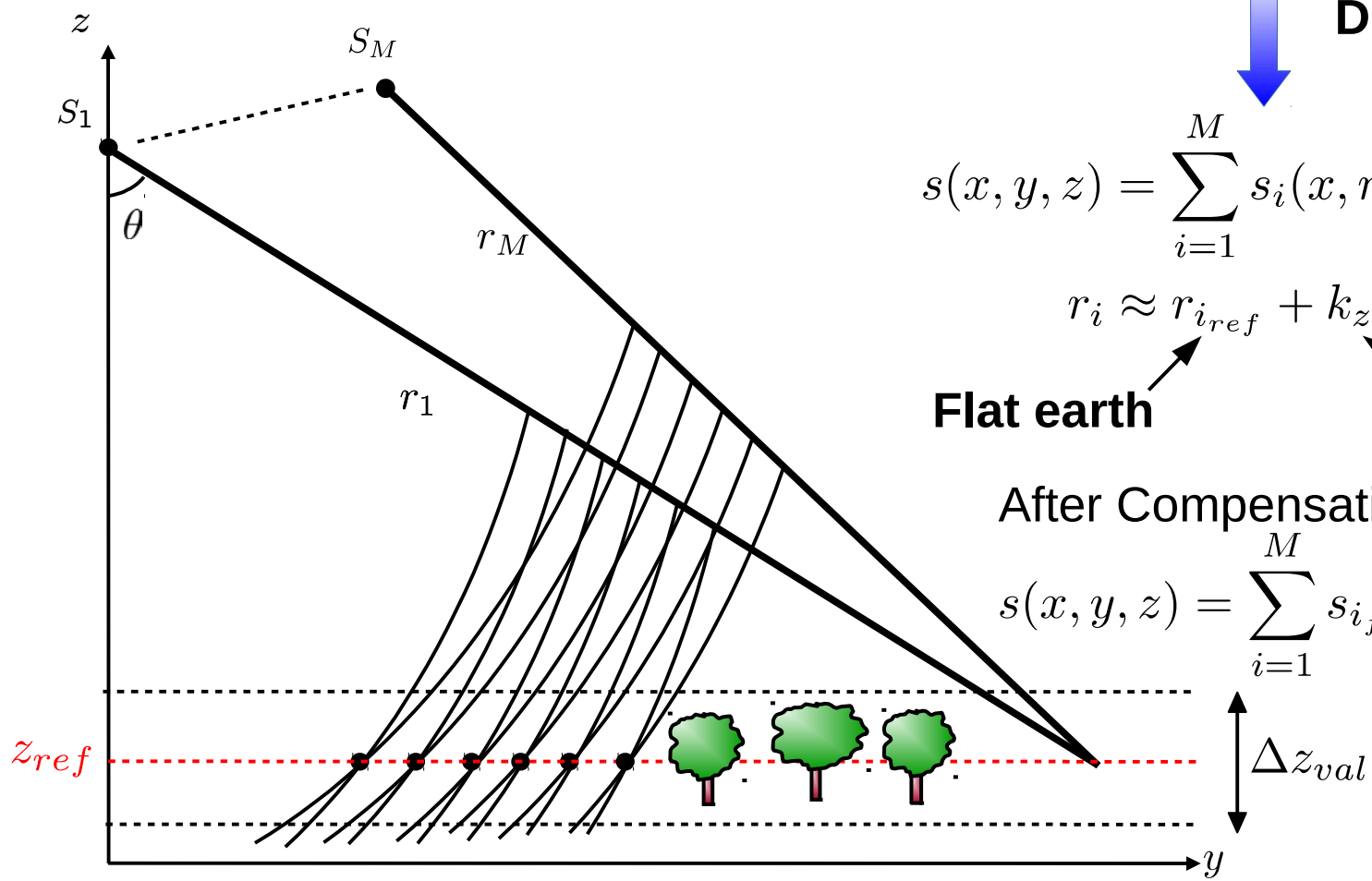

$$s(x,y,z) = \sum_{i=1}^{M} s_i(x, r(y,z))\, \mathrm{e}^{jk_c r(y,z)}$$

Discretization
NN-interp.

$$s(x,y,z) = \sum_{i=1}^{M} s_i(x, r_{i_{ref}})\, \mathrm{e}^{jk_c r_i}$$

$$r_i \approx r_{i_{ref}} + k_{z_i} z$$

Flat earth **Elevation**

After Compensation

$$s(x,y,z) = \sum_{i=1}^{M} s_{i_{flat}}(x, r_{i_{ref}})\, \mathrm{e}^{jk_{z_i} z}$$

3-D SAR imaging

3-D Synthetic Aperture imaging

$$s(x,y,z) = \sum_{i=1}^{M} s_i(x, r_{i_{ref}})\, \mathrm{e}^{jk_{z_i} z}$$

Filter-like formulation for a given resolution cell

Coregistered Resampled Flattened SLC data

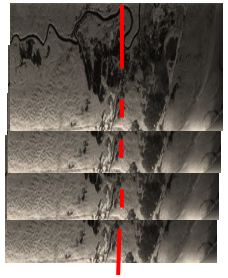

$$\Rightarrow \mathbf{y} = \begin{bmatrix} y_1 \\ \vdots \\ y_M \end{bmatrix} = \begin{bmatrix} s_1(x, r_{1_{ref}}) \\ \vdots \\ s_M(x, r_{M_{ref}}) \end{bmatrix}$$

$$\boxed{s(z) = \mathbf{a}^H(z)\mathbf{y}}$$

Steering vector

$$\mathbf{a} = [1, \mathrm{e}^{-jk_{z_2} z}, \ldots, \mathrm{e}^{-jk_{z_M} z}]^T$$

3-D Fourier imaging is equivalent to the Beamformer spectral analysis method

PolTomSAR imaging using Monodimensional Spectral Analysis Techniques

Intuitive interpretation of Beamforming

Estimation of a single scatterer: InSAR way

$$\begin{aligned} s_1 &= a_c\, \mathrm{e}^{j\xi} \\ s_2 &= a_c\, \mathrm{e}^{j\xi+\Delta\phi} \end{aligned} \Rightarrow \begin{cases} \Delta\hat{\phi} = \arg(s_2 s_1^*) \\ \hat{I} = \frac{|s_1|^2+|s_2|^2}{2} \end{cases}$$

Estimation of a single scatterer: linear filtering way

$$\mathbf{y} = \begin{bmatrix} s_1 \\ s_2 \end{bmatrix}, \mathbf{a}(\phi) = \begin{bmatrix} 1 \\ \mathrm{e}^{j\phi} \end{bmatrix} \qquad \boxed{f(\phi) = \frac{\mathbf{a}^H(\phi)\mathbf{y}}{2} = \frac{s_1 + s_2\, \mathrm{e}^{-j\phi}}{2}}$$

$$\Rightarrow \begin{cases} \Delta\hat{\phi} = \arg\max_\phi |f(\phi)|^2 \\ \hat{I} = |f(\Delta\hat{\phi})|^2 \end{cases}$$

- Phase estimation → linear filtering & search
- Filter output: reflectivity
- $\mathbf{a}(\phi)$ steering vector: Discrete Fourier Transform filter

Intuitive interpretation of Beamforming

Estimation of several scatterers: MB InSAR way

$$\{s_1, \ldots, s_M\}, \quad s_m = \sum_{t=1}^{N_t} a_{c_t}\, \mathrm{e}^{j\xi_t}\, \mathrm{e}^{jk_{z_m} z_t} \quad \Rightarrow \quad ???$$

Estimation of several scatterers: linear filtering way

$$\mathbf{y} = \begin{bmatrix} s_1 \\ \vdots \\ s_M \end{bmatrix}, \mathbf{a}(z) = \begin{bmatrix} 1 \\ \vdots \\ \mathrm{e}^{jk_{z_M} z} \end{bmatrix} \qquad \boxed{f(z) = \frac{\mathbf{a}^H(z)\mathbf{y}}{M} = \frac{\sum_m s_m\, \mathrm{e}^{-jk_{z_m} z}}{M}}$$

$$\Rightarrow \begin{cases} \hat{z}_t = \arg\max_{loc} |f(z)|^2 \\ \hat{I}_t = |f(\hat{z}_t)|^2 \end{cases}$$

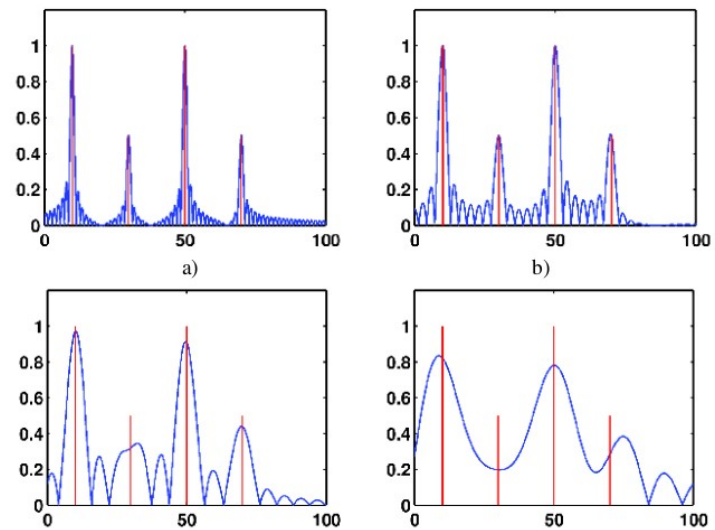

- Tomographic focusing: spectral estimation problem
- Estimation quality: depends on MB-inSAR configuration

Tomographic imaging using specan

Acquired signal (single scatterer)

$$\mathbf{y} = a_c\,\mathbf{a}(z_0) + \mathbf{n}$$

$$\text{with} \quad \mathbf{a}(z_0) = [1, \mathrm{e}^{jk_{z_2} z_0}, \ldots, \mathrm{e}^{jk_{z_M} z_0}]^T$$

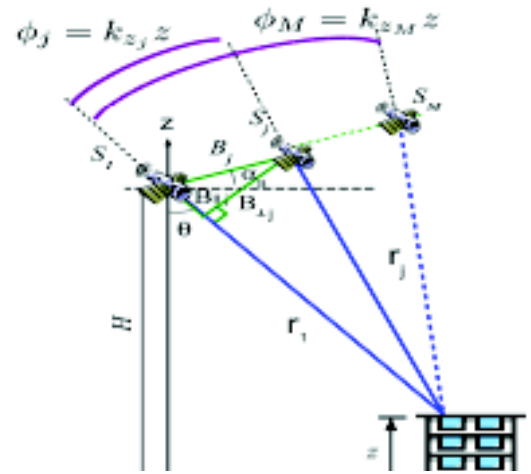

Second order statistics

$$\mathbf{y}(l) = a_c(l)\mathbf{a}(z_0) + \mathbf{n}(l) \quad l = 1, \ldots, L$$

$$\mathbf{R} = \mathrm{E}(\mathbf{y}\mathbf{y}^H) = \mathbf{P}\widetilde{\mathbf{R}}\mathbf{P} \qquad \widehat{\mathbf{R}} = \frac{1}{L}\sum_{l=1}^{L} \mathbf{y}(l)\mathbf{y}^H(l)$$

$$\mathbf{P} = \begin{bmatrix} \sqrt{I_1} & & & \\ & \sqrt{I_2} & & \\ & & \ddots & \\ & & & \sqrt{I_M} \end{bmatrix} \qquad \widetilde{\mathbf{R}} = \begin{bmatrix} 1 & \gamma_{12} & \cdots & & \gamma_{1M} \\ \gamma_{12}^* & 1 & \gamma_{23} & \cdots & \gamma_{2M} \\ & & \ddots & & \\ \gamma_{1M}^* & & & & 1 \end{bmatrix}$$

Tomographic imaging using specan

Acquired signal (single scatterer)

$$\mathbf{y} = a_c\,\mathbf{a}(z_0) + \mathbf{n}$$

$$\text{with} \quad \mathbf{a}(z_0) = [1, \mathrm{e}^{jk_{z_2} z_0}, \ldots, \mathrm{e}^{jk_{z_M} z_0}]^T$$

Beamformer

$$\boxed{\mathbf{v}_{BF} = \frac{\mathbf{a}(z)}{M}}$$

- Unbiased: $\mathrm{E}(f(\mathbf{v})) = a_c$
- BF maximizes output SNR at z = z_0
- Use:
  - compute $P_{BF}(z) = \mathrm{E}(|\mathbf{v}_{BF}^H(z)\mathbf{y}|^2)$
  - estimate parameters from the max

Linear filtering (fast)

$$f(\mathbf{v}) = \mathbf{v}^H\mathbf{y} = \sum_{i=1}^{M} v_i^* y_i$$

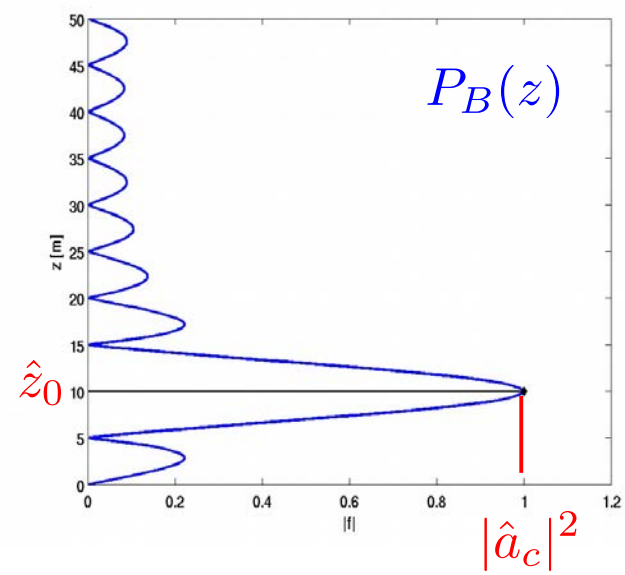

Tomographic imaging using specan

Uniform baseline sampling

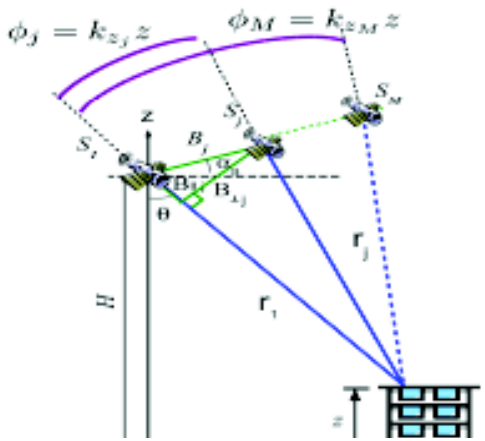

$$B_{\perp_i} = (i-1)B_\perp$$

$$\mathbf{a}(z) = [1, \mathrm{e}^{j\mathrm{d}k_z z}, \ldots, \mathrm{e}^{j(M-1)\mathrm{d}k_z z}]^T$$

Spectral sampling: $\mathrm{d}k_z = \dfrac{k_c B_\perp}{r \sin\theta}$

Spectral bandwidth: $\Delta k_z = M \mathrm{d}k_z$

Ideal response $\mathbf{y} = a_c \mathbf{a}(z_0)$

$$|f(z)| = |a_c| \frac{|\mathbf{a}^H(z)\mathbf{a}(z_0)|}{M} = \frac{|a_c|}{M} \frac{|\sin(\pi \Delta k_z (z - z_0))|}{|\sin(\pi \mathrm{d}k_z (z - z_0))|}$$

Fast

M times Slower

Tomographic imaging using specan

Uniform baseline sampling $\mathbf{a}(z) = [1, \mathrm{e}^{j\mathrm{d}k_z z}, \ldots, \mathrm{e}^{j(M-1)\mathrm{d}k_z z}]^T$

$$|f(z)| = |a_c| \frac{|\mathbf{a}^H(z)\mathbf{a}(z_0)|}{M} = \frac{|a_c|}{M} \frac{|\sin(\pi \Delta k_z (z - z_0))|}{|\sin(\pi \mathrm{d} k_z (z - z_0))|}$$

Fast → resolution

Slow → ambiguity

Spatial features of a tomogram

- **rapid oscillations: resolution**
- **band-limited: sidelobes**
- **sampled spectrum : spatial ambiguities**

$$\delta z = \frac{2\pi}{\Delta k}, \quad z_{amb} = \frac{2\pi}{\mathrm{d}k}, \quad \delta z = \frac{z_{amb}}{M}$$

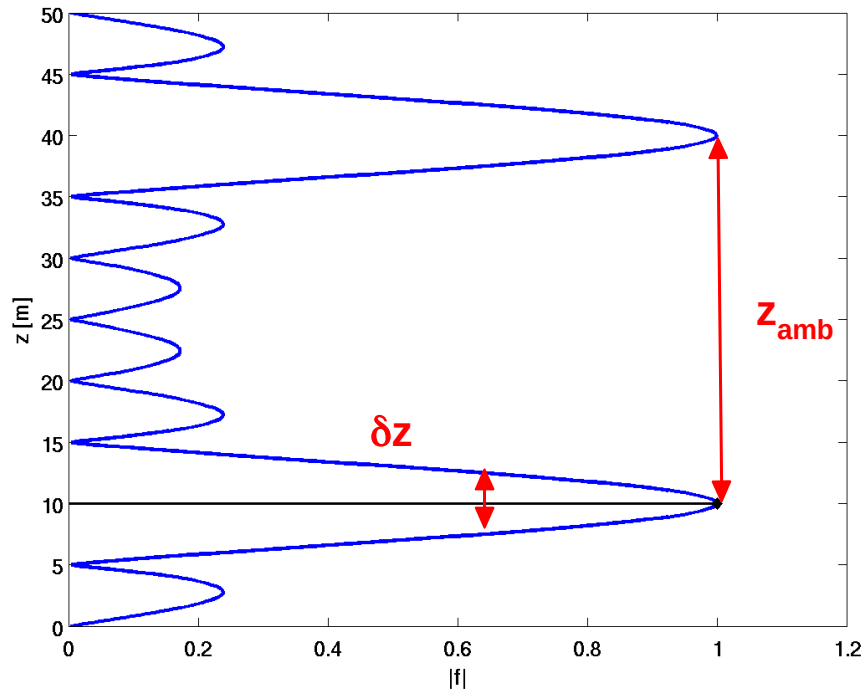

M=6

Tomographic imaging using specan

M=6

$$\Delta k_z \propto M B_\perp$$

$$\mathrm{d}k_z = \frac{\Delta k_z}{M}$$

M=12

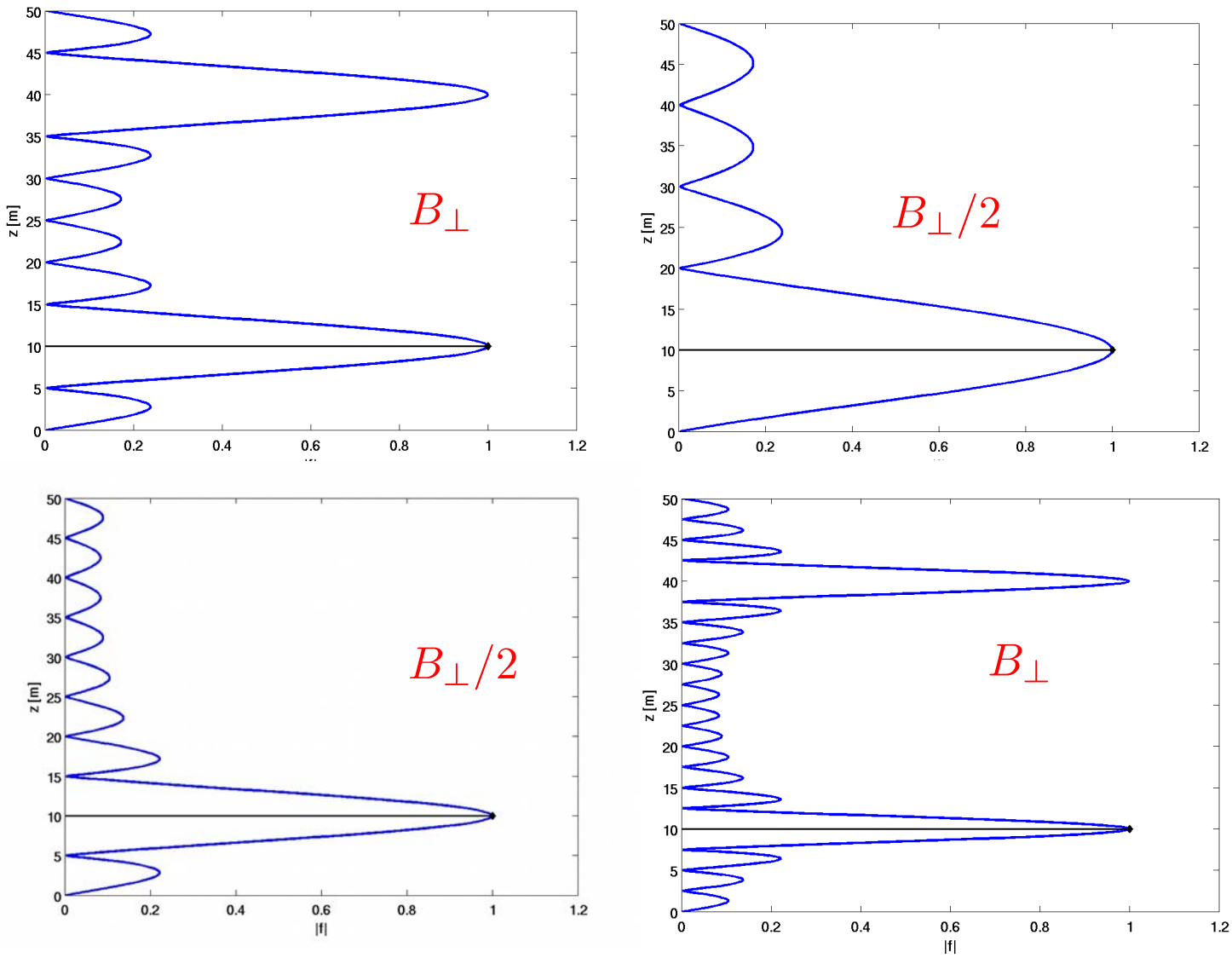

Tomographic imaging using specan

M=6

$$\Delta k_z \propto M B_\perp$$

$$\mathrm{d}k_z = \frac{\Delta k_z}{M}$$

M=12

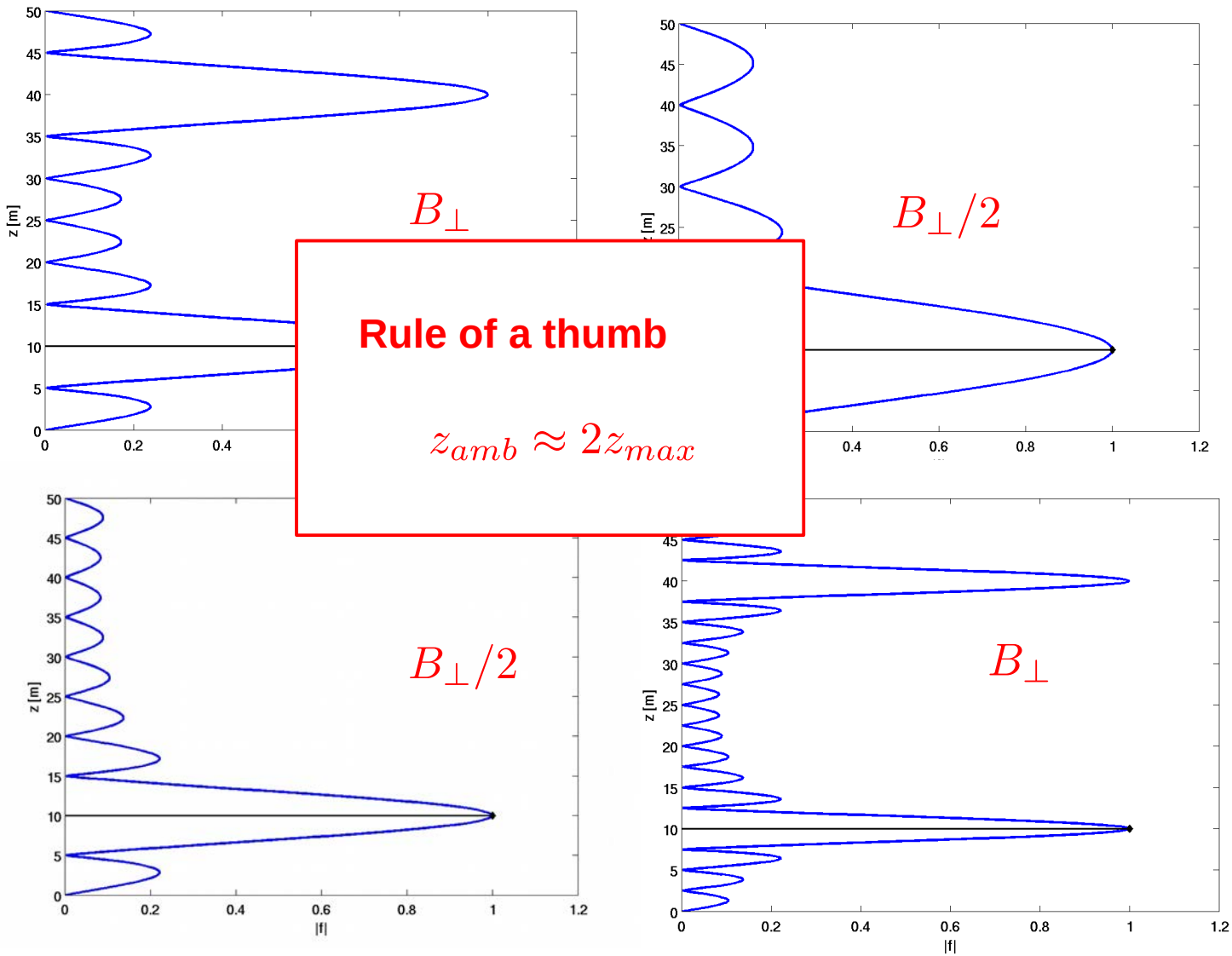

Rule of a thumb

$$z_{amb} \approx 2 z_{max}$$

Tomographic imaging using specan

Beamformer features

- Excellent statistical accuracy
- Fourier resolution (depends on Δk)
- Cannot handle closely spaced scatterers

Capon's approach

- Also a linear filter (fast)
- Aims to minimize spatial perturbations & sidelobes

Capon's solution: constrained beamformer

Minimize output power, with unitary gain at the height of interest

$$\mathbf{v}_C = \arg\min_{\mathbf{v}} \mathrm{E}(|\mathbf{v}^H\mathbf{y}|^2) \quad \text{s.t,} \quad \mathbf{v}^H\mathbf{a}(z) = 1$$

$$\mathbf{v} = \frac{\mathbf{R}^{-1}\mathbf{a}(z)}{\mathbf{a}^H(z)\mathbf{R}^{-1}\mathbf{a}(z)} \qquad \mathbf{R} = \mathrm{E}(\mathbf{y}\mathbf{y}^H)$$

Tomographic imaging using specan

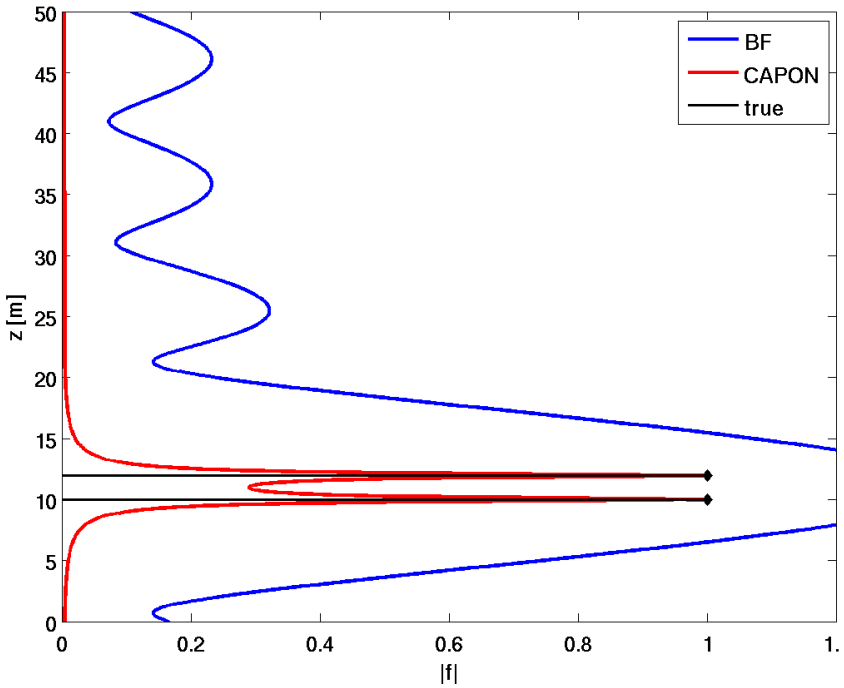

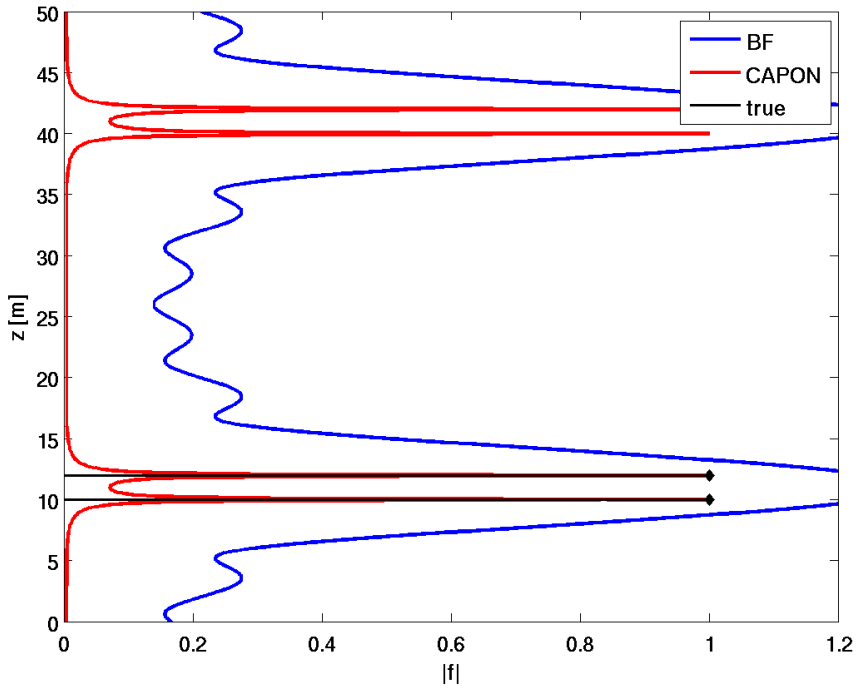

- **Capon: significantly improved resolution**
- **Resolution improvement is a function of the Signal to Noise Ratio (SNR)**
- **For regular baselines, BF & Capon are equally affected by ambiguities**

Irregular baseline sampling: logscale distribution

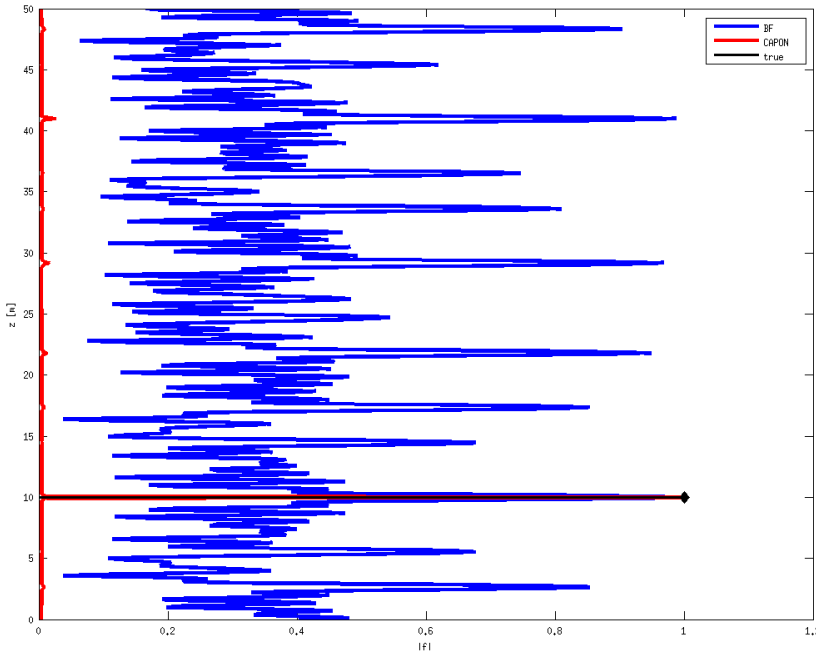

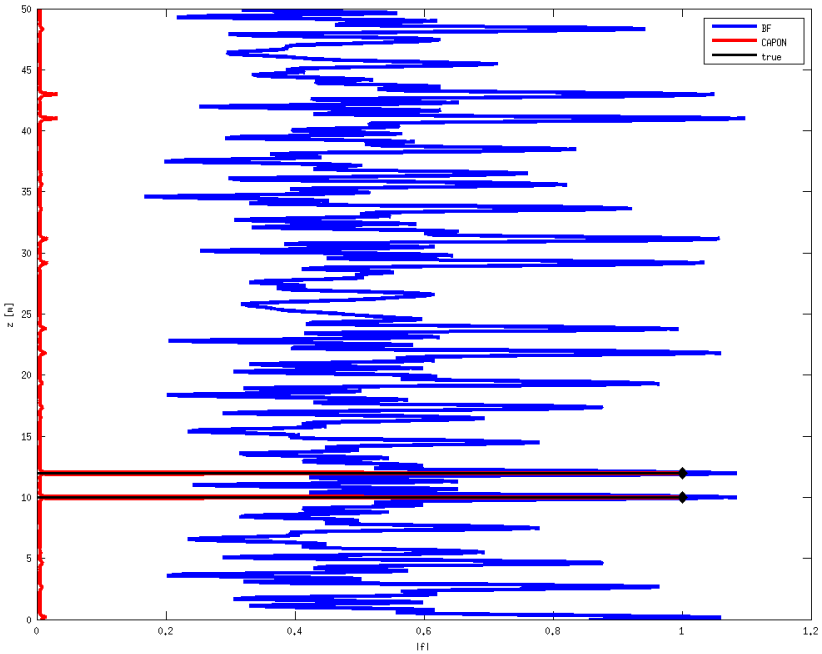

- BF: strongly affected by ambiguities
- CAPON: unsynchronized ambiguities are considered as perturbations and filtered. Good resolution performance preserved

Over speckle affected environments

- $\hat{a}_c = \mathbf{v}^H \mathbf{y}$ is a Random Variable (1 realization is not representative)
- Power Spectral Density: Intensity

$$P(z) = \mathrm{E}(|a_c|^2) = \mathrm{E}(|\mathbf{v}^H \mathbf{y}|^2) = \mathbf{v}^H \mathbf{R} \mathbf{v}$$

$$\boxed{P_B(z) = \frac{\mathbf{a}^H(z)\mathbf{R}\mathbf{a}(z)}{M^2}} \qquad \boxed{P_C(z) = \frac{1}{\mathbf{a}^H(z)\mathbf{R}^{-1}\mathbf{a}(z)}}$$

- In practice

$$\widehat{\mathbf{R}} = \frac{1}{L}\sum_{l=1}^{L} \mathbf{y}(l)\mathbf{y}^H(l)$$

- BF: quite stable w.r.t L

- Capon may suffer from a poor covariance matrix conditioning

$\Rightarrow$ Diagonal Loading $\widetilde{\mathbf{R}} = \widehat{\mathbf{R}} + \alpha \mathbf{I}_M, \quad \alpha \geq 0$

Tomographic imaging using specan

Tropical forest profile at P band with residual phase errors

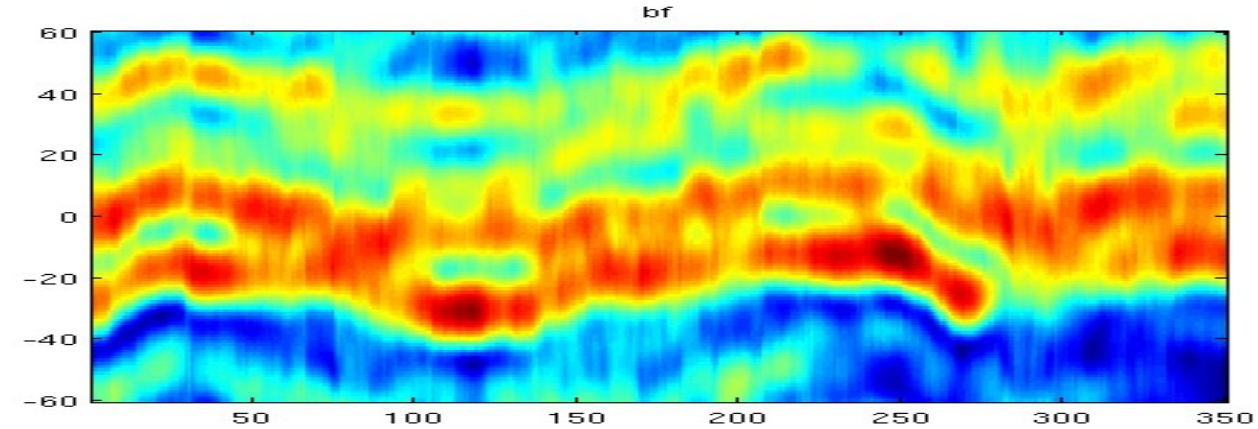

Z

BF

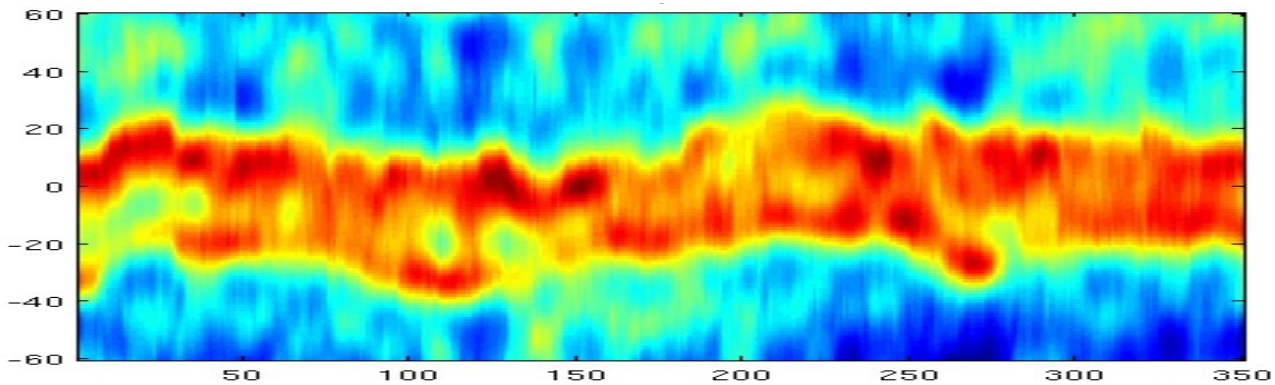

Z

Capon

Tomographic imaging using specan

Critical configuration **(3 images)** in an urban environment at L band

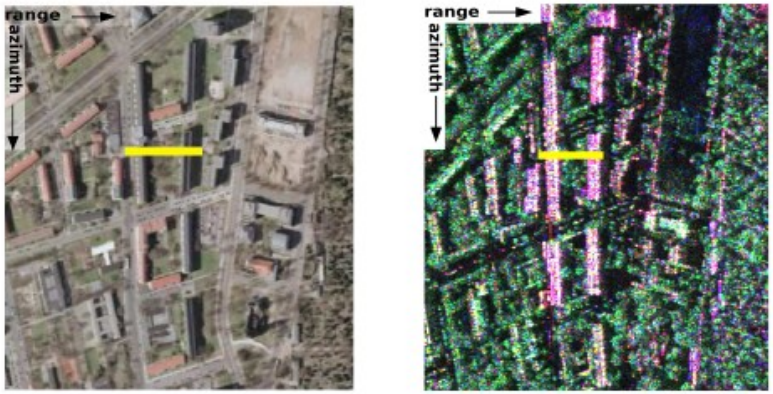

(a) Optical image (b) SAR

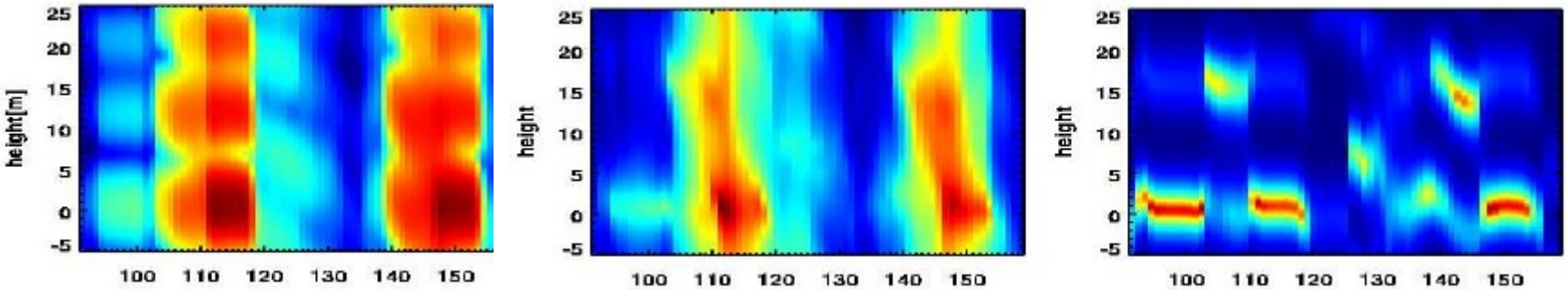

BF CAPON MUSIC

- Strictly speaking, Capon's technique is not HR, but is very convenient
- MUSIC (and some other techniques) is HR

Case study: BIOSAR 2 data

Forest height

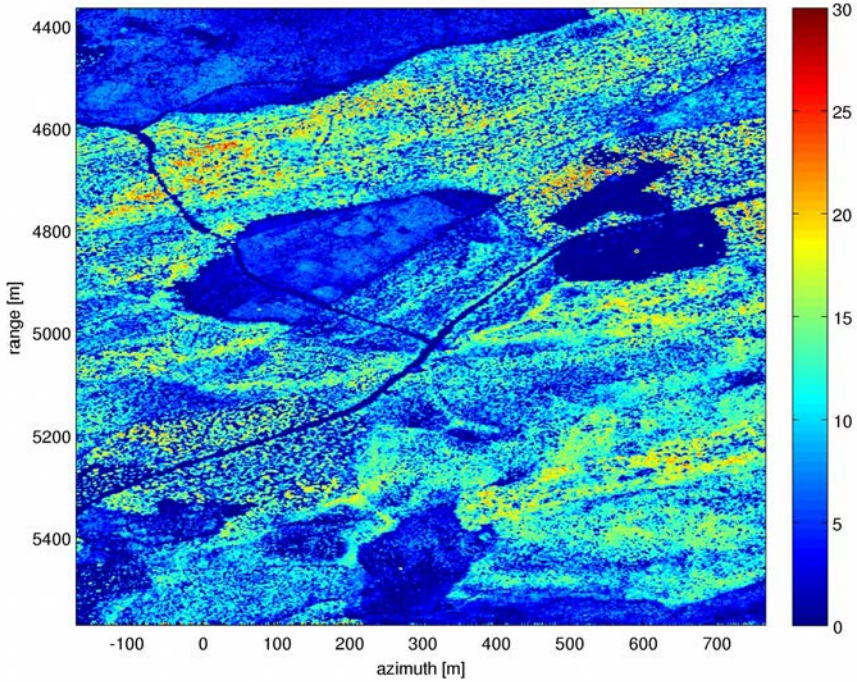

HH intensity

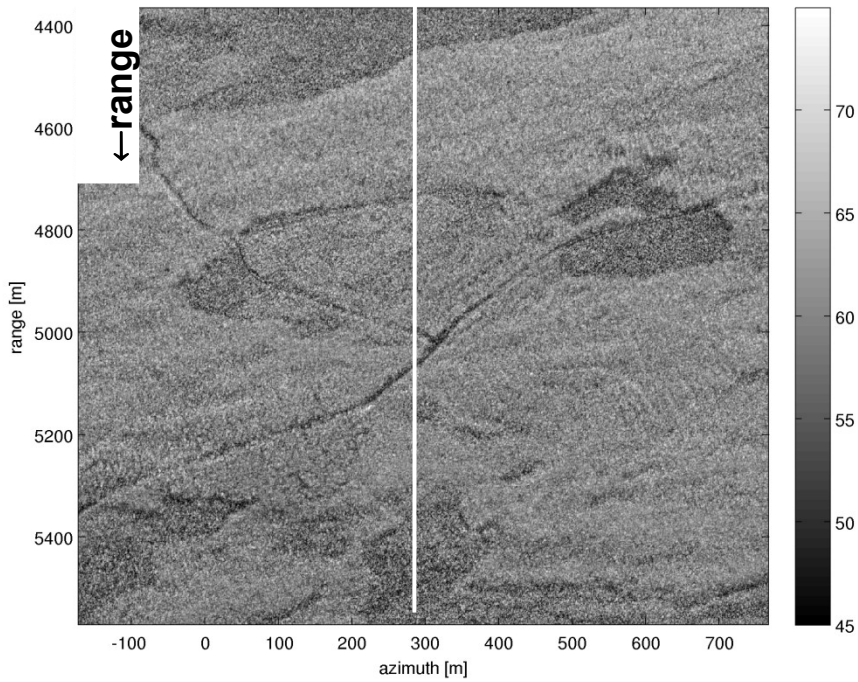

DEM

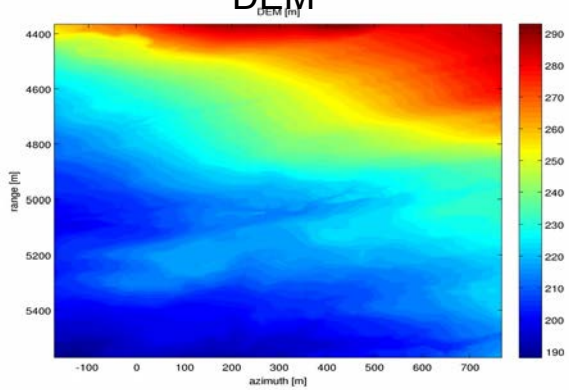

Case study: BIOSAR 2 data

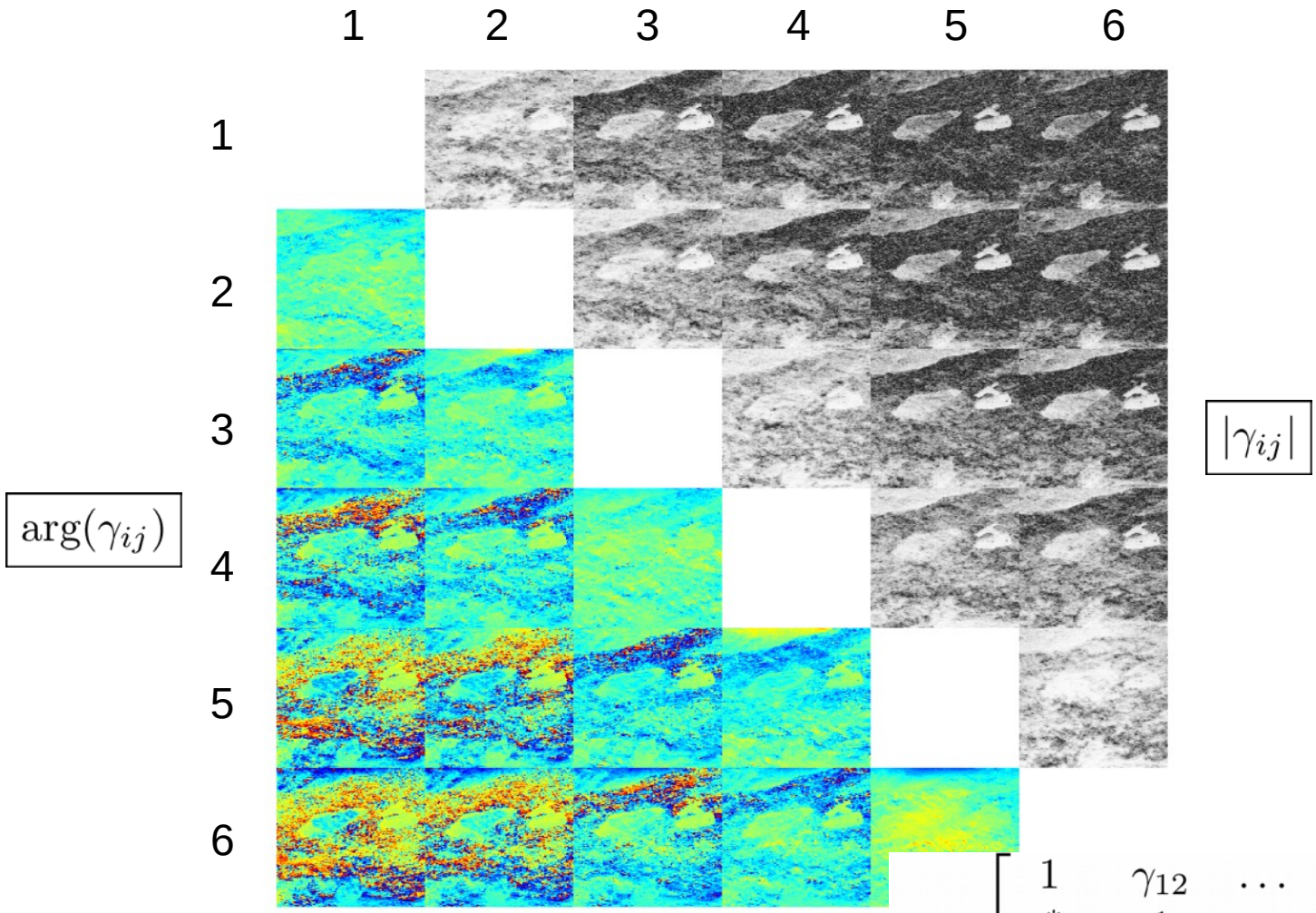

$$\widetilde{\mathbf{R}} = \begin{bmatrix} 1 & \gamma_{12} & \cdots & & \gamma_{1M} \\ \gamma_{12}^* & 1 & \gamma_{23} & \cdots & \gamma_{2M} \\ & & \ddots & & \\ \gamma_{1M}^* & & & & 1 \end{bmatrix}$$

Case study: BIOSAR 2 data

BF

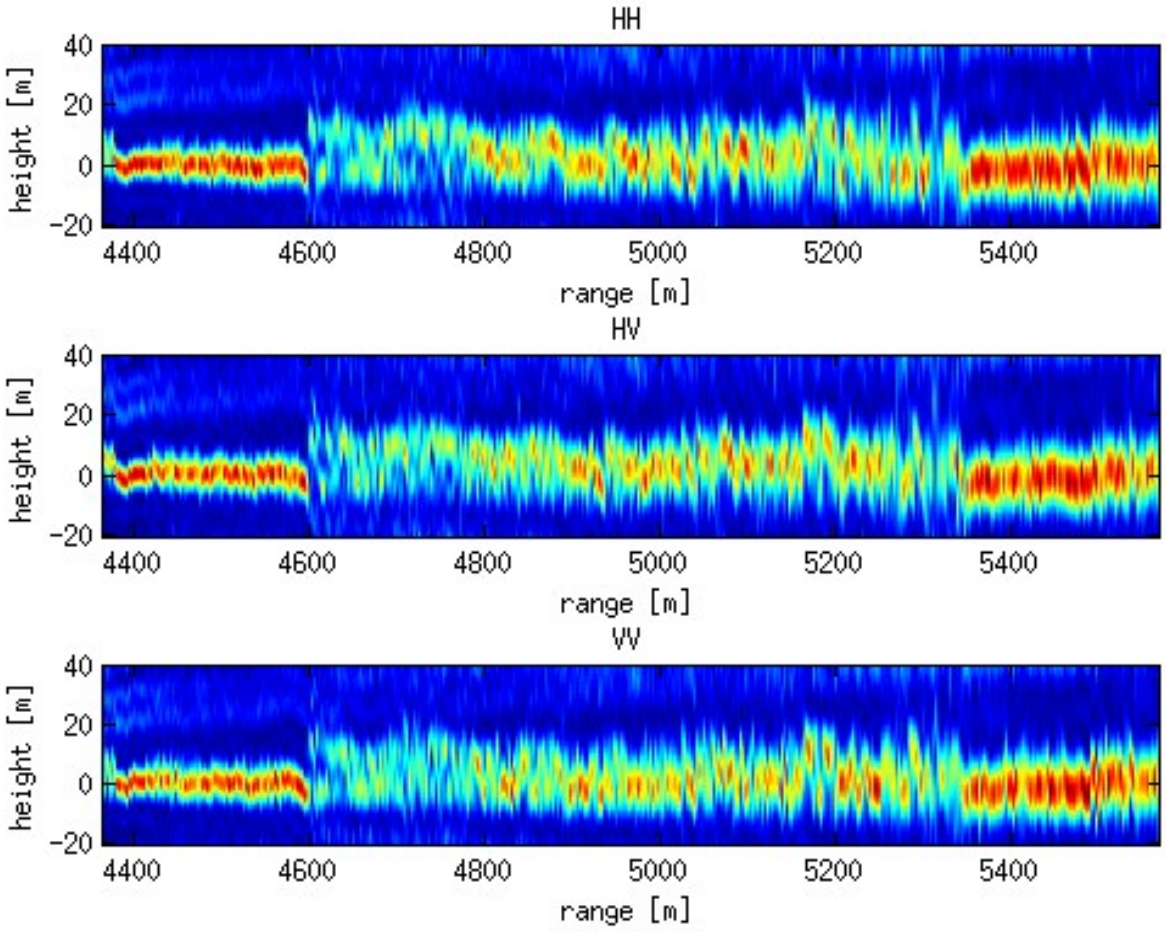

CAPON: processing OK ?

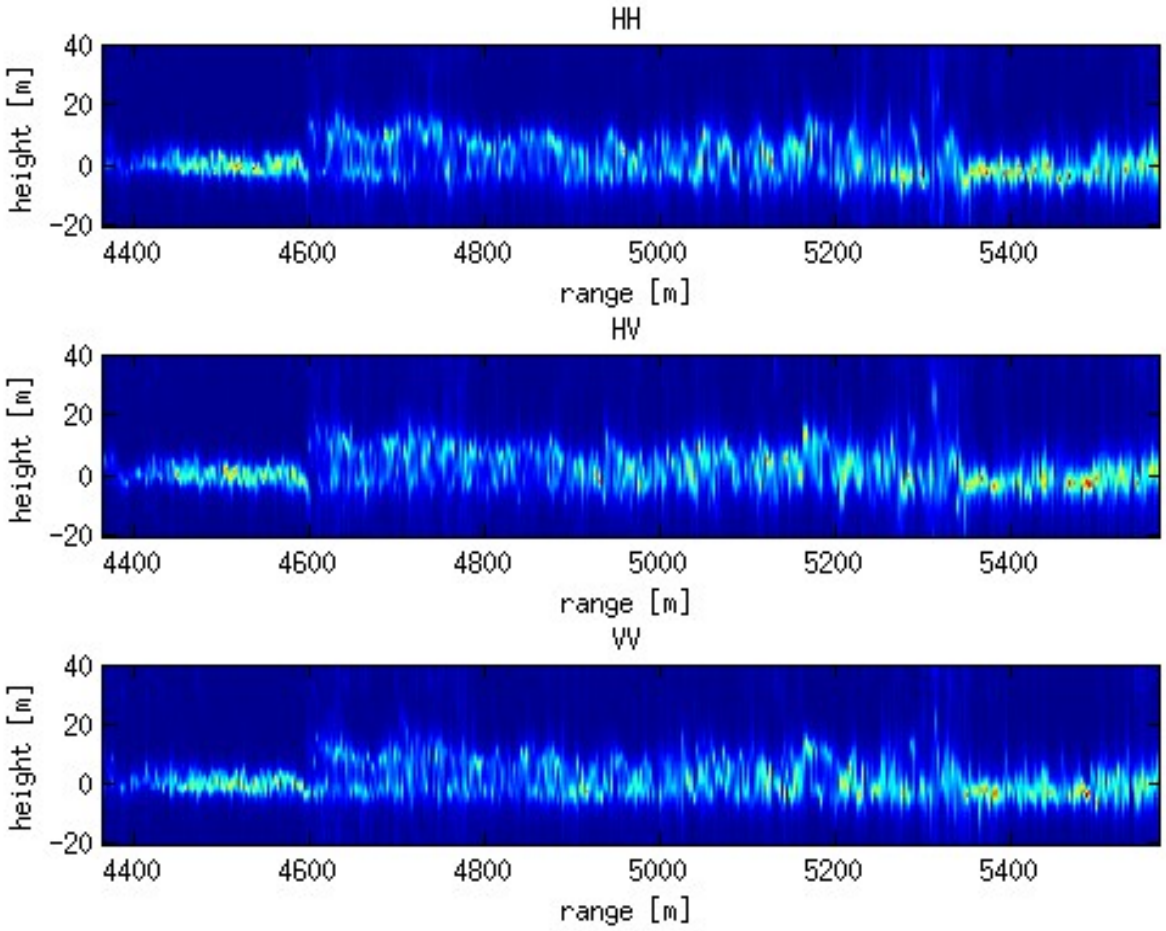

Advanced PolTomSAR imaging Using Specan methods

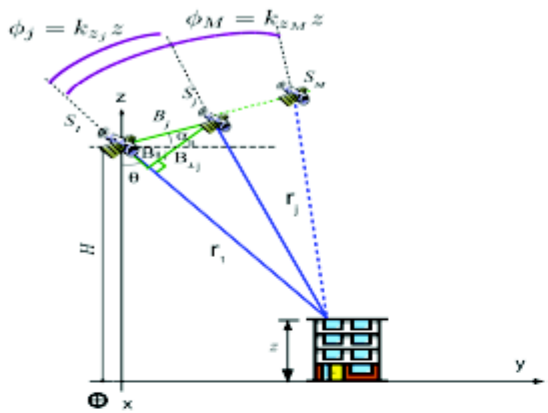

- M coherent acquisitions

$$\mathbf{y} = [y_1, \ldots, y_M]^T$$

- Steering vector

$$\mathbf{a}(z) = [1, e^{jk_{z_2} z}, \ldots, e^{jk_{z_M} z}]^T$$

Ideal scatterers (D sources)

$$\begin{aligned} \mathbf{y}(l) &= \mathbf{A}(\mathbf{z})\mathbf{s}(l) + \mathbf{n}(l) \\ \mathbf{A}(\mathbf{z}) &= [\mathbf{a}(z_1), \ldots, \mathbf{a}(z_D)] \end{aligned}$$

Fluctuating scatterers

- $\mathbf{s}(l) = \sqrt{\boldsymbol{\sigma}} \odot \mathbf{x}(l)$ varies over the M inSAR acquisitions
- Observed signal

$$\mathbf{y}(l) = \sum_{i=1}^{D} \sqrt{\sigma_i}\mathbf{x}_i(l) \odot \mathbf{a}(z_i) + \mathbf{n}(l)$$

- InSAR coherence matrix: $\mathbf{R_{ii}} = \mathrm{E}(\mathbf{x}_i(l)\mathbf{x}_i(l)^\dagger)$

MB-InSAR signal models

CM

$\mathbf{x}_{c_i} = \mathbf{1}_{(M\times 1)}$

UM

$\mathbf{x}_{u_i} \sim \mathcal{N}(0, \mathbf{R}_{ii})$

HM

PolTomSAR analysis of complex environments

UM: Speckle-affected distributed scatterers

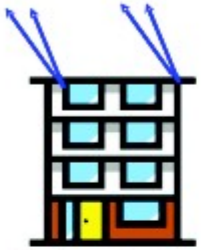

Roof scattering

Truck top scattering

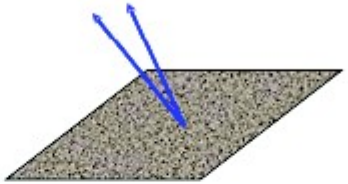

Rough surface scattering

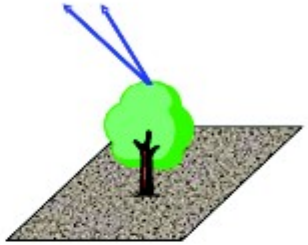

Volume scattering

CM: Deterministic scatterers

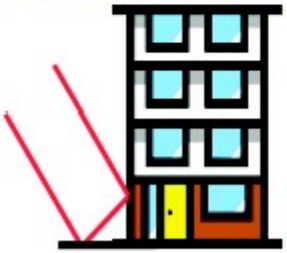

Wall-ground reflection

Double bounce reflection

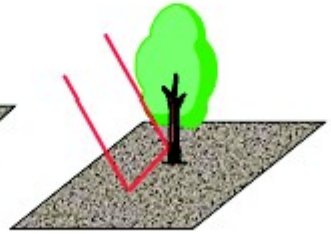

Ground-trunk reflection

coherent point scatterer

Single source

- POLSAR unitary target vector

$$\mathbf{k} = [k_1, k_2, k_3]^T, \ \mathbf{k}^\dagger \mathbf{k} = 1$$

- Polarimetric steering vector

$$\mathbf{a}(z, \mathbf{k}) = \mathbf{k} \otimes \mathbf{a}(z)$$

- 3-M element MB-POLinSAR signal

$$\mathbf{y}_P(l) = \begin{bmatrix} \mathbf{y}_1(l) \\ \mathbf{y}_2(l) \\ \mathbf{y}_3(l) \end{bmatrix} = s(l)\mathbf{a}(z, \mathbf{k}) + \mathbf{n}(l)$$

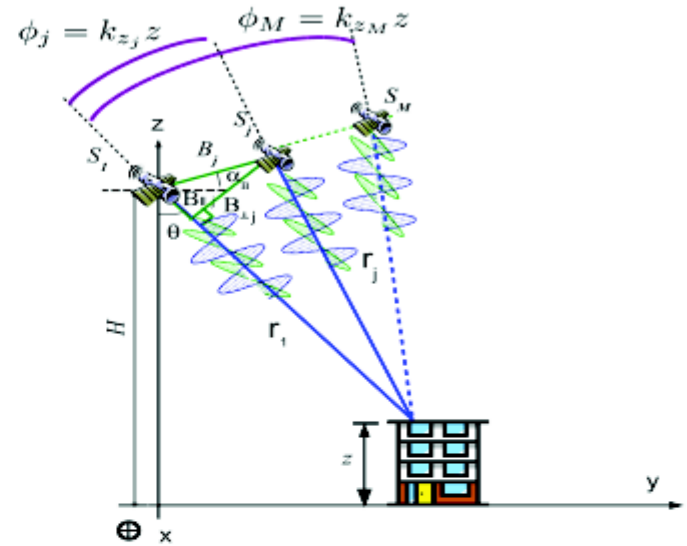

D sources

- Polarimetric steering matrix

$$\mathbf{A}(\mathbf{z}, \mathbf{K}) = [\mathbf{a}(z_1, \mathbf{k}_1), \ldots, \mathbf{a}(z_D, \mathbf{k}_D)]$$

- 3-M element MB-POLinSAR signal

$$\mathbf{y}_P = \mathbf{A}(\mathbf{z}, \mathbf{K})\mathbf{s} + \mathbf{n}$$

PolTomSAR analysis of complex environments

Discrete case (N_s *sources*)

- Heights: $\hat{\mathbf{z}}$
- Reflectivities: $\hat{\sigma}$
- Polarimatric mech.: $\hat{\mathbf{K}}$

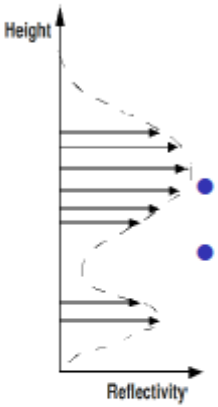

Continuous case

- Reflectivity: $\hat{\sigma}(z)$
- Polarimatric mech.: $\mathbf{k}(z)$

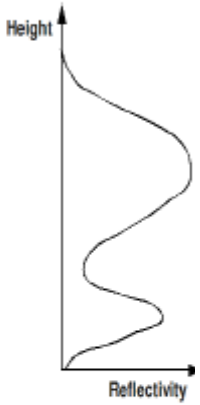

Practical implementation

- Parameters estimated from $\hat{\mathbf{R}} = \frac{1}{L}\sum_{l=1}^{L} \mathbf{y}(l)\mathbf{y}(l)^{\dagger}$
- N_s: estimated using MOS techniques

PolTomSAR analysis of complex environments

Nonparametric estimators

Beamforming

$$\hat{\sigma}(z) = \mathbf{a}^{\dagger}(z)\hat{\mathbf{R}}\mathbf{a}(z)$$

☺ Continuous, fast & robust

☹ Limited vertical resolution

Capon

$$\hat{\sigma}(z) = \frac{1}{\mathbf{a}^{\dagger}(z)\hat{\mathbf{R}}^{-1}\mathbf{a}(z)}$$

Parametric estimators (N_s sources)

MUSIC: subspace based 1-D method

- $\hat{\mathbf{z}} = \arg\max_{loc,z}\left(\frac{1}{\mathbf{a}^{\dagger}(z)\hat{\mathbf{E}}_n\hat{\mathbf{E}}_n^{\dagger}\mathbf{a}(z)}\right)$
- $\hat{\boldsymbol{\sigma}} = \arg\min_{\mathbf{s}} ||\sum_l \mathbf{y}(l) - \mathbf{A}(\hat{\mathbf{z}})\mathbf{s}||^2$

☺ High resolution & relatively fast (1-D)

☹ Unadapted to CM scatterers

Maximum Likelihood (ML) estimators

- $(\hat{\mathbf{z}}, \hat{\boldsymbol{\sigma}}, \hat{\sigma_n}) = \arg\max \mathcal{L}(\mathbf{z}, \boldsymbol{\sigma}, \sigma_n)$
- $\mathcal{L}_{CM} \Rightarrow$ Deterministic ML (DML)
- $\mathcal{L}_{UM} \Rightarrow$ Stochastic ML (SML)

☺ High resolution

☹ Computationally intensive ($N_s - D$)

Subspaces (N_s sources)

$$\begin{aligned} \mathbf{R} = E(\mathbf{y}\mathbf{y}^\dagger) &= \mathbf{A}(\mathbf{z})\mathbf{S}\mathbf{A}(\mathbf{z})^\dagger + \sigma_n \mathbf{I} \\ &= \mathbf{E}_s \mathbf{\Lambda}_s \mathbf{E}_s^\dagger + \sigma_n \mathbf{E}_n \mathbf{E}_n^\dagger \end{aligned}$$

- Signal subspace: $\mathbf{E}_s = \mathbf{A}(\mathbf{z})\mathbf{T}$
- Noise subspace: $\mathbf{E}_n^\dagger \mathbf{A}(\mathbf{z}) = \mathbf{0}$

Weighted LS subspace fit

- $\hat{\mathbf{R}} = \hat{\mathbf{E}}_s \hat{\mathbf{\Lambda}}_s \hat{\mathbf{E}}_s^\dagger + \hat{\mathbf{E}}_n \hat{\mathbf{\Lambda}}_n \hat{\mathbf{E}}_n^\dagger \qquad \hat{N}_s$
- Signal subspace fitting (SSF): $\hat{\mathbf{z}}, \hat{\mathbf{T}} = \arg\min \|\hat{\mathbf{E}}_s \mathbf{W}_s^{1/2} - \mathbf{A}\mathbf{T}\|_F^2$
- Noise subspace fitting (NSF): $\hat{\mathbf{z}} = \arg\min \|\mathbf{W}_n^{1/2} \mathbf{E}_n^\dagger \mathbf{A}\|_F^2$

Weighted Subspace Fitting (WSF) Estimators

Weighting matrix	Method	Performance
$\mathbf{W}_S = \mathbf{W}_N = \mathbf{I}$	MUSIC	☹CM scatterers
$\mathbf{W}_S = \mathbf{\Lambda}_s - \sigma^2\mathbf{I}$, $\mathbf{W}_N = \hat{\mathbf{R}}_x$	DML	☹close CM scatterers
$\mathbf{W}_{S\,opt} = (\mathbf{\Lambda}_s - \sigma^2\mathbf{I})^2 \mathbf{\Lambda}_s^{-1}$	SSF	☺Optimal CM/UM scatterers
$\mathbf{W}_{N\,opt} = (\mathbf{A}^\dagger \hat{\mathbf{E}}_s (\mathbf{\Lambda}_s - \sigma^2\mathbf{I})^{-2} \mathbf{\Lambda}_s \hat{\mathbf{E}}_s^\dagger \mathbf{A})^{-1}$	NSF	☺Optimal UM scatterers

Influence of vertical resolution, δz and source correlation ρ

$SNR = 20\,\text{dB}$, vertical resolution $\delta z = 30/M$ (m)

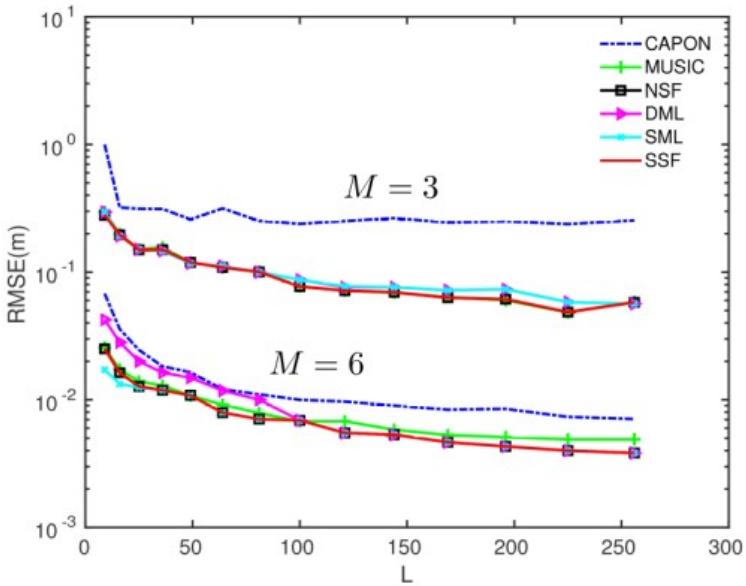

$\rho = 0, \Delta z = 4$ m

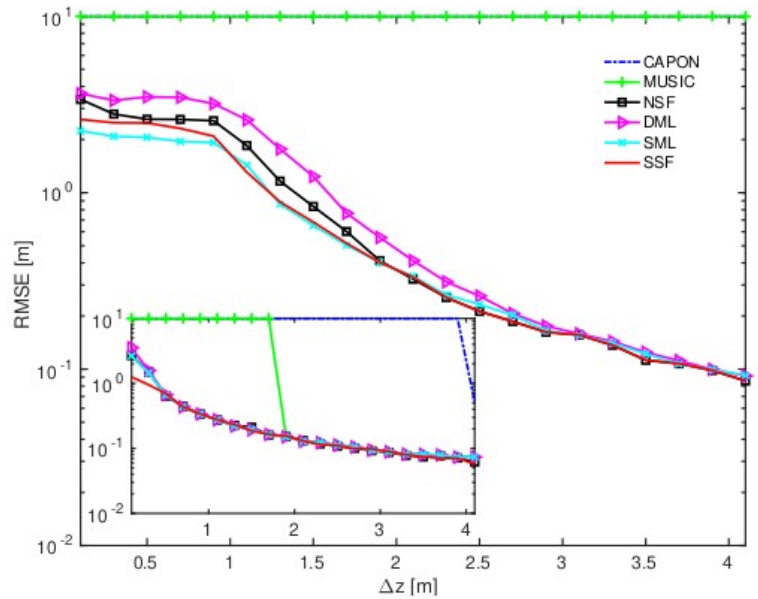

$M = 3$, $\rho = 0.995$ **(outer)**. $\rho = 0$ **(inner)**

- M, ρ: huge influence on tomographic performance. Non-parametric methods: unadapted
- ML and WSF: can cope with high-correlation cases (urban areas).
- NSF and DML: may reach limitations

Influence of polarization diversity

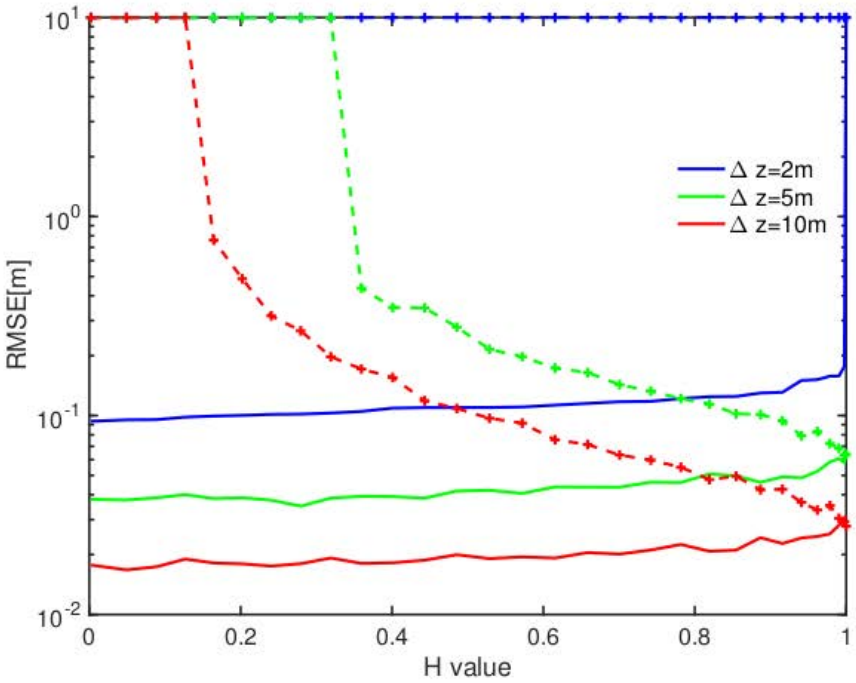

Single-pol processing: most (solid) and least (dashed) favorable cases

- Deterministic PolSAR response ($H = 0$):
  polarimetric processing may provide a huge gain
- Unpolarized responses ($H = 1$):
  same performance than single-pol processing

Required spectral estimation method

Method selection

- High-resolution & able to cope with $\rho \approx 1$
- Adapted to low M values & polarimetric

$\Rightarrow$ Polarimetric Weighted Signal Subspace Fitting P-SSF

Optimization criterion

$$\widehat{\mathbf{z}}, \widehat{\mathbf{K}} = \arg\max_{\mathbf{z},\mathbf{K}} Q(\mathbf{z},\mathbf{K}) \quad \text{with } Q(\mathbf{z},\mathbf{K}) = \mathrm{tr}(\mathbf{P}_{\mathbf{A}_{(\mathbf{z},\mathbf{K})}}\mathbf{M}), \qquad \mathbf{M} = \begin{cases} \widehat{\mathbf{R}}_{\mathbf{yy}} & \rightarrow \text{P-DML} \\ \widehat{\mathbf{E}}_s \mathbf{W} \widehat{\mathbf{E}}_s^H & \rightarrow \text{P-SSF} \end{cases}$$

$\Rightarrow N_p \times N_s$-D search!

Proposed solution: Polarimetric Alternating Projections

- Iterative 1-D search: alternating directions
- Polarimetric optimization at each step: constrained beamforming

$\Rightarrow$ Generalized eigen-decomposition

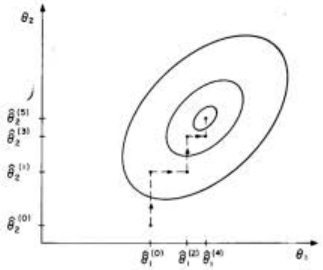

Ziskind & Wax, "Maximum likelihood localization of multiple sources by alternating projection," IEEE T&SSP, 1988

3-D IMAGING OF AN URBAN AREA USING A MINIMAL POL-TOMSAR CONFIGURATION

Urban area test site

- Images over Dresden, 2000
- DLR's E-SAR at L-Band
- Resolution : 0.5 m $\times$ 2.5 m
- Fully polarimetric
- Dual-baseline InSAR

Baselines	H_{am}
10 m	55-73 m
40 m	14-18 m

3 PolSAR images

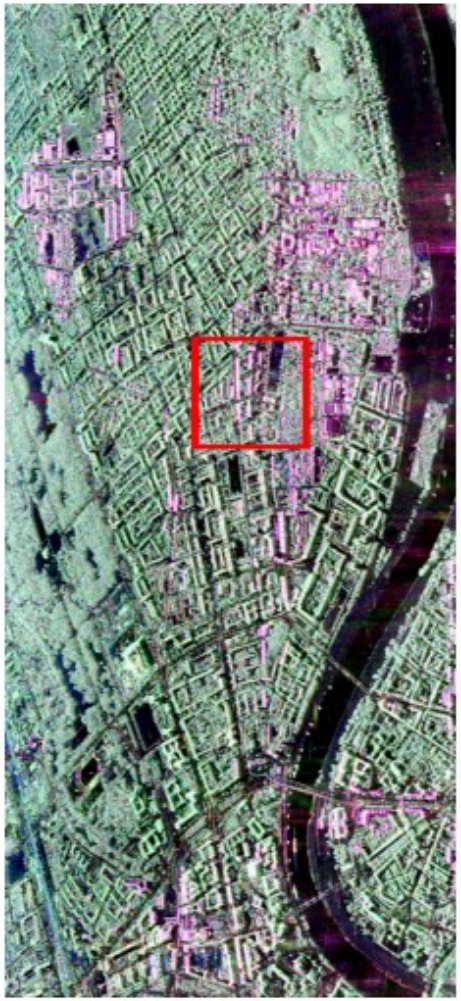

Pauli-coded SAR image

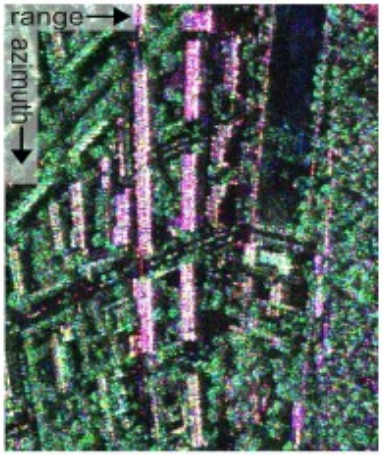

Optical image

Polarimetric SAR tomography over urban areas

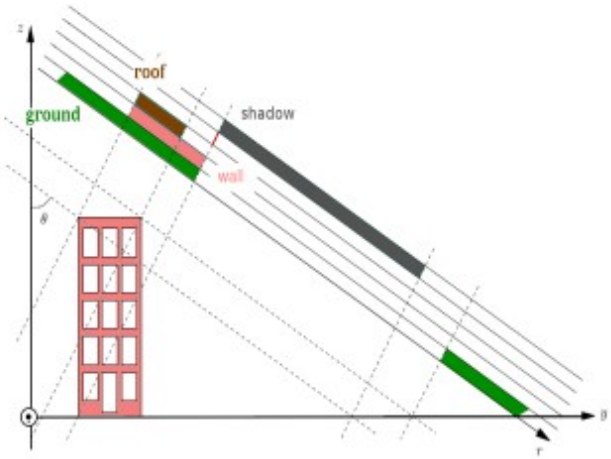

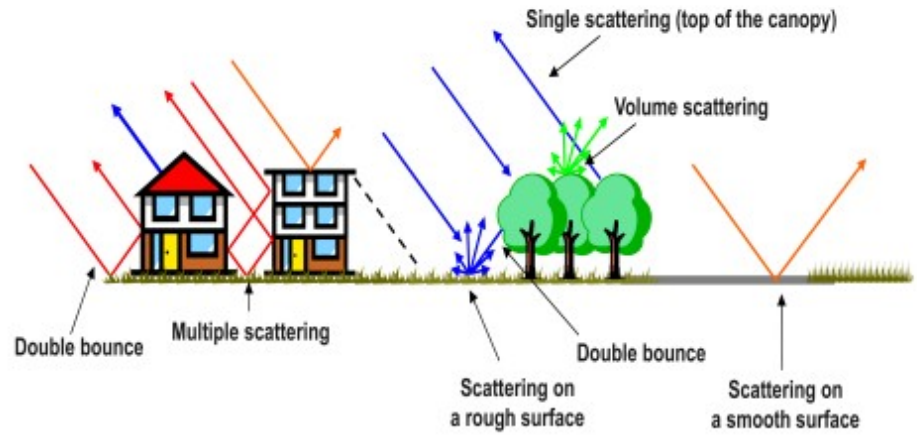

- L-band intermediate-resolution data sets
  $\Rightarrow$ High-Resolution (HR) tomographic estimators
- 3 images
  $\Rightarrow N_s = 2$

Polarimetric SAR tomography over urban areas

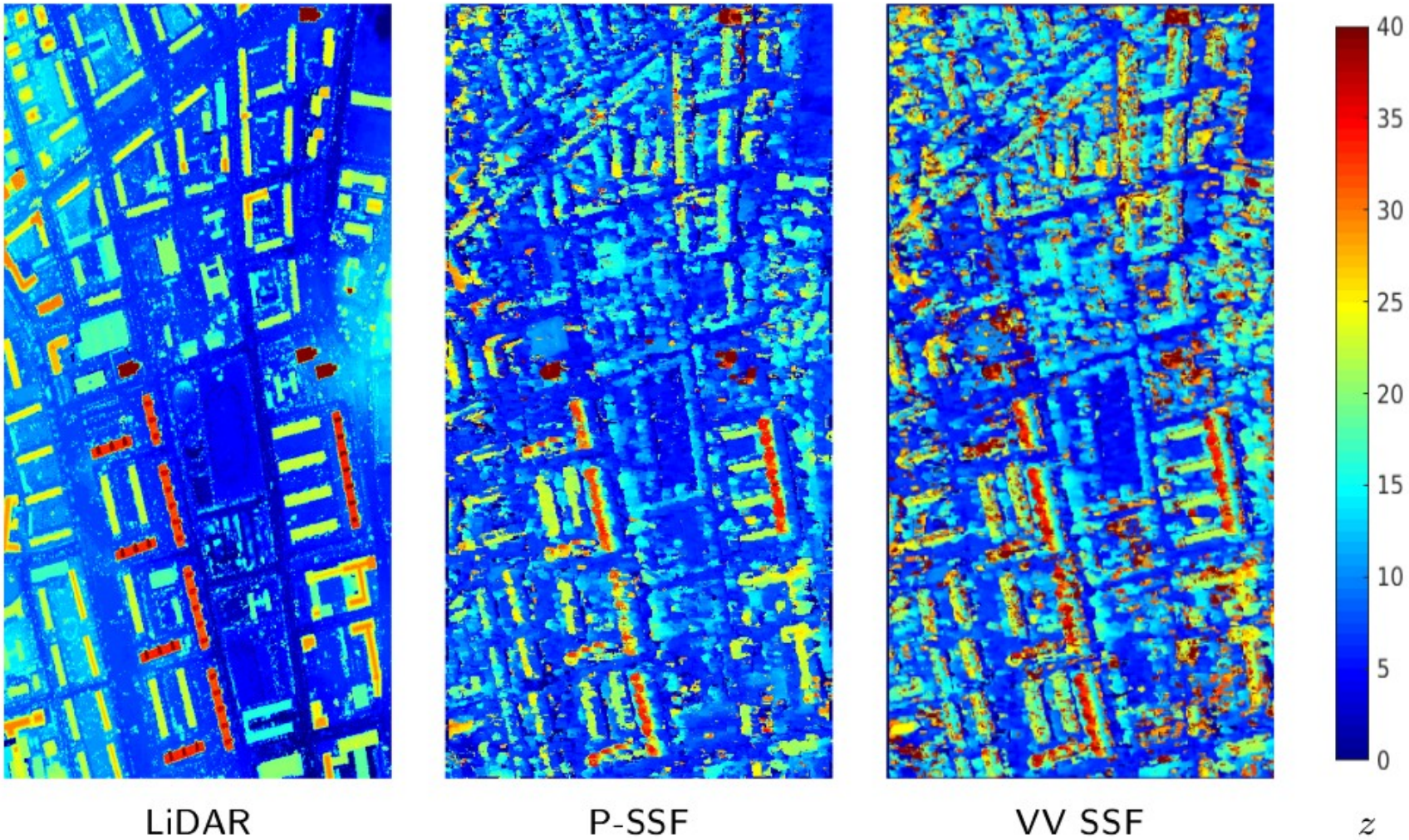

Polarimetric SAR tomography over urban areas

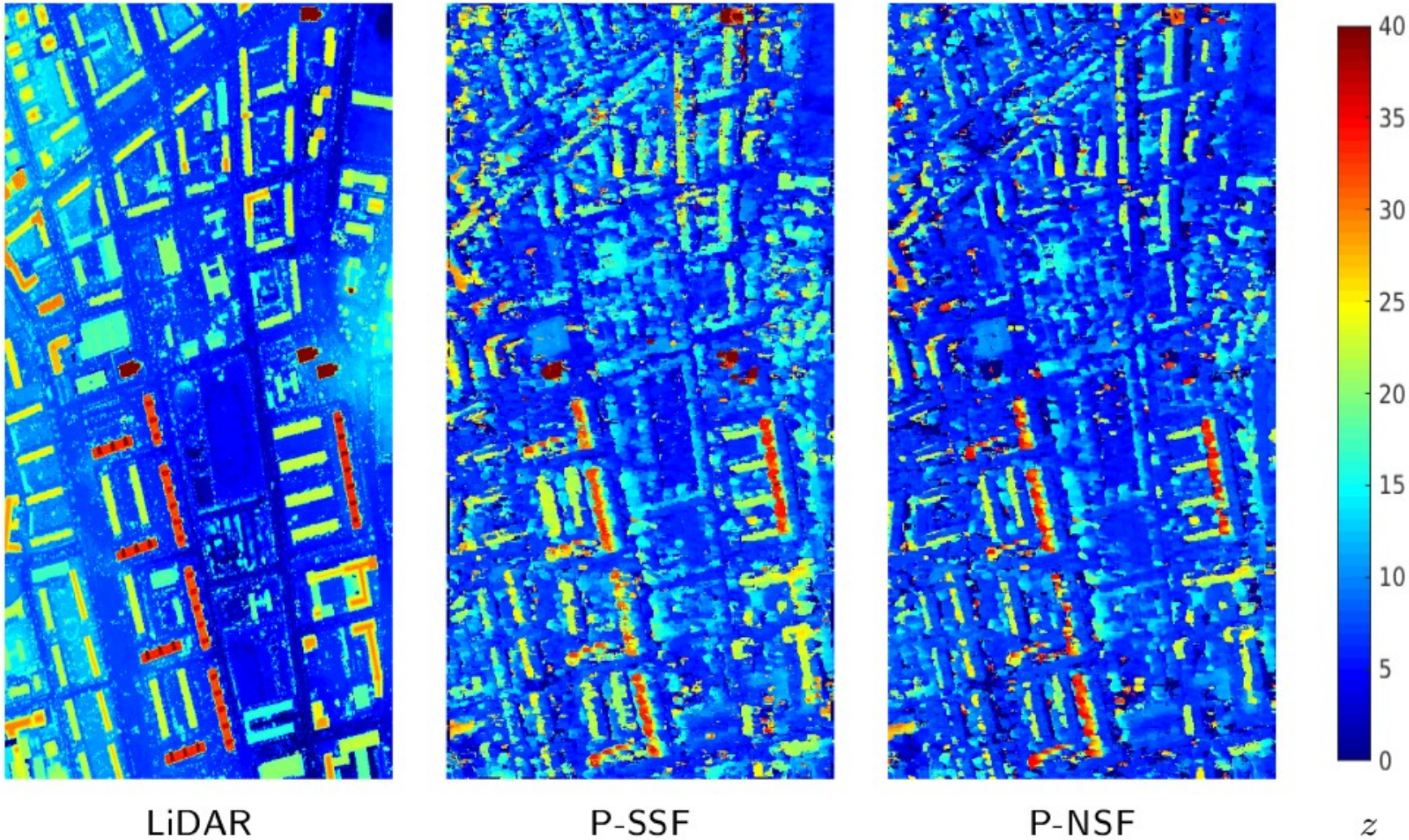

Polarimetric SAR tomography over urban areas

Building reconstruction

Google map

Pauli-coded

LiDAR

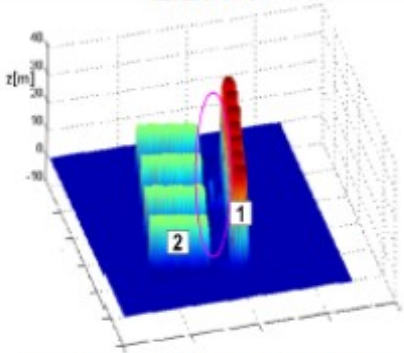

Estimated by FP-NSF
($N_s = 2$)

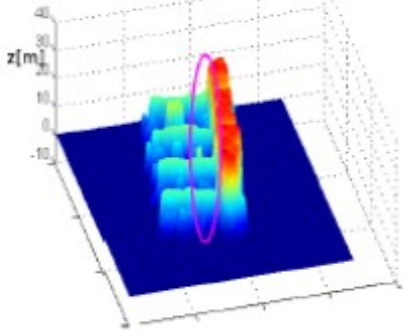

Difference between LiDAR and estimated surface

- projection of SAR imaging
- vegetation between B1 and B2

Polarimetric SAR tomography over urban areas

Building reconstruction

Google map

Bing map

LiDAR

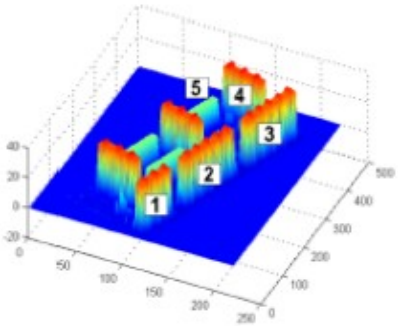

Estimated by FP-NSF
($N_s = 2$)

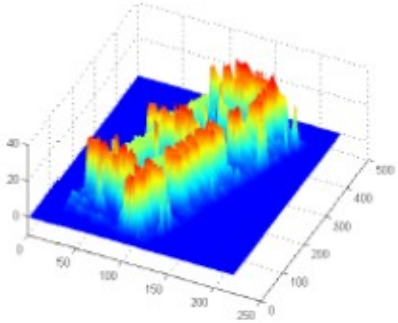

Averaged z[m]	B1	B2	B3	B4	B5
LIDAR	30.0	30.2	30.1	30.8	16.3
Estimated	27.5	27.8	27.5	27.3	16.1

Polarimetric SAR tomography over urban areas

Full-rank polarimetric Capon tomographic estimator

- Classical unitary-rank PolTomoSAR $\mathbf{k}(z) \in \mathbb{C}^{N_p \times 1}$
- Full-rank PolTomoSAR

$$\boxed{\widehat{\mathbf{T}}(z) \quad \text{with} \quad \mathbf{T}(z) = \mathrm{E}(\mathbf{k}(z)\mathbf{k}^H(z))}$$

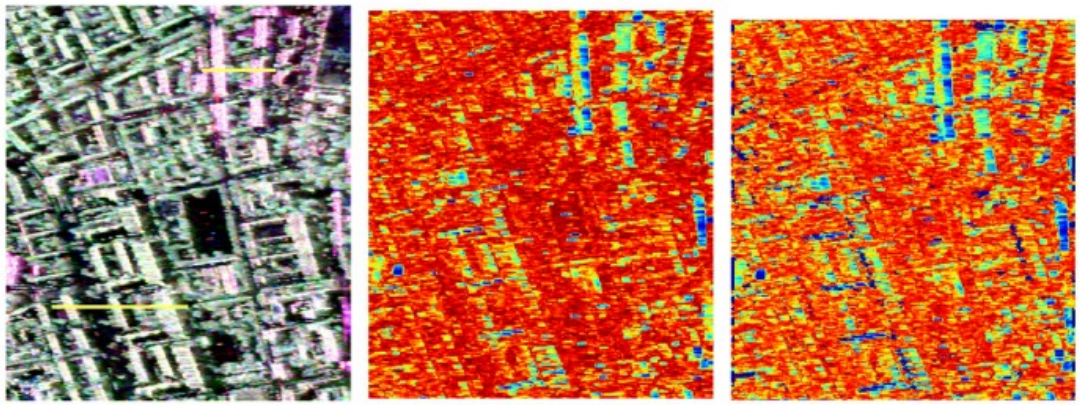

PolSAR image | 2-D H | 3-D H, 1st source

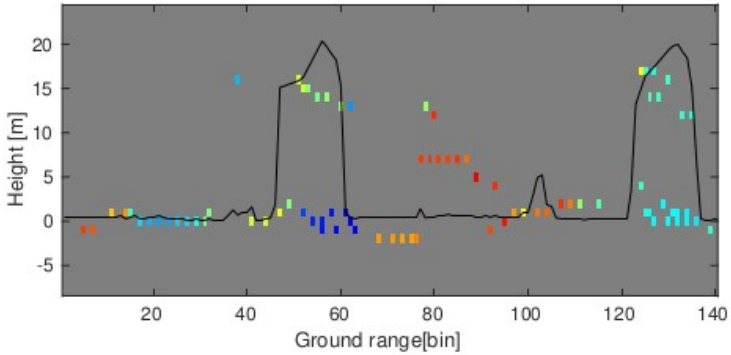

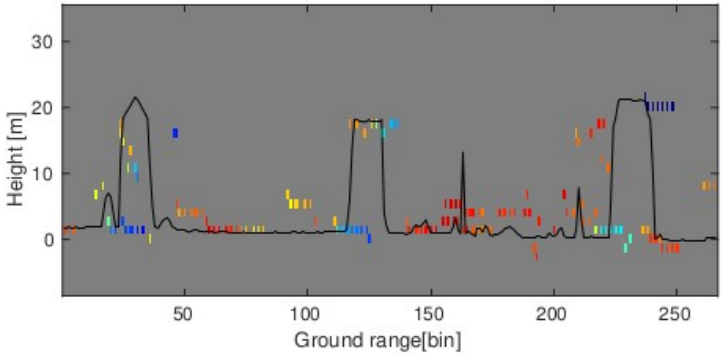

POL-TOMSAR IMAGING OF CONCEALED OBJECTS

Above ground and under foliage objects observed at L band

- DLR E-SAR image over Dornstetten, Germany
- L-Band
- 21 tracks : average baseline 20m
- $\delta_z = 2$m

Horizontal baseline distribution

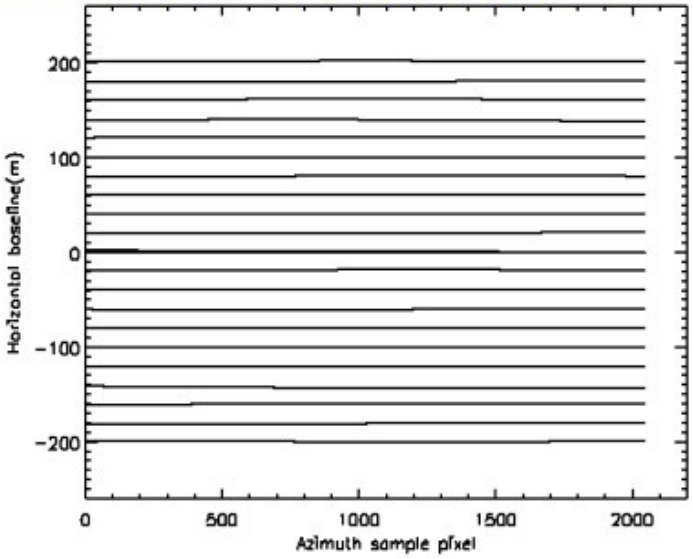

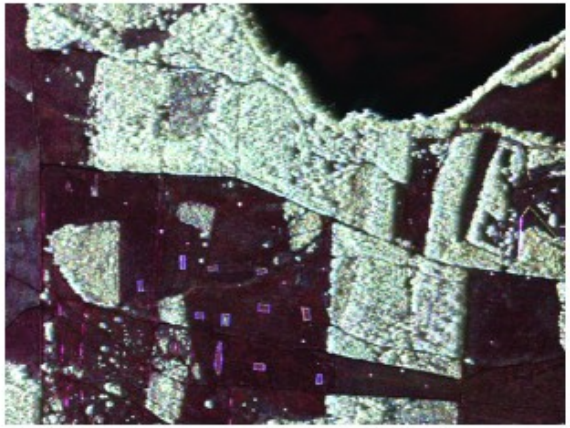

Huang, Y.; Ferro-Famil, L. & Reigber, A. "Under-Foliage Object Imaging Using SAR Tomography and Polarimetric Spectral Estimators", IEEE TGRS 2011

POL-TOMSAR IMAGING OF CONCEALED OBJECTS

VV refectivity tomograms

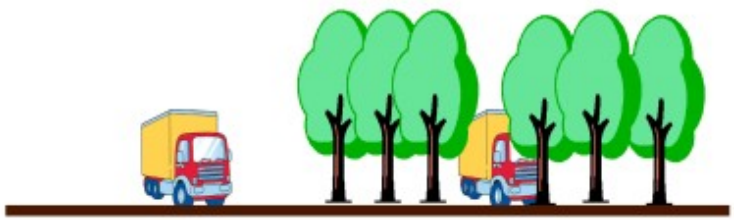

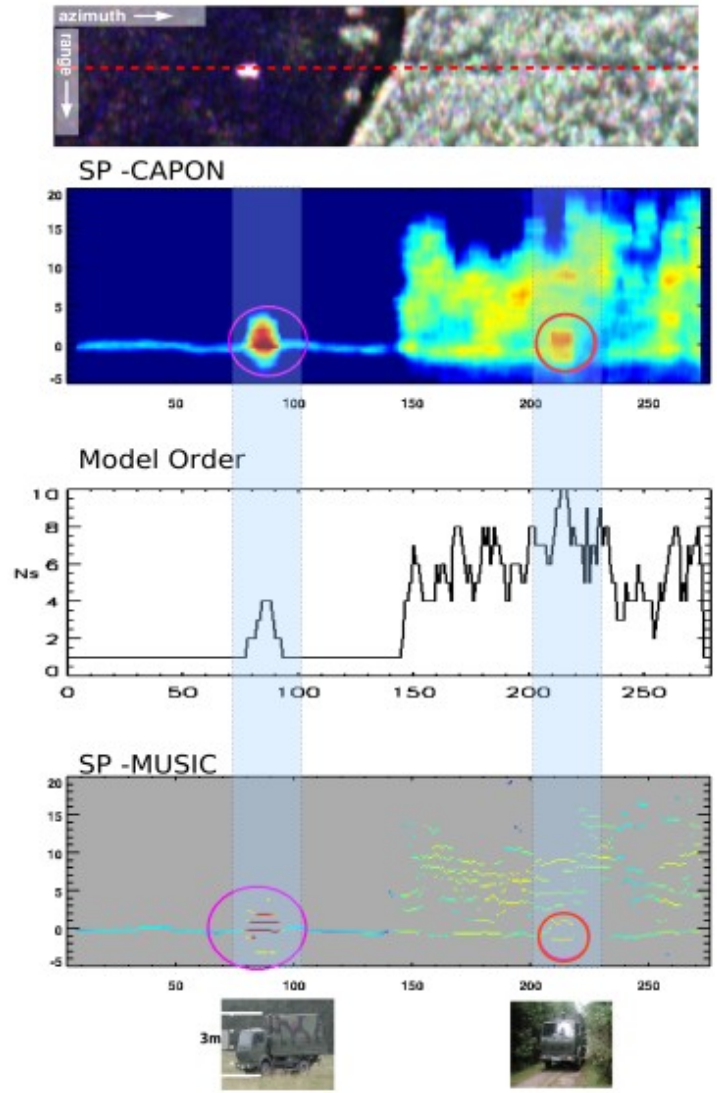

Capon :

limited resolution
$\Rightarrow$ overestimated H_{truck}

MUSIC :

- ☺ Sub-canopy truck
  $\Rightarrow$ hybrid scatterer
- ☹ Uncovered
  $\Rightarrow$ coherent scatterer
- ☹ Spurious sidelobes.

POL-TOMSAR IMAGING OF CONCEALED OBJECTS

High Resolution tomograms of underfoliage objects

SSF : shape and reflectivity

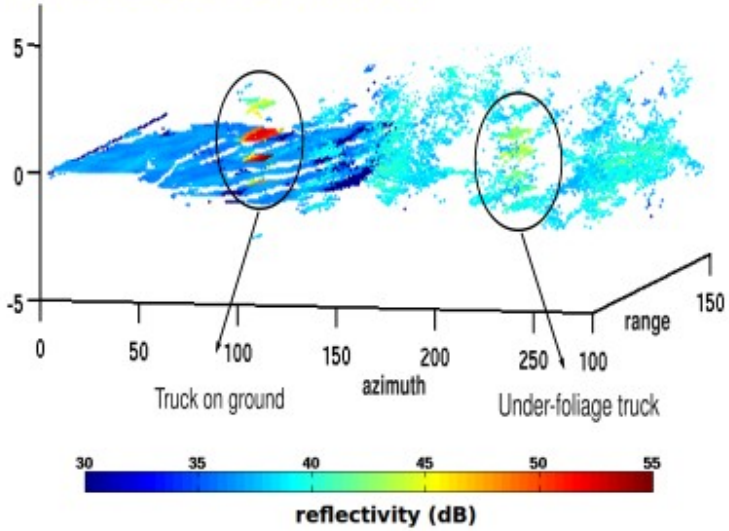

FP-NSF : scattering mechanisms

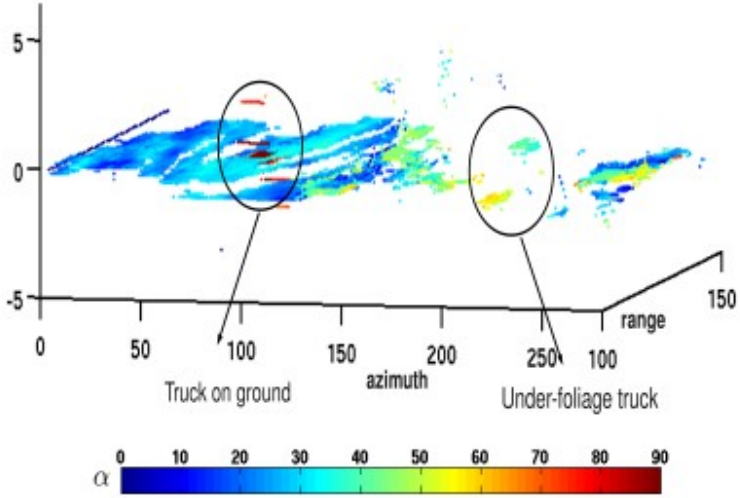

Sparse (compressive) sensing solution

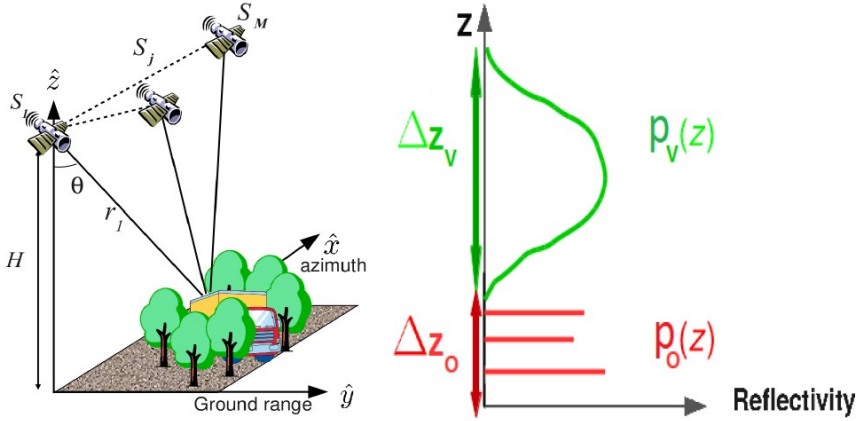

- a few wavelet components
- a few discrete contributions

$$\min_{\mathbf{p}} ||\mathbf{B}\mathbf{p}||_1 \text{ subject to } \quad ||\mathbf{R} - \widehat{\mathbf{R}}||_F \leq \epsilon \qquad \widehat{\mathbf{R}} = \mathbf{A}(\mathbf{z})\,\mathrm{diag}(\mathbf{p})\mathbf{A}^H(\mathbf{z})$$

$$\mathbf{B} = \begin{bmatrix} \mathbf{I}_{(N_o \times N_o)} & \mathbf{0} \\ \mathbf{0} & \mathbf{\Psi}_{(N_v \times N_v)} \end{bmatrix} \in \mathbb{R}^{(N_s \times N_s)} \qquad \mathbf{p} = [\mathbf{p}_o^T \quad \mathbf{p}_v^T]^T \in \mathbb{R}^{+N_s \times 1}$$

POL-TOMSAR IMAGING OF CONCEALED OBJECTS

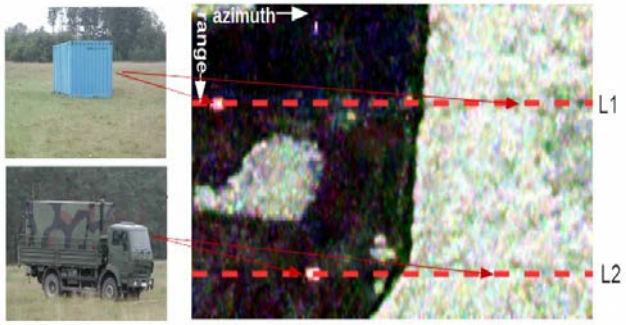

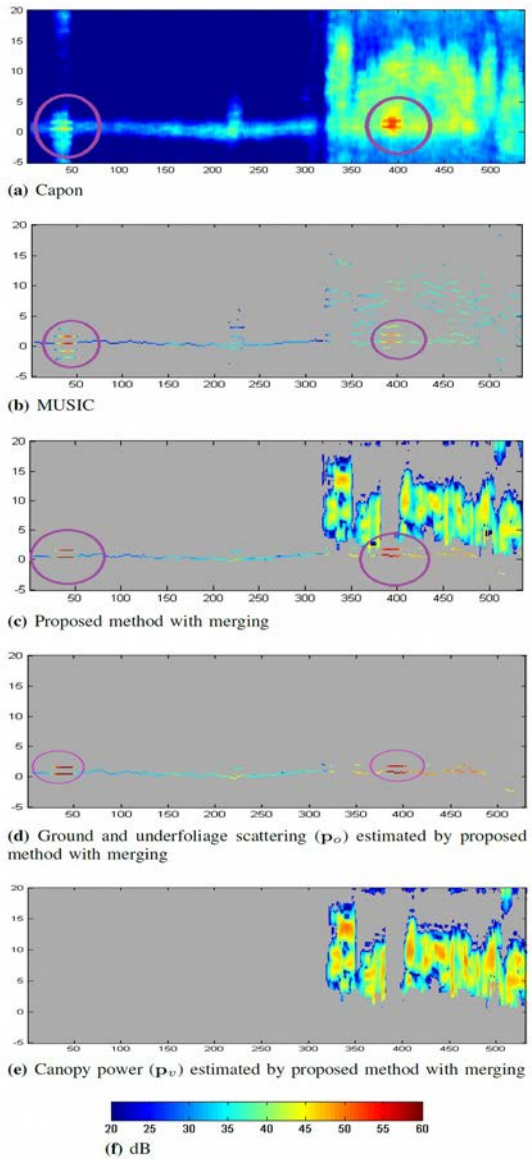

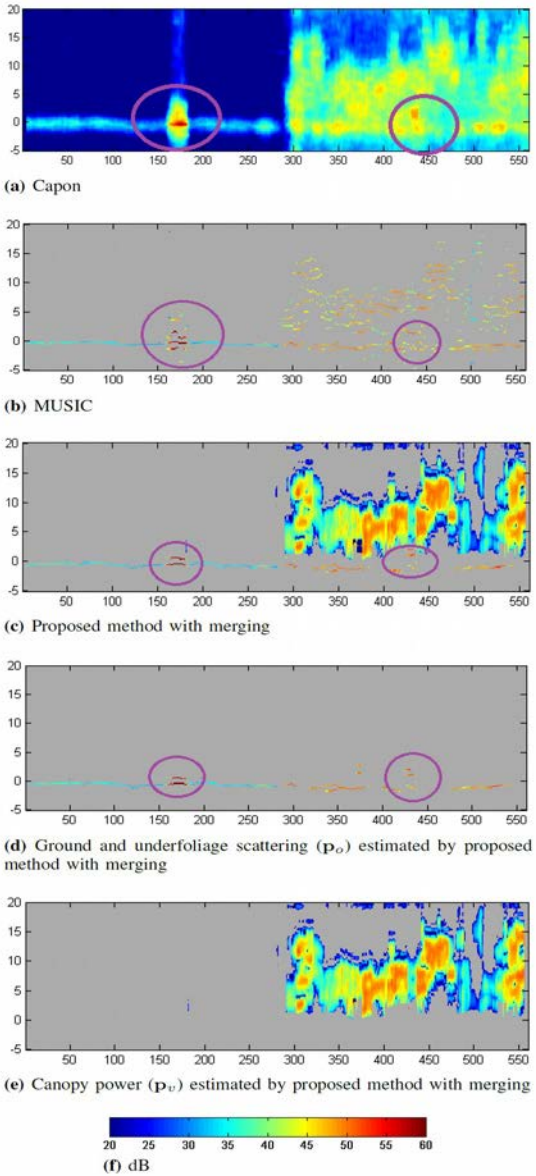

Tropical forest characterization

Tropical forest test site and objectives

- TropiSAR Campaign, 2009
- ONERA SETHI
- P-Band
- 6 tracks
- $\delta_{az} = 1.245m$
  $\delta_{rg} = 1m$
- $\delta_z = 12.5m$
- Ground truth
  - LiDAR data
  - Biomass measurements for 16 ROIs

The ECOFOG Sites
- Nouragues
- Paracou
- Arbocel

The Calibration site
- Rochambeau

Other site
- Marais de Kaw

Courtesy ONERA

Objectives

- Tree height,underlying ground topography estimation
- Forest vertical structure characterization
- Biomass monitoring

Tropical forest characterization

Tropical forest test site : Paracou

Optical image

SAR image

LiDAR z_g

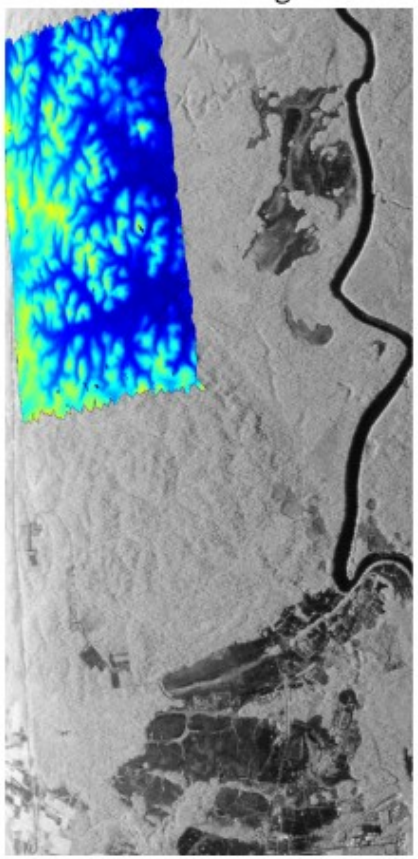

LiDAR z_{top}

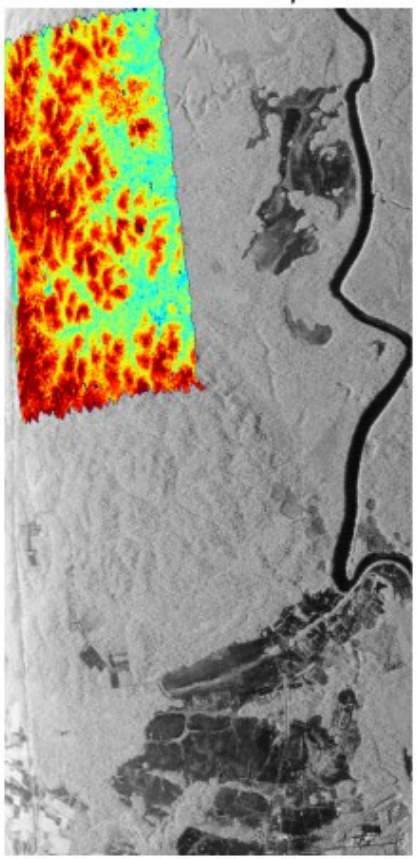

- Tropical forest environments (savannah, undisturbed forests, logged plots...)
- Highly varying ground topography

Tropical forest characterization

Tree height and ground topography estimation

Hybrid spectral approach

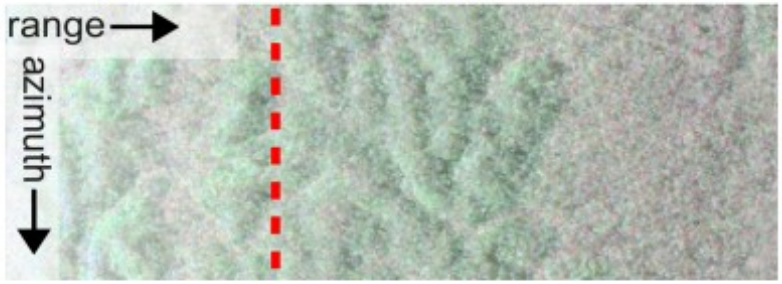

- Estimated profiles match LiDAR
- HH profiles : similar to FP case

LiDAR — TomSAR —

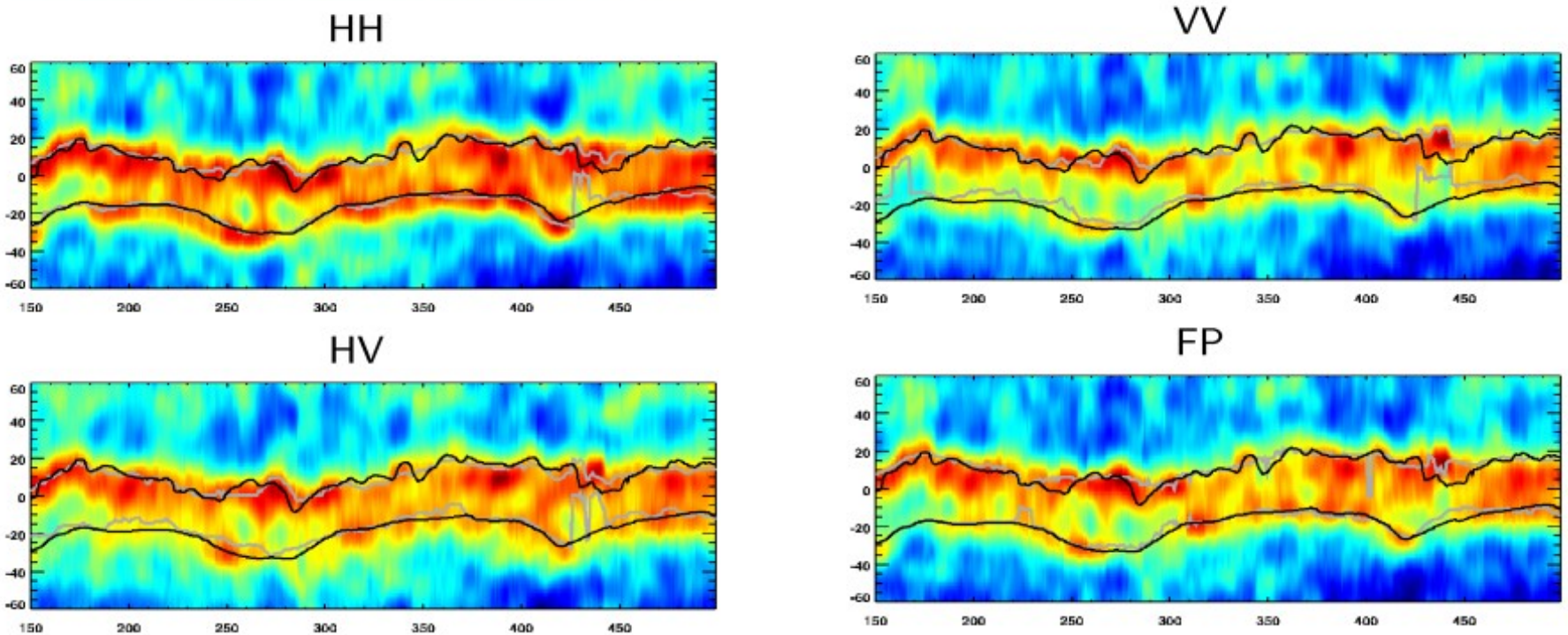

Tropical forest characterization

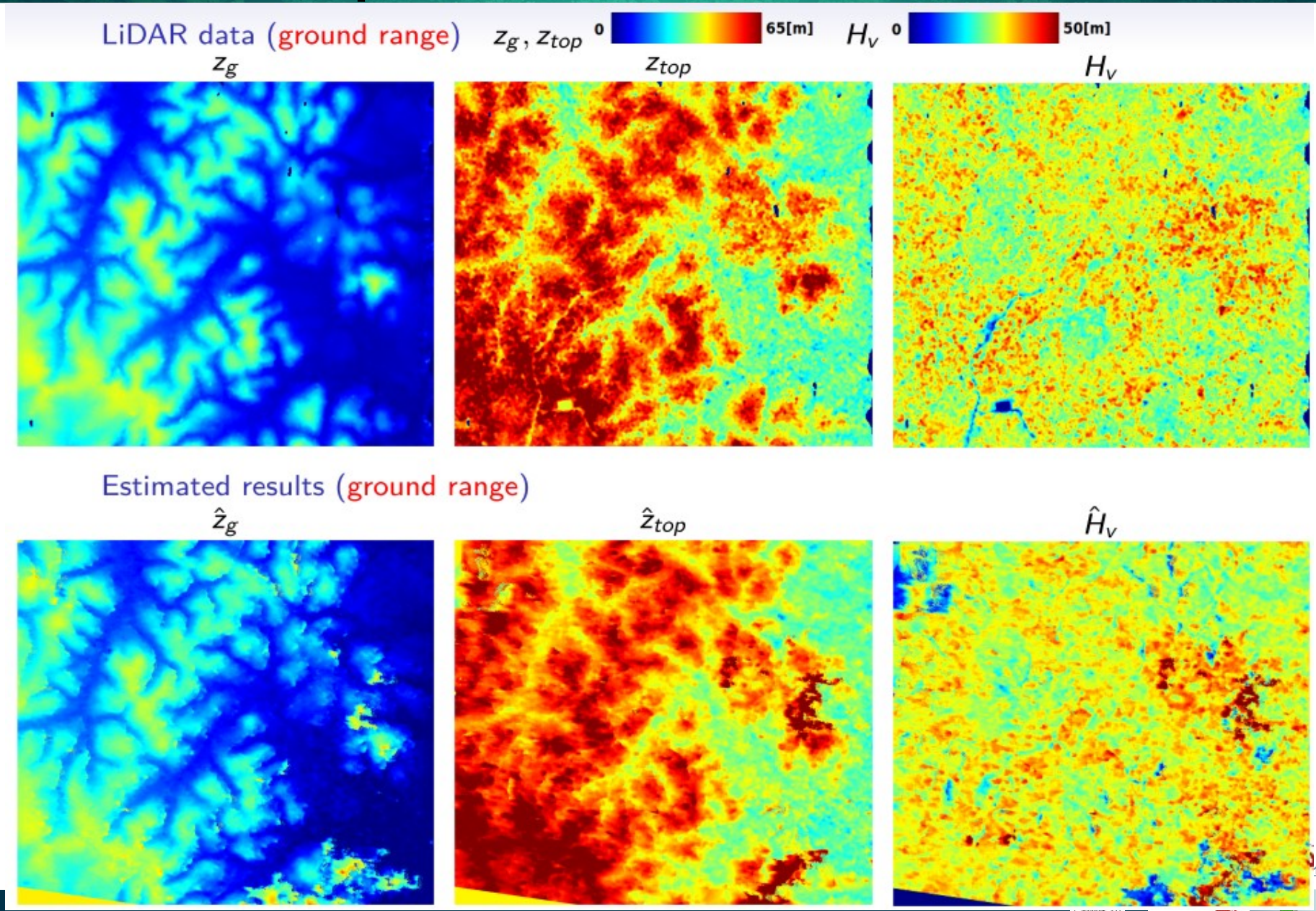

Tropical forest characterization

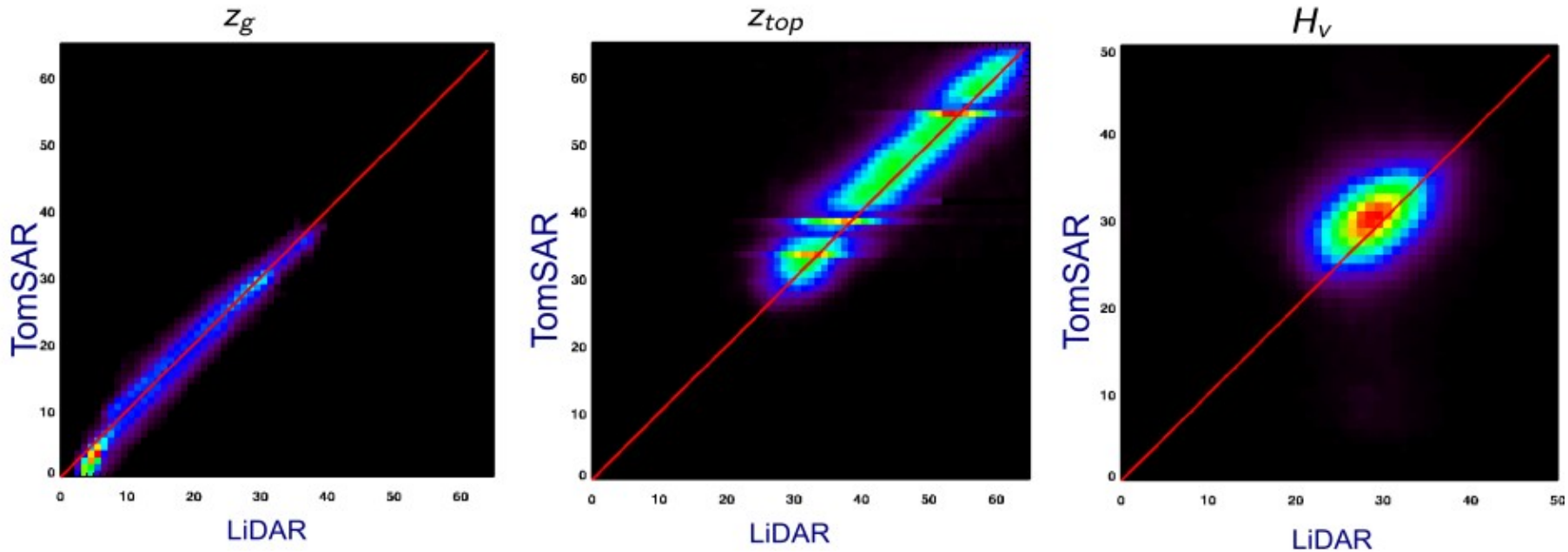

TomSAR-LiDAR [m]	Mean	Std
Δz_g	0.005	4.6
Δz_{top}	1.6	7.4
ΔH_v	0.9	7.7

Analysis of natural volumes using Polarimetric SAR tomography

Full-Rank specan techniques and SKP algebraic decomposition

Need for full-rank Polarimetric SAR Tomography

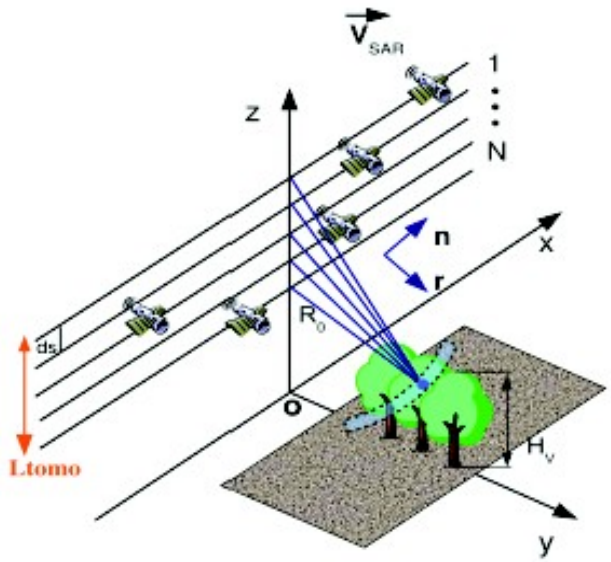

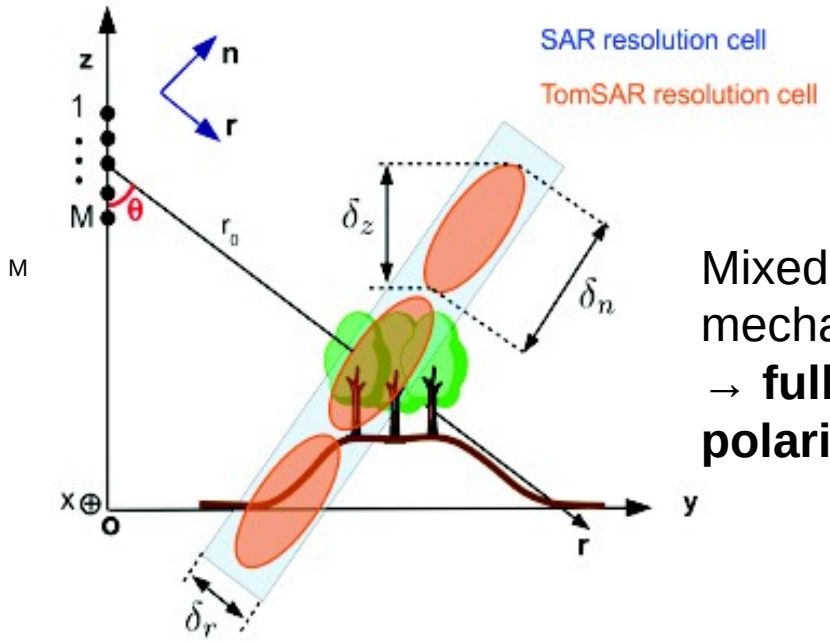

Mixed scattering mechanisms → **full rank polarimetry**

Intensity
σ(x,r)

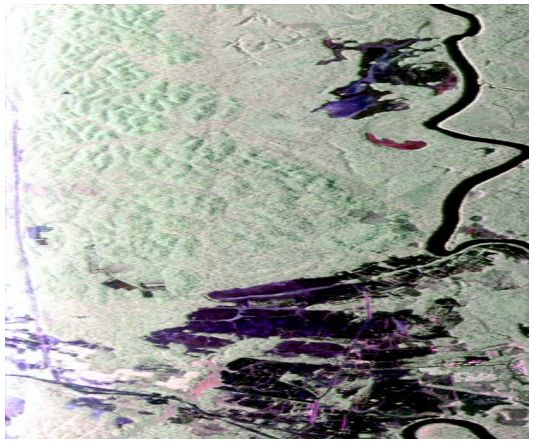

Rank 1 polarimetry (Pauli)
k(x,r)

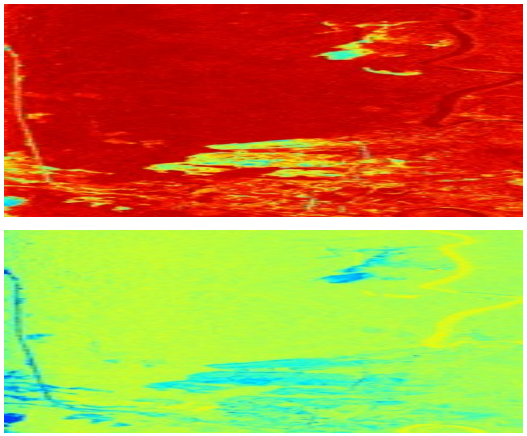

H

α

Full rank polarimetry
T(x,r)

Need for full-rank Polarimetric SAR Tomography

Multibaseline polarimetric SAR tomography

MB SAR Tomography

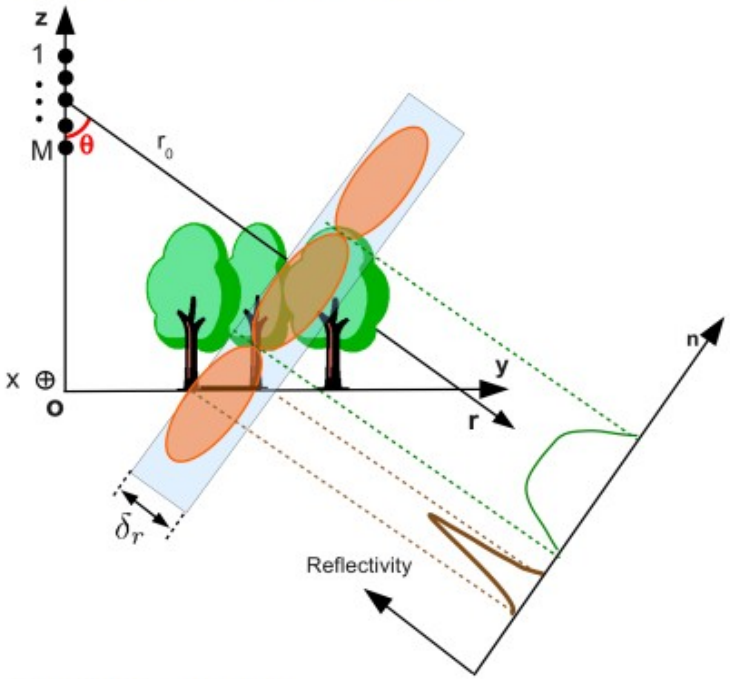

TomoSAR : reflectivity

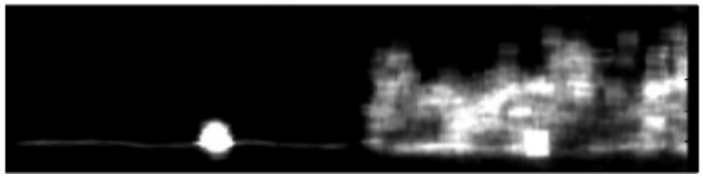

Polarimetric MB SAR Tomography

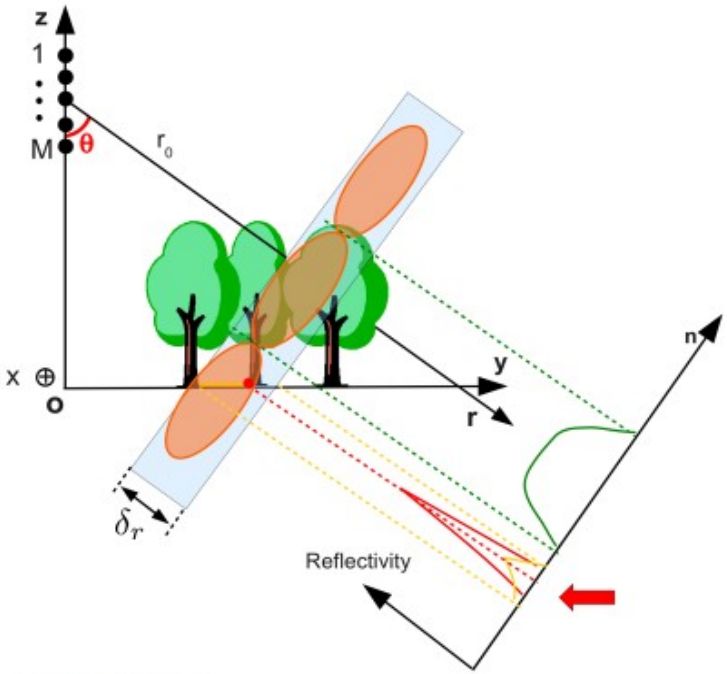

PolTomSAR: α

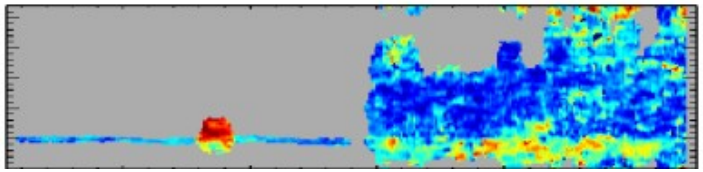

M PolSAR images

$$\mathbf{y}_{PS} = \begin{bmatrix} \mathbf{y}_1 \\ \mathbf{y}_2 \\ \mathbf{y}_3 \end{bmatrix} \in \mathbb{C}^{3M}$$

$$\mathbf{R}_{PS} = \begin{bmatrix} \mathbf{R}_{11} & \mathbf{R}_{12} & \mathbf{R}_{13} \\ & \mathbf{R}_{22} & \mathbf{R}_{23} \\ & & \mathbf{R}_{33} \end{bmatrix}$$

$\gamma_{ij}(w_1, w_k)$

$\gamma_{ij}(w_2, w_k)$

$\gamma_{ij}(w_3, w_k)$

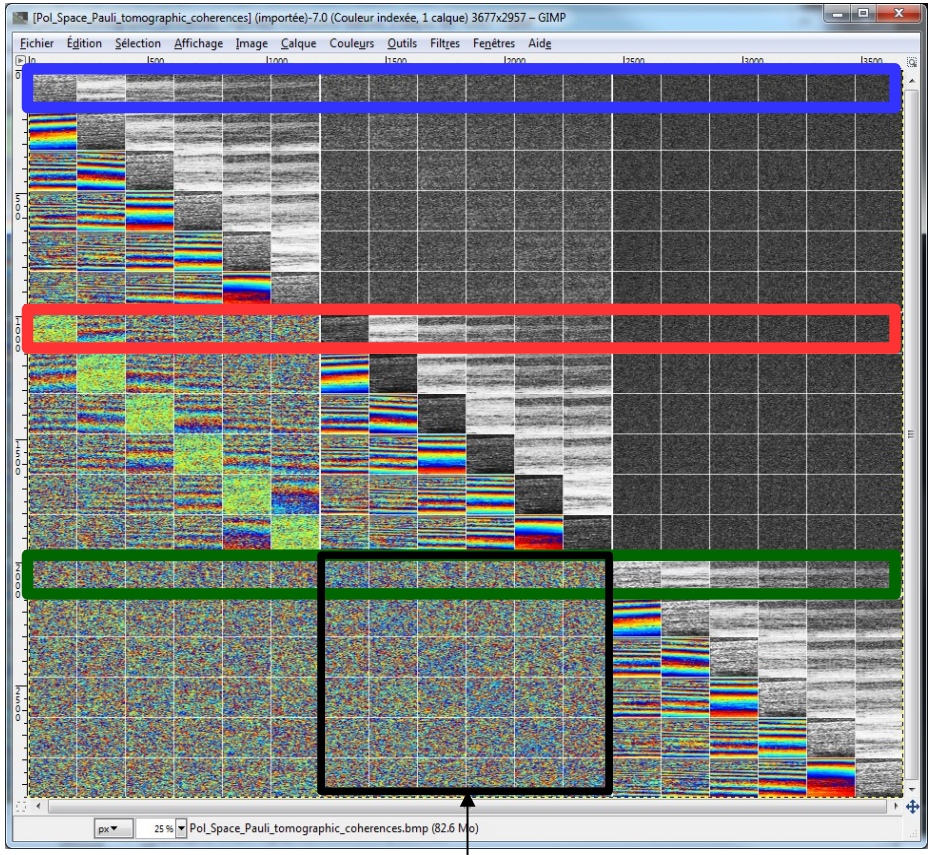

$\mathbf{R}_{ij} \in \mathbb{C}^{M \times M}$

Full rank analysis strategies

- Full-rank P-Capon (LFF et al. 2012)

$$\mathbf{R}_{PS} \longrightarrow \sigma(z)\mathbf{T}(z)$$

- SKP decomposition (Tebaldini 2009)

$$\mathbf{R}_{PS} = \sum_i \mathbf{T}_{P_i} \otimes \mathbf{R}_{S_i} \longrightarrow \sum_i \sigma_i(z)\mathbf{T}_{P_i}$$

Pol ch. 1 $\gamma_{ij}(w_1, w_k)$

Pol ch. 2 $\gamma_{ij}(w_2, w_k)$

Pol ch. 3 $\gamma_{ij}(w_3, w_k)$

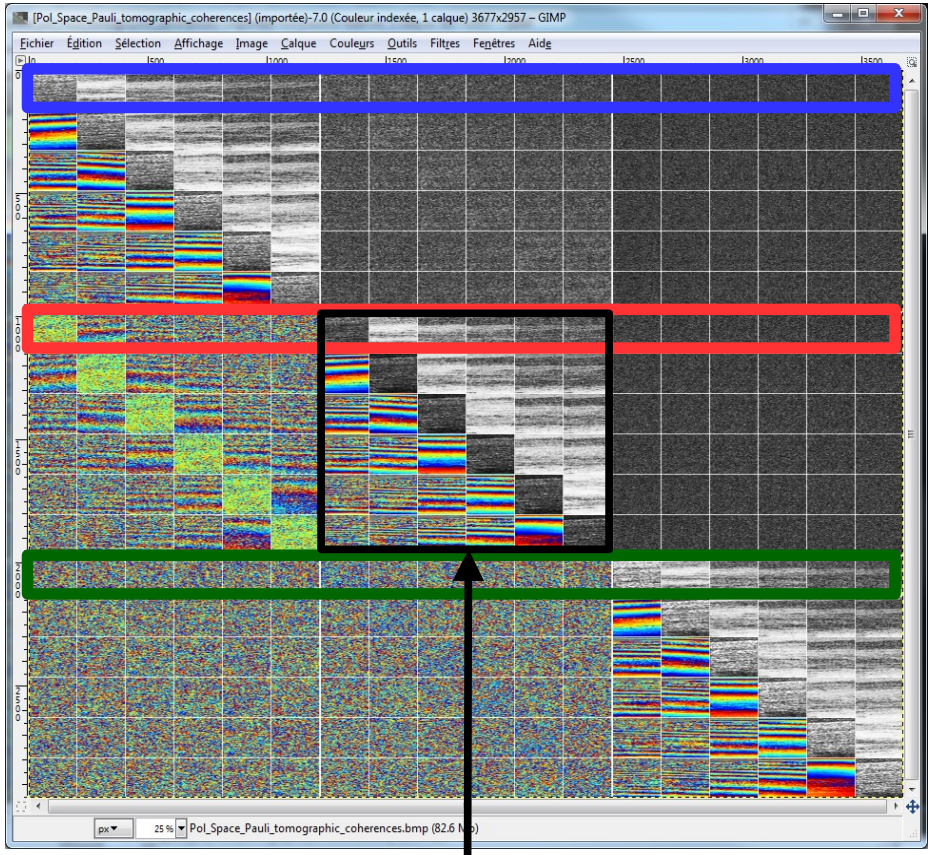

$\mathbf{R}_{ij} \in \mathbb{C}^{M \times M}$

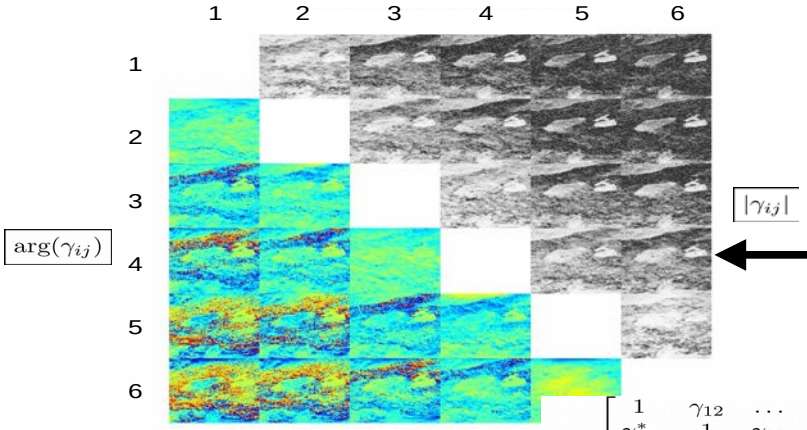

$$\widetilde{\mathbf{R}} = \begin{bmatrix} 1 & \gamma_{12} & \cdots & & \gamma_{1M} \\ \gamma_{12}^* & 1 & \gamma_{23} & \cdots & \gamma_{2M} \\ & & \ddots & & \\ \gamma_{1M}^* & & & & 1 \end{bmatrix}$$

Combined spatial & polarimetric correlations

Single-pol or rank-one polarimetric CAPON

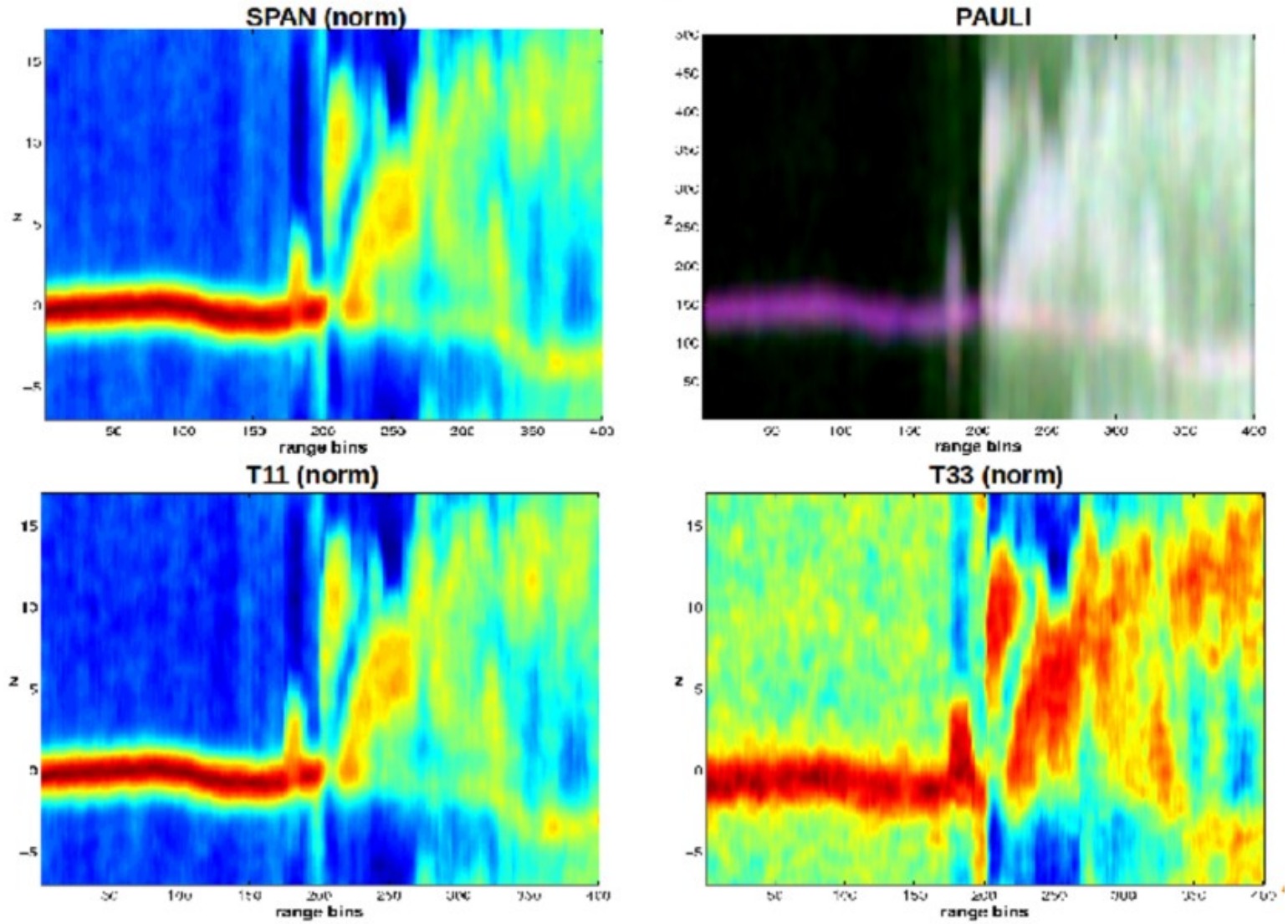

Full-Rank Polarimetric CAPON

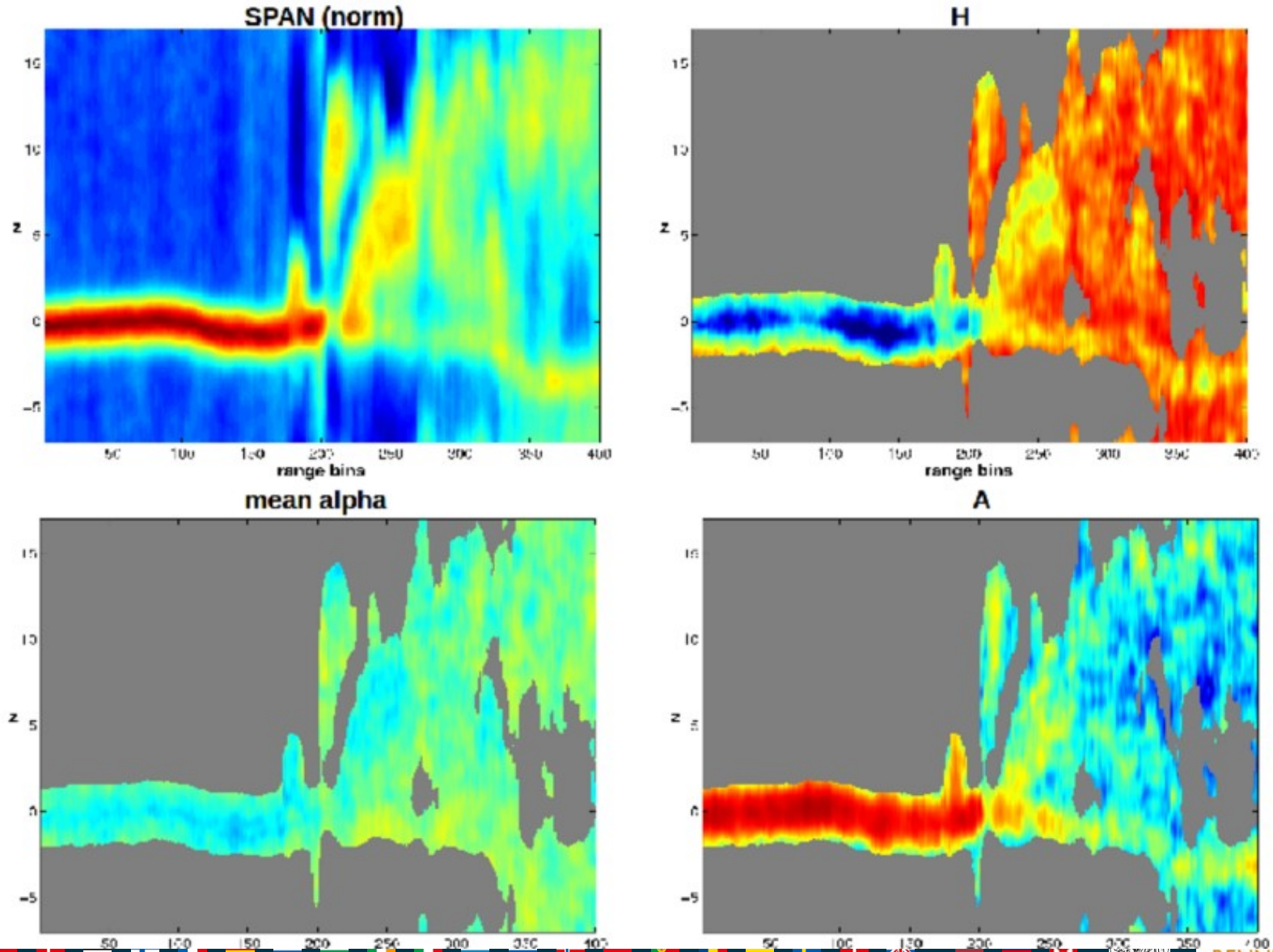

FR-P-CAPON over the Dornstetten temperate forest at L band

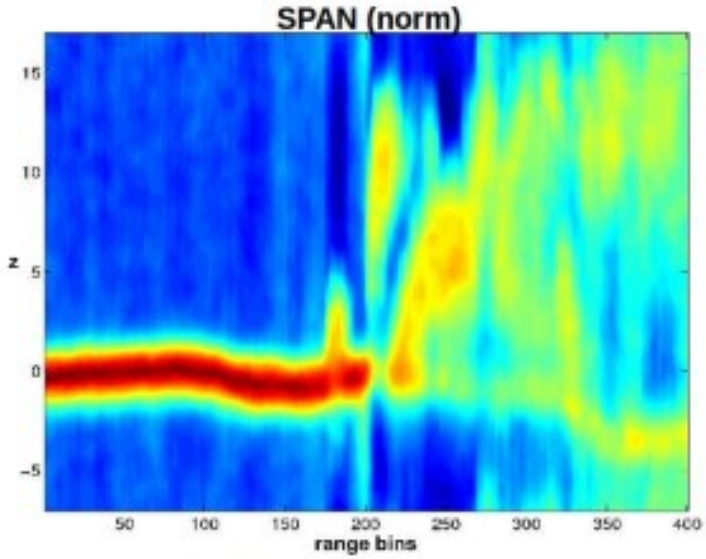

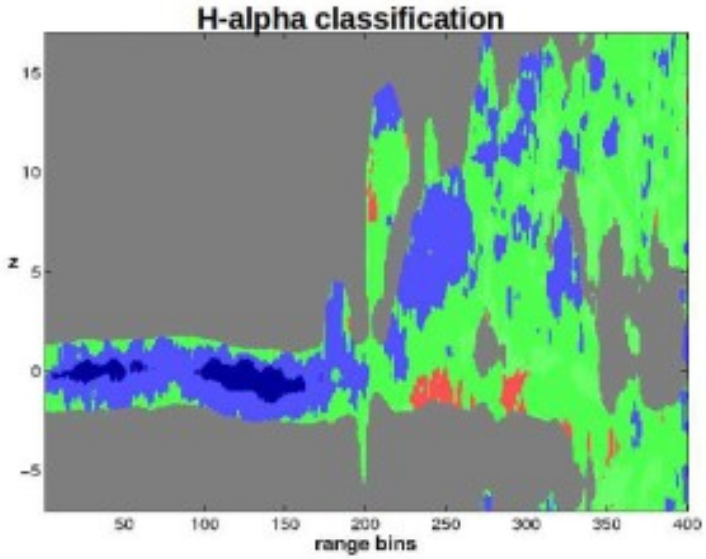

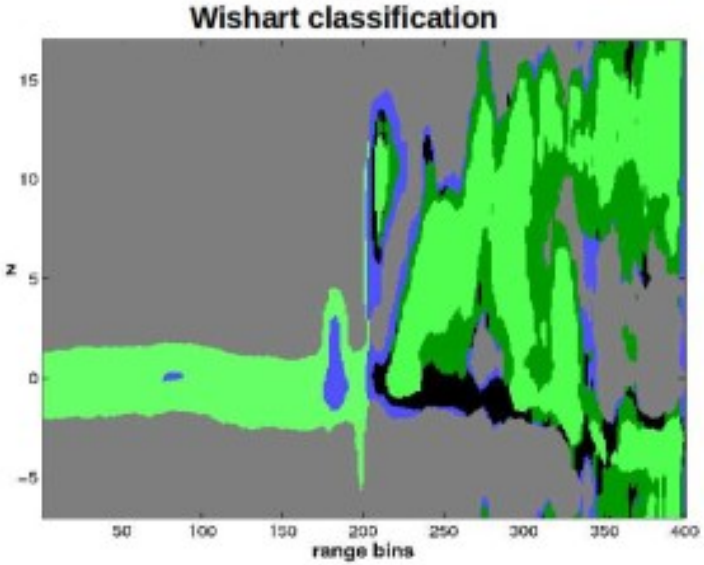

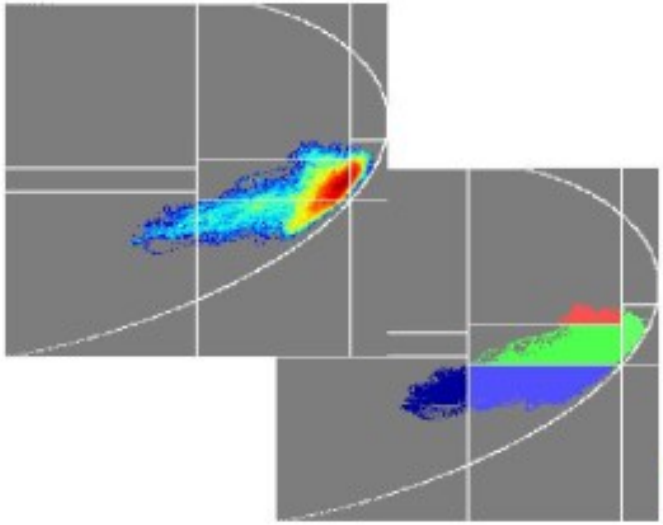

FR-P-CAPON over the Dornstetten temperate forest at L band

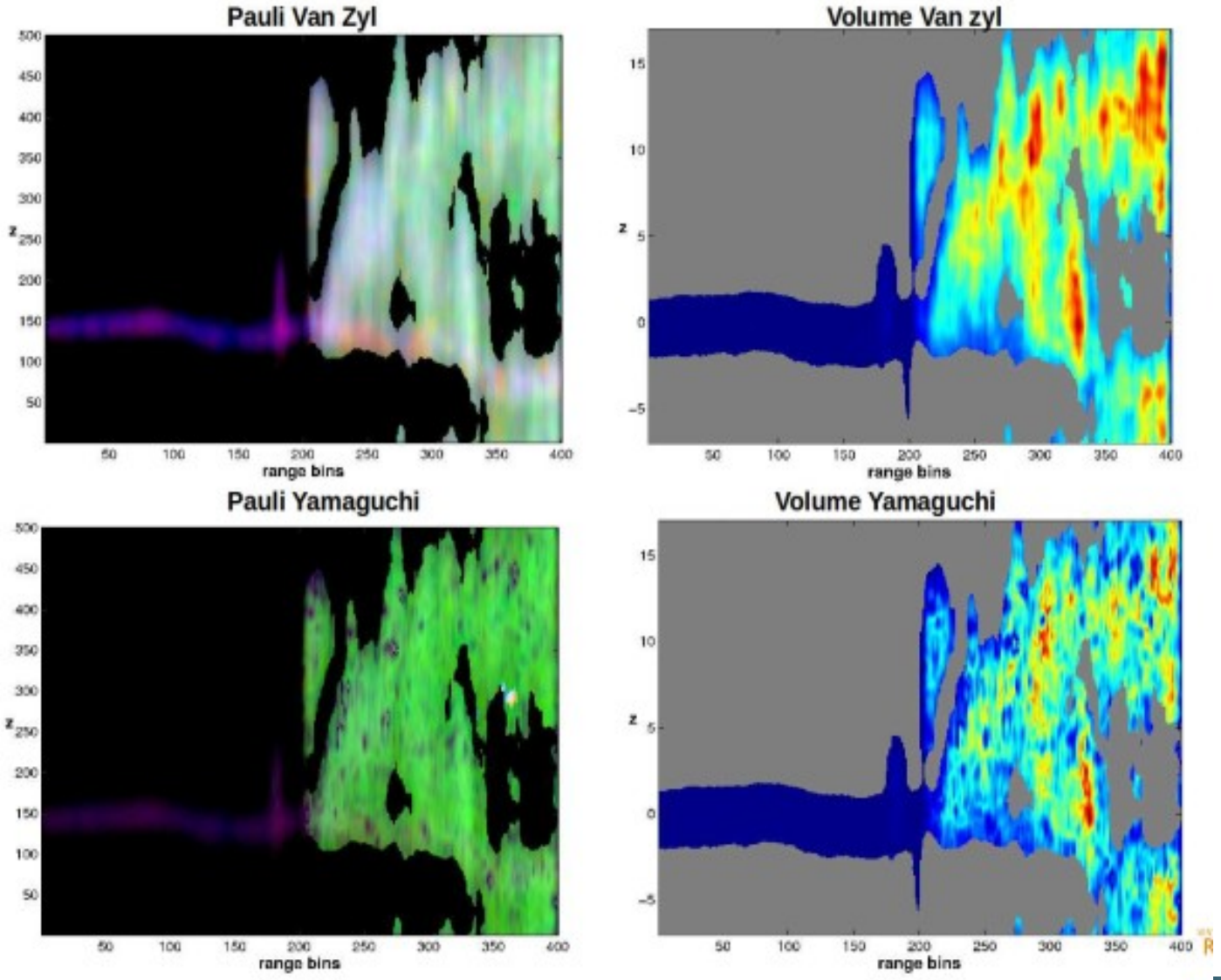

Under foliage vehicle detection using FR-P-CAPON and POLSAR techniques

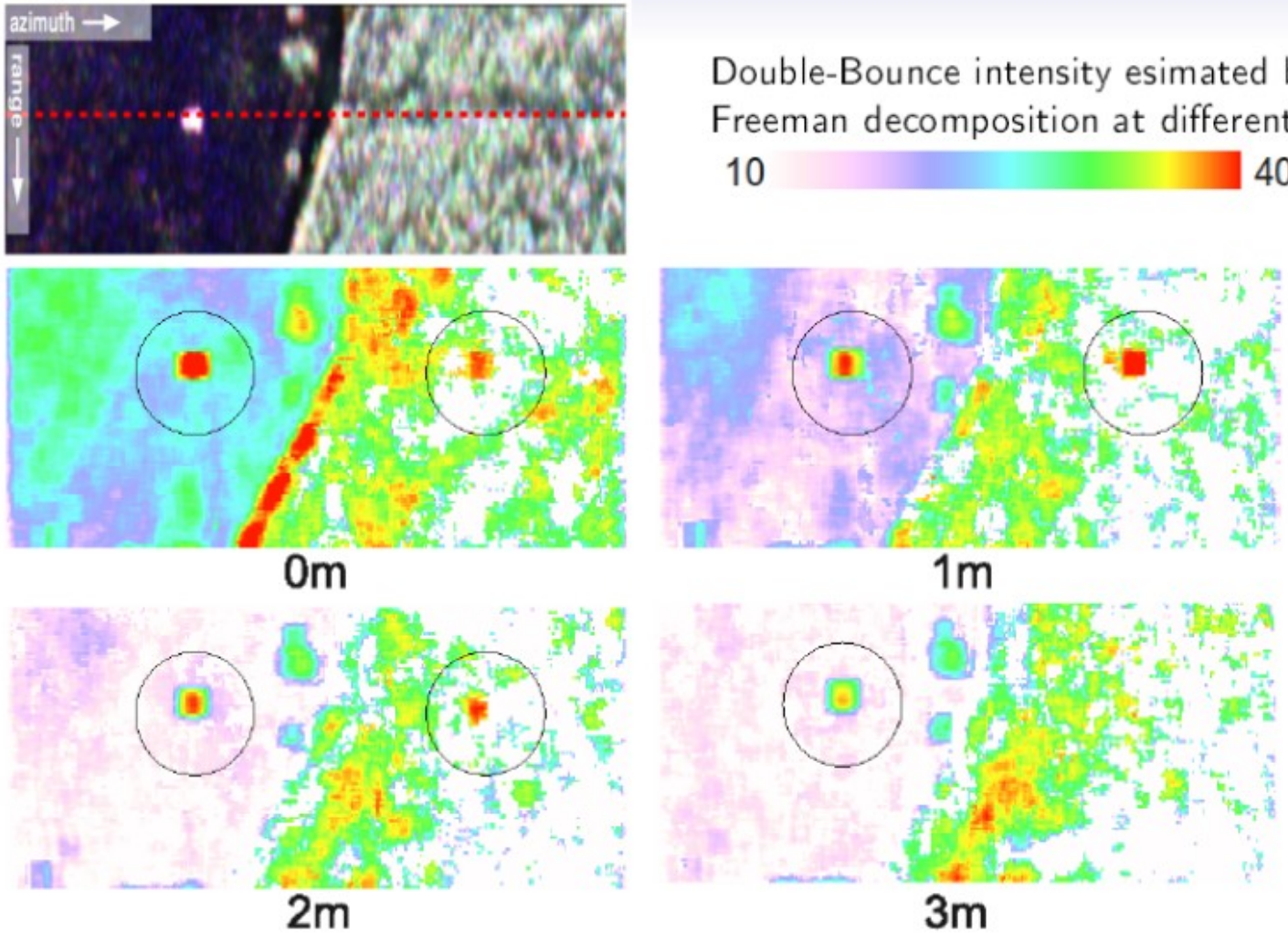

3-D SAR imaging using PolTomSAR

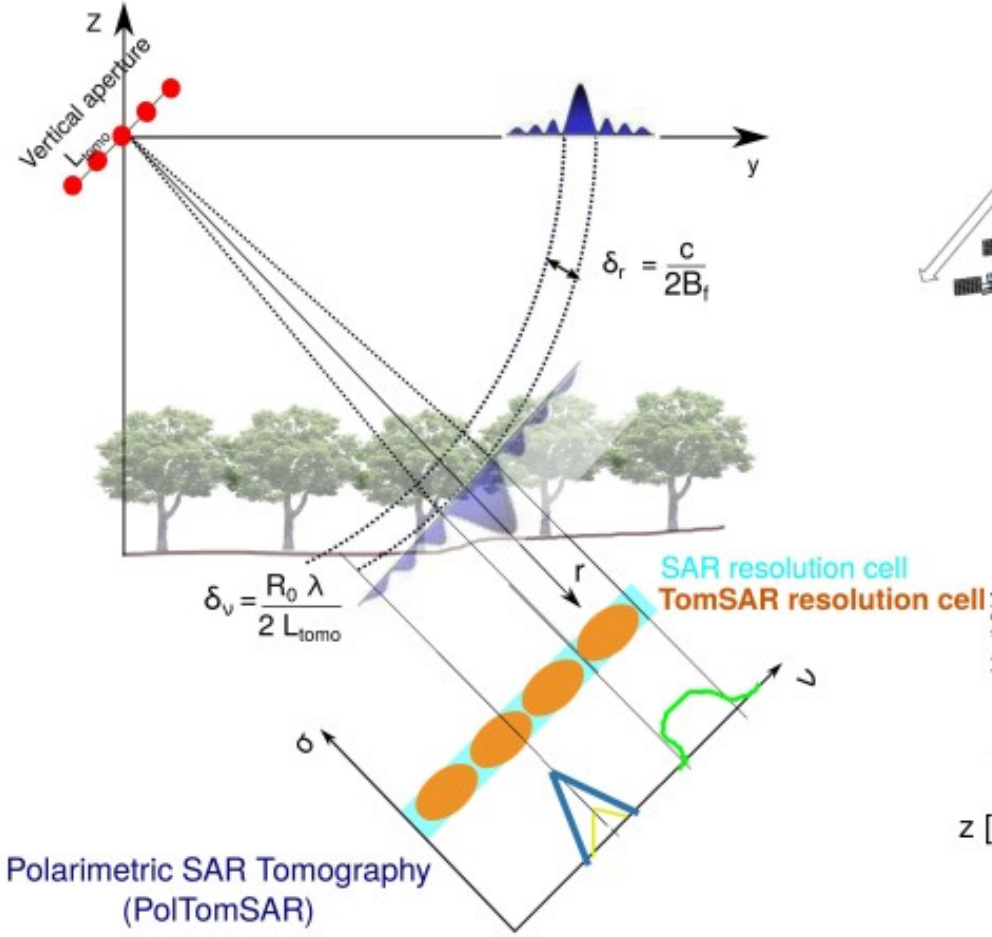

Polarimetric SAR Tomography
(PolTomSAR)

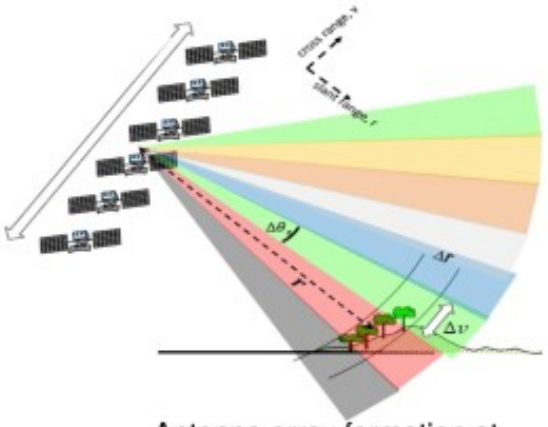

Antenna array formation at
each (x,r) position

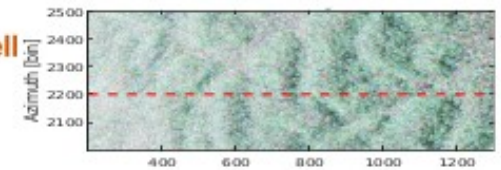

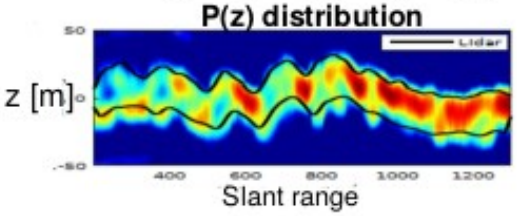

RVoG characterization using PolinSAR

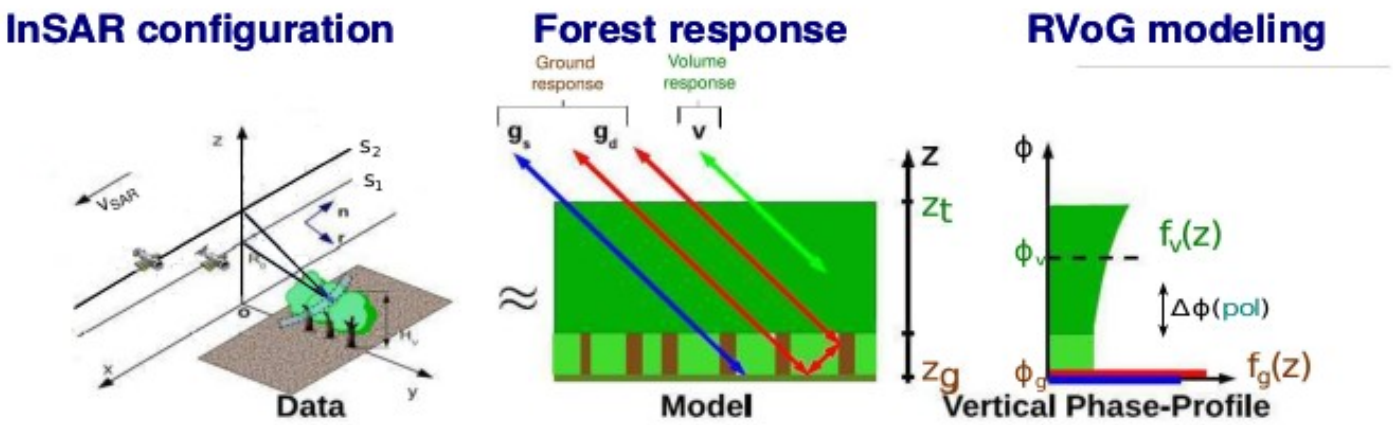

- Vertical structure: $f(z) = f_g(z) + f_v(z)$
- Coherence: $\gamma = \frac{\int f(z) e^{jk_{z12} z} dz}{\int f(z) dz} = L\gamma_v + (1 - L)\gamma_g$

  Volume-Contribution-Ratio (VCR): $L = \frac{I_v}{I_v + I_g}$

γ_v, γ_g, L estimation $\rightarrow$ PolInSAR: $\gamma(\text{pol}) = L(\text{pol})\gamma_v + (1 - L(\text{pol}))\gamma_g$

Using Multi-Baseline inSAR: TomSAR

TomSAR configuration | **Forest response** | **RVoG modeling**

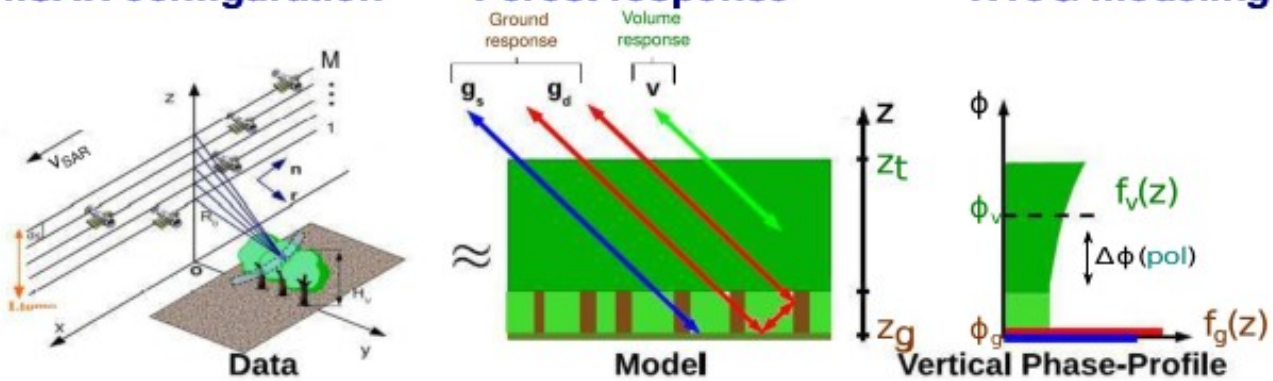

Spatial baseline diversity: $M(M-1)/2$ coherences

$$\gamma_{12} = \frac{\int f(z) e^{jk_z z_{12} z} dz}{I}$$

$$\vdots$$

$$\gamma_{1M} = \frac{\int f(z) e^{jk_z z_{1M} z} dz}{I} \longrightarrow \hat{f}(z)$$

$$\vdots$$

$$\gamma_{(M-1)M} = \frac{\int f(z) e^{jk_z (M-1)M z} dz}{I}$$

Polarimetric diversity
required for separating
$f_g(z)/f_v(z)$

Using PolTomSAR

TomSAR configuration | **Forest response** | **RVoG modeling**

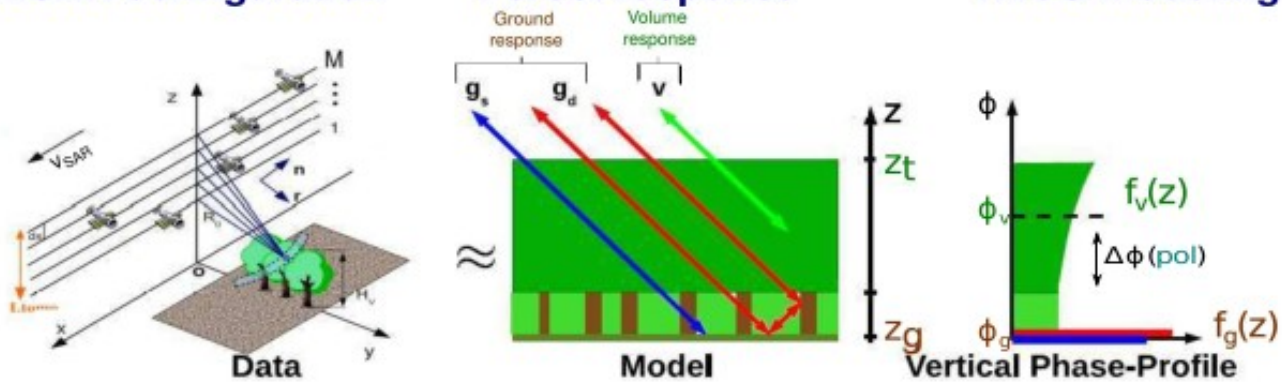

$$\begin{bmatrix} \gamma_{12}(\text{pol}) \\ \vdots \\ \gamma_{1M}(\text{pol}) \\ \vdots \\ \gamma_{(M-1)M}(\text{pol}) \end{bmatrix} = L(\text{pol}) \begin{bmatrix} \gamma_{v_{12}} \\ \vdots \\ \gamma_{v_{1M}} \\ \vdots \\ \gamma_{v_{(M-1)M}} \end{bmatrix} + (1 - L(\text{pol})) \begin{bmatrix} \gamma_{g_{12}} \\ \vdots \\ \gamma_{g_{1M}} \\ \vdots \\ \gamma_{g_{(M-1)M}} \end{bmatrix}$$

PolTomSAR covariance matrix

$$\gamma_{ij}(\text{pol}_{1,2,3}) \longrightarrow \boxed{\mathbf{R}_{P-S} = \mathbf{C}_g \otimes \mathbf{R}_g + \mathbf{C}_v \otimes \mathbf{R}_v} \in \mathbb{C}^{3M \times 3M}$$

SKP2-decomposition

Ground-volume decomposition implies:

- Separation of Structural Properties

=> Separated Tomographic Imaging of Ground-only and Volume-only Contributions

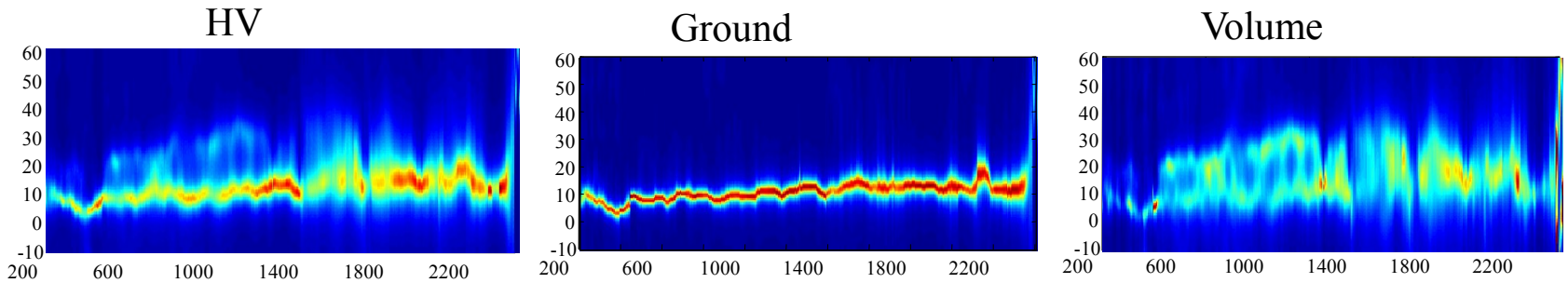

- Separation of Polarimetric Properties

=> Evaluation of the Ground to Volume Backscattered Power Ratio for each polarization

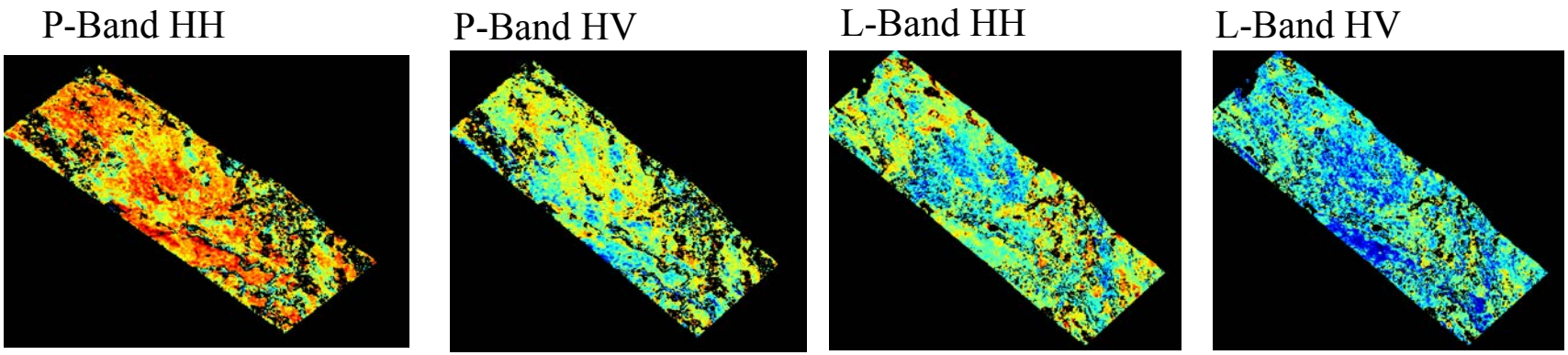

SKP Decomposition

General procedure for ground and volume decomposition

Approximate W by retaining the first two KPs of the SKP Decomposition

Choose the proper values of *a*, *b* :

1. **Select values of *a*, *b* that give rise to (semi) positive definite R_g, R_v, C_g, C_v**

   → physical validity of the solution

2. **Optimize some criterion in order to pick a unique solution**

Region of physical validity for the ground and volume coherences in the interferometric pair formed between tracks 1 and 2 (Numerical simulation)

Coherence Locus – N = 2

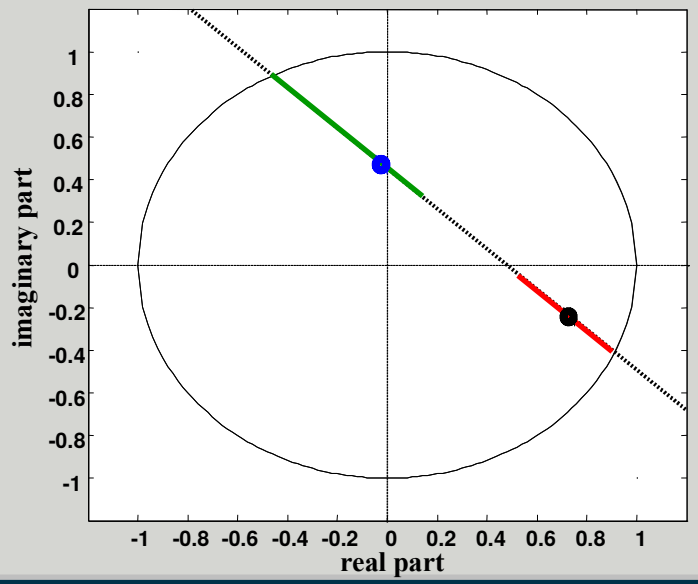

Single Baseline case :

The region of physical validity is formed by two branches, spanned by the parameters *a, b*

The union of branches *a, b* results in the same region of physical validity as in PolInSAR

Physically valid solutions

Branch a

Branch b

True Volume Coherence

True Ground Coherence

SKP Decomposition

General procedure for ground and volume decomposition

Approximate W by retaining the first two KPs of the SKP Decomposition

Choose the proper values of *a*, *b* :

1. **Select values of *a*, *b* that give rise to (semi) positive definite R_g, R_v, C_g, C_v**

   🔔 **physical validity of the solution**

2. **Optimize some criterion in order to pick a unique solution**

Region of physical validity for the ground and volume coherences in the interferometric pair formed between tracks 1 and 2 (Numerical simulation)

Coherence Locus – N = 3

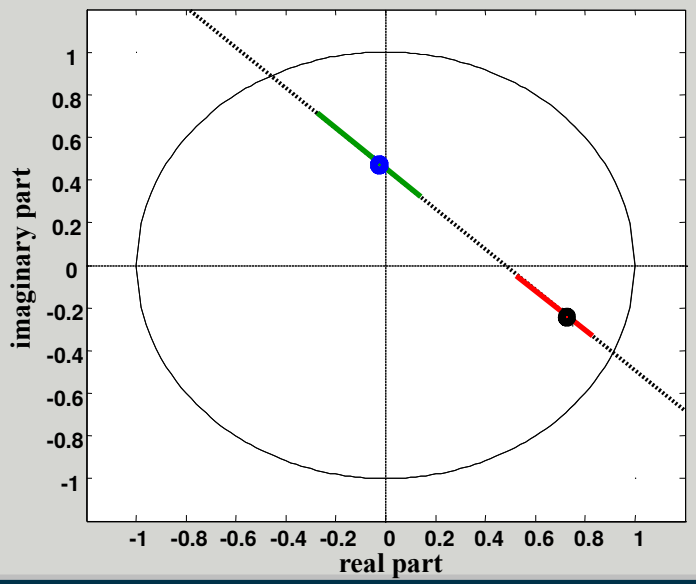

Multi-Baseline case : the region of physical validity tends to *shrink*, depending on the number of available tracks

Physically valid solutions

Branch a

Branch b

True Volume Coherence

True Ground Coherence

SKP Decomposition

General procedure for ground and volume decomposition

Approximate W by retaining the first two KPs of the SKP Decomposition

Choose the proper values of *a*, *b* :

1. **Select values of *a*, *b* that give rise to (semi) positive definite R_g, R_v, C_g, C_v**

   → physical validity of the solution

2. **Optimize some criterion in order to pick a unique solution**

Region of physical validity for the ground and volume coherences in the interferometric pair formed between tracks 1 and 2 (Numerical simulation)

Coherence Locus – N = 10

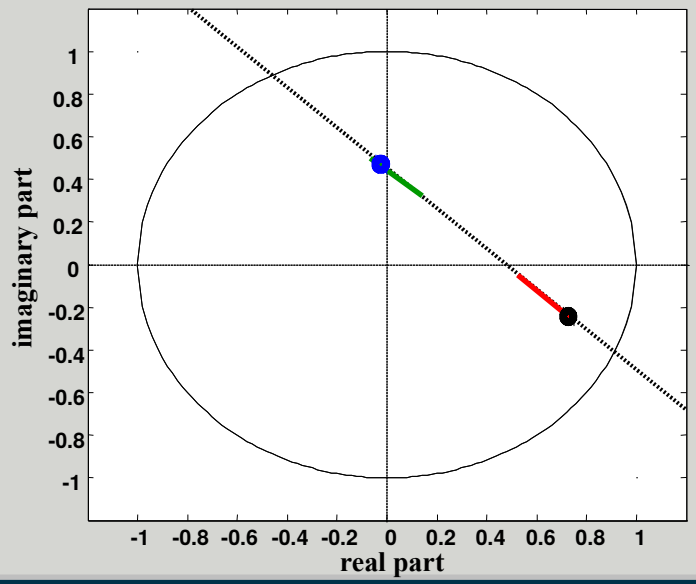

Multi-Baseline case : the region of physical validity tends to *shrink*, depending on the number of available tracks

- **The higher the number of tracks, the easier it is to pick the correct solution**

Physically valid solutions

Branch a

Branch b

True Volume Coherence

True Ground Coherence

Case Studies

Campaign	BioSAR 2007 - ESA
System	E-SAR - DLR
Period	Spring 2007
Site	Remningstorp, South Sweden
Scene	Semi-boreal forest
Topography	Flat
Tomographic tracks	9 – Fully Polarimetric
Carrier frequency	350 MHz
Slant range resolution	2 m
Azimuth resolution	1.6 m
Vertical resolution	10 m (near range) to 40 m (far range)

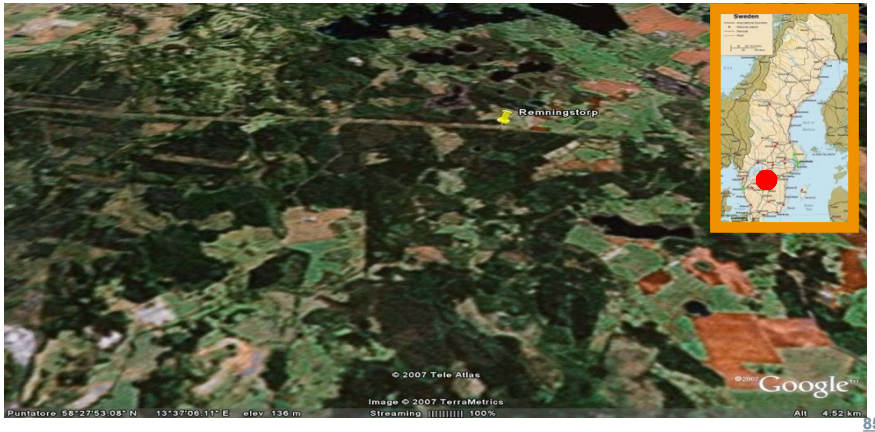

Case Studies

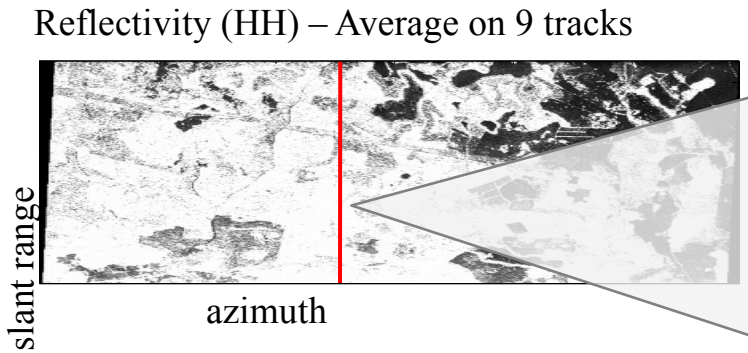

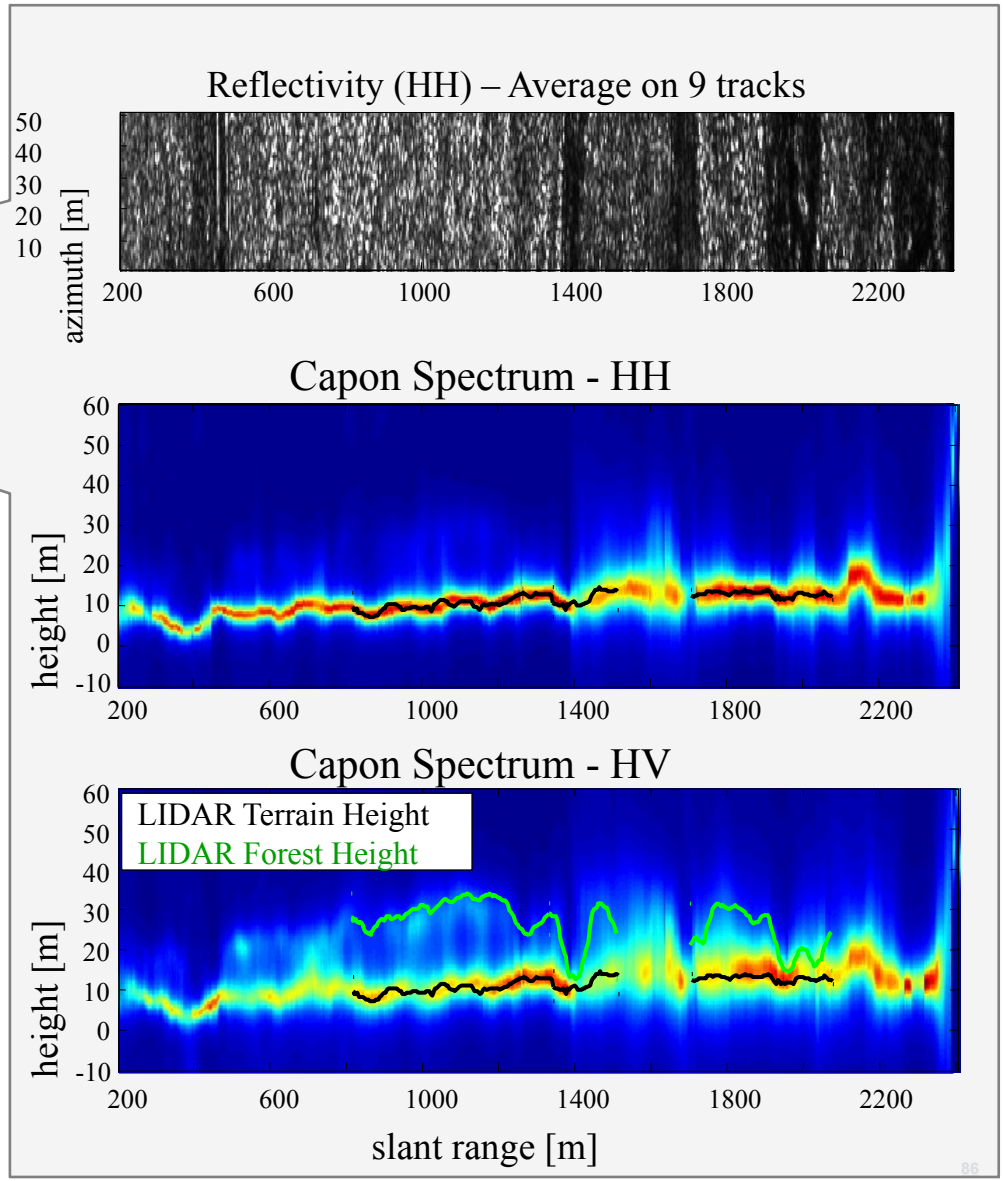

The analyzed profile is almost totally forested, except for the dark areas

HH:

Dominant phase center is ground locked
Vegetation is barely visible

Similar conclusions for VV

HV:

Dominant phase center is ground locked
Vegetation is much more visible

Case Studies

Model validation: $\mathbf{W} \overset{?}{=} \mathbf{C}_g \otimes \mathbf{R}_g + \mathbf{C}_v \otimes \mathbf{R}_v$

Methodology:

evaluation of the error between the sample covariance matrix and its best L2 approximation with $K = \{1,2,3,4\}$ KPs

$$\hat{\mathbf{W}}_K = \arg\min_{\mathbf{W}_k} \left\{ \left\| \hat{\mathbf{W}} - \mathbf{W}_K \right\|_F \right\}$$

$$error = \frac{\left\| \hat{\mathbf{W}} - \mathbf{W}_K \right\|_F}{\left\| \hat{\mathbf{W}} \right\|_F}$$

Remark: the best L2 approximation is obtained simply by taking the dominant K terms of the SKP decomposition

$$\left\| \hat{\mathbf{W}} - \hat{\mathbf{W}}_2 \right\|_F < 0.1 \cdot \left\| \hat{\mathbf{W}} \right\|_F$$

> 90 % of the information can be represented by the sum of just two KPs

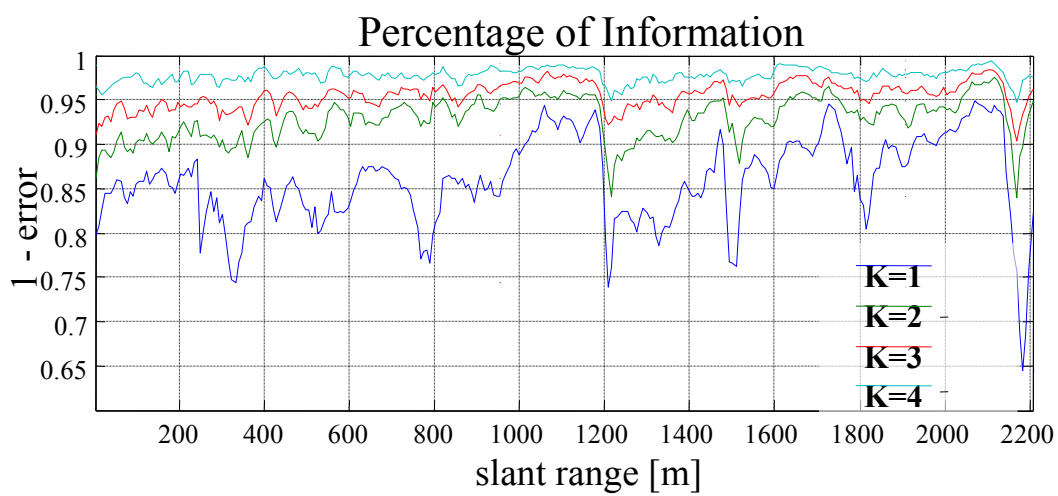

Inner boundary solutions

RPV

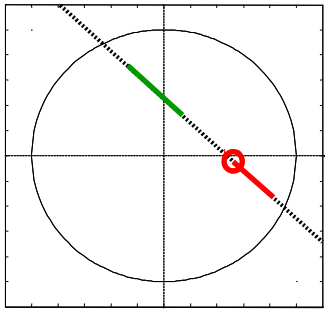

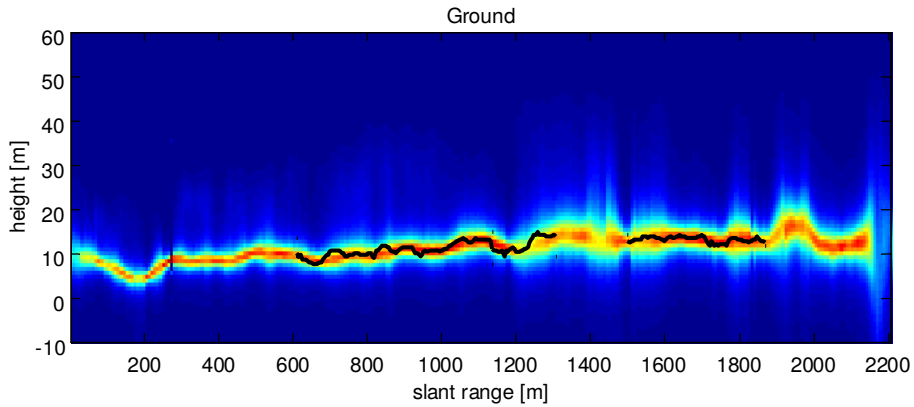

Residual volume contributions visible above the ground

Significant contributions from the ground level.
Volumetric scattering at the ground level
Consistent with:

- Backscattering from understorey or lower tree branches
- Multiple interactions of volumetric scatterers with the ground

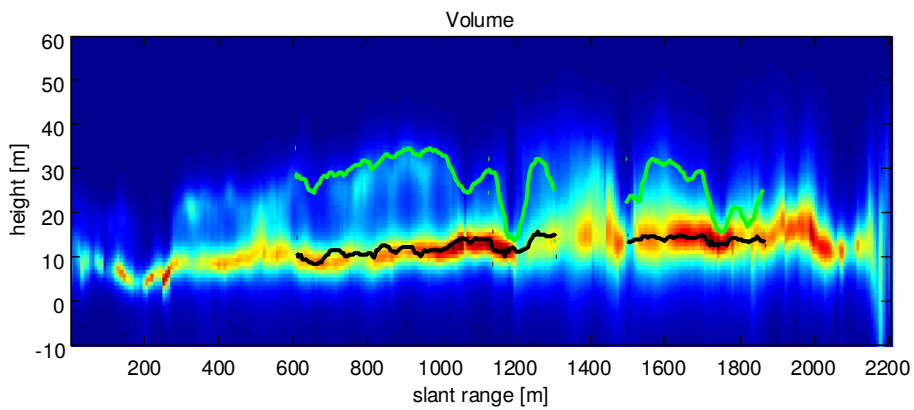

RPV

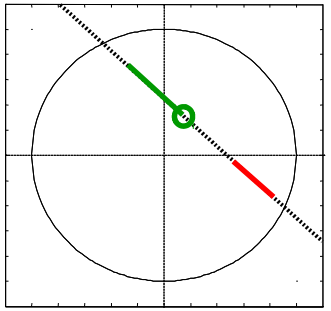

LIDAR Terrain Height
LIDAR Forest Height

RPV

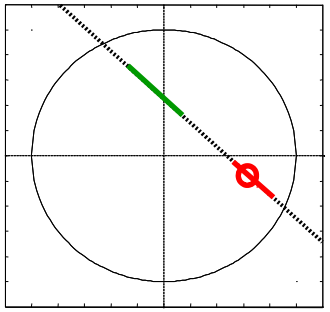

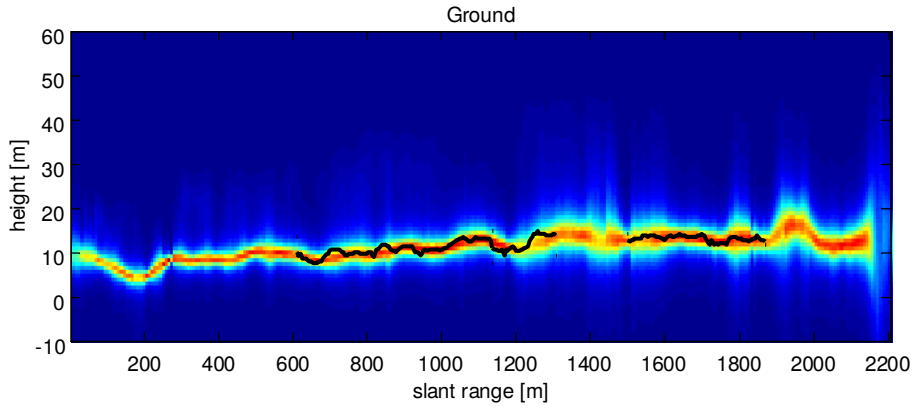

Improved volume rejection

Volumetric contributions from the ground level are partly rejected

Backscattering contributions from the whole volume structure are emphasized

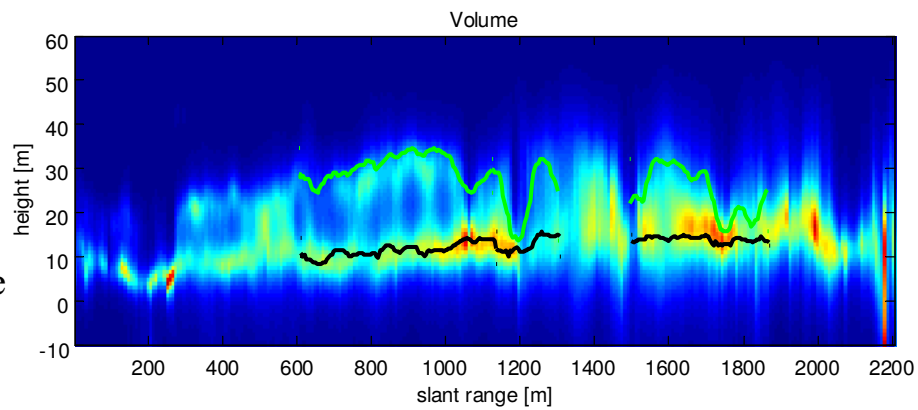

RPV

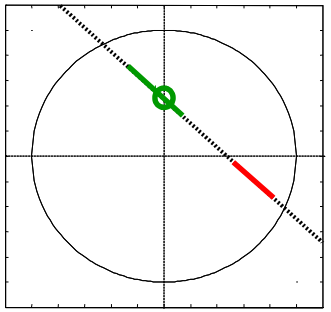

LIDAR Terrain Height
LIDAR Forest Height

RPV

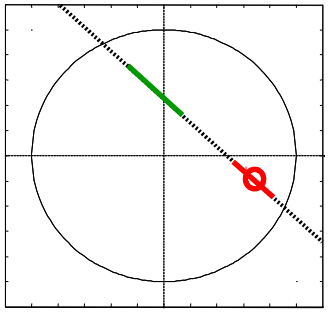

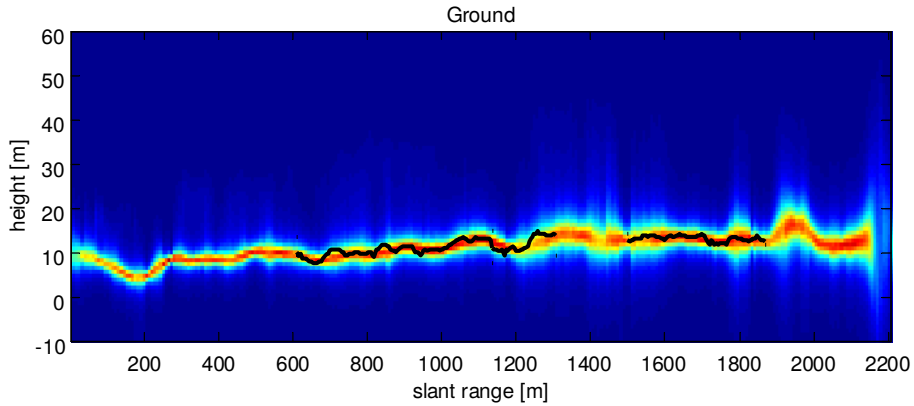

Improved volume rejection

Improved ground rejection

Backscattering contributions from the whole volume structure are emphasized

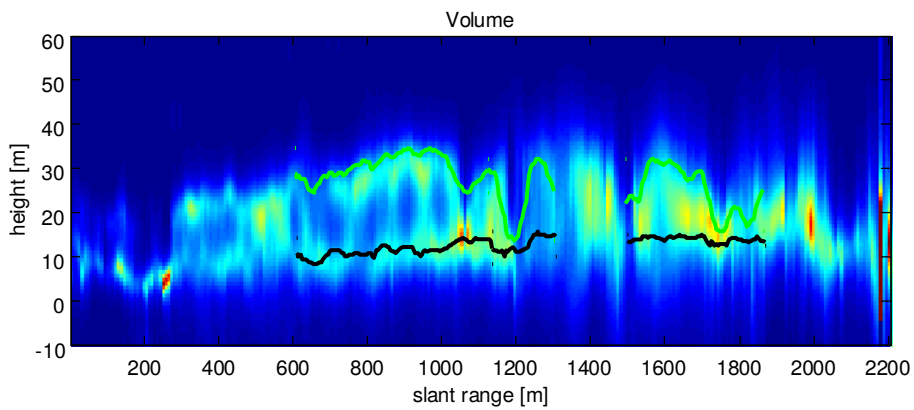

RPV

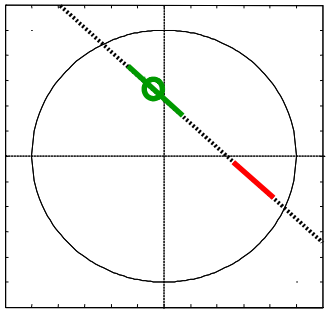

LIDAR Terrain Height
LIDAR Forest Height

Intermediate solutions

RPV

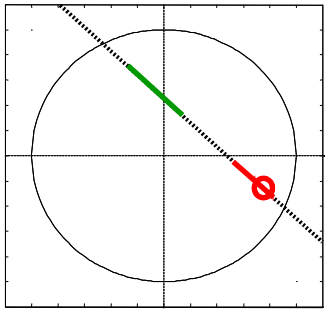

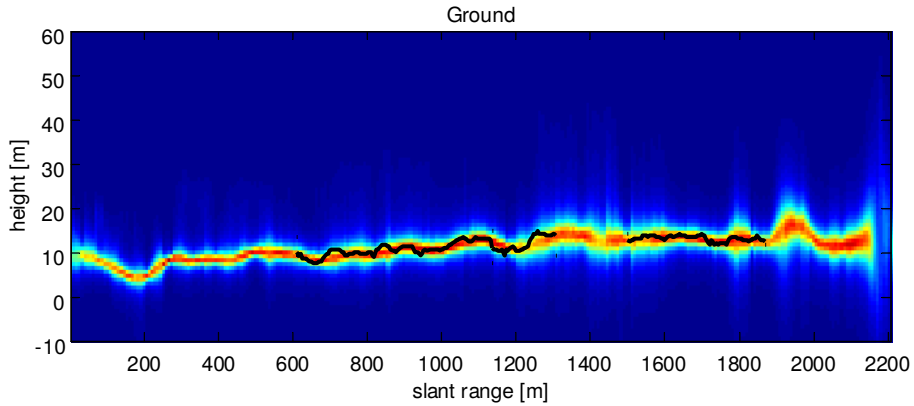

Improved volume rejection

Ground contributions rejected

Contributions from the lower canopy are partly rejected

Backscattering contributions from the upper volume structure are emphasized

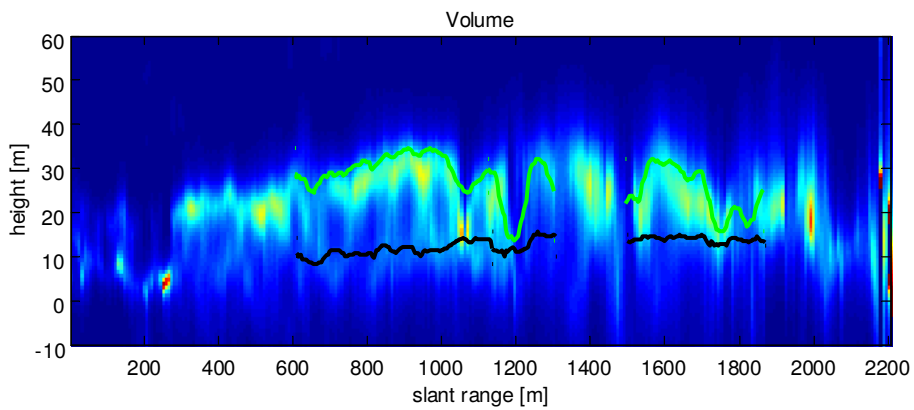

RPV

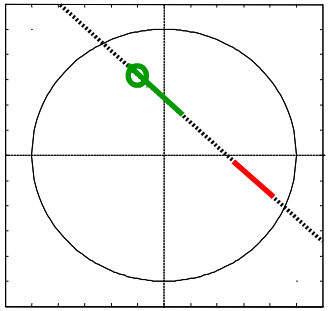

LIDAR Terrain Height
LIDAR Forest Height

Outer boundary solutions

RPV

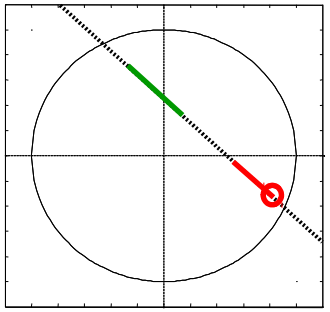

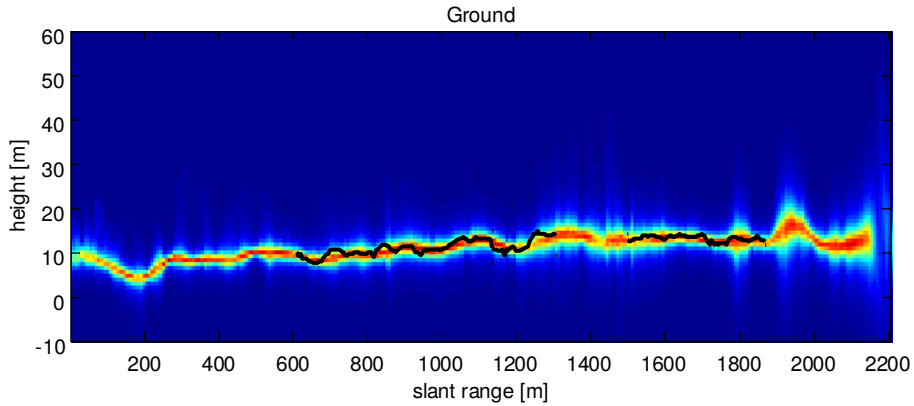

Maximum volume rejection

Ground structure is maximally coherent

Ground and lower canopy contributions are rejected

Only upper canopy contributions are visible

Volume structure is maximally coherent

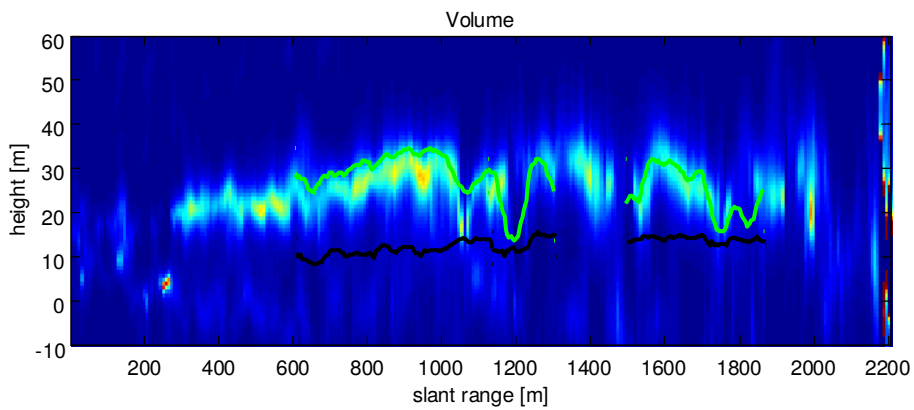

RPV

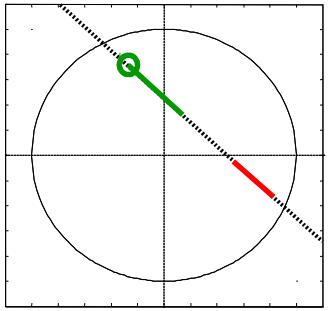

Volume top height is nearly invariant to the choice of the solution, therefore constituting a robust indicator of the volume structure

LIDAR Terrain Height
LIDAR Forest Height

Tropical forest biomass estimation at P band (TropiSAR campaign)

Biomass estimation procedure

Main processing principle: Ground/Volume separation

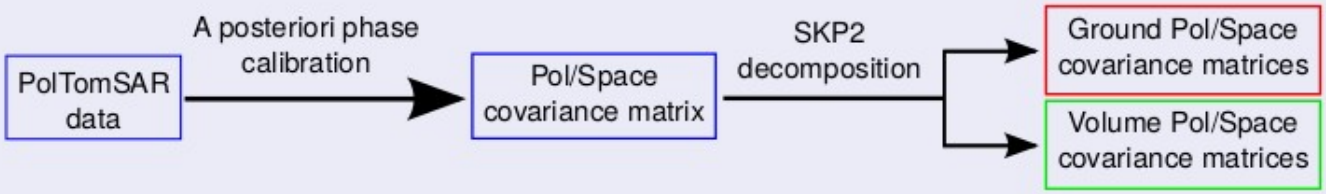

1- Ground/tree-top height estimation

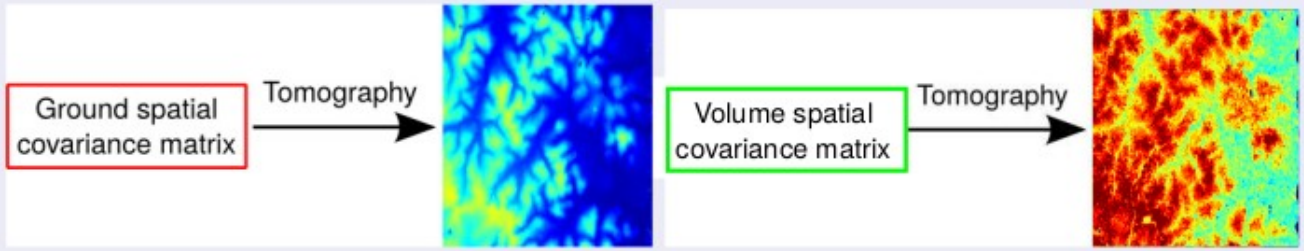

2- Refined Biomass estimation

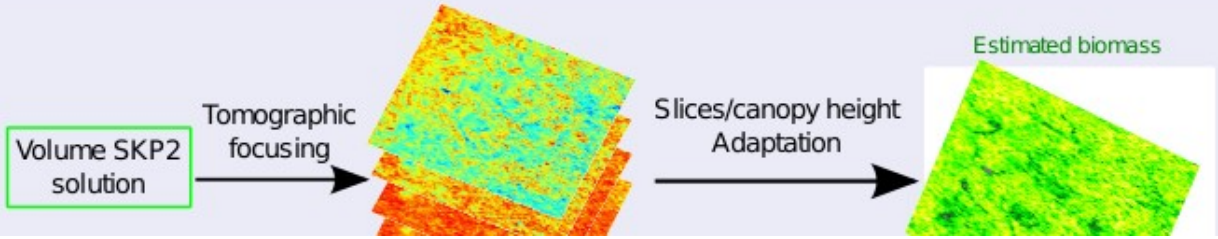

Forest vertical extent estimation procedure

Ground/volume separation

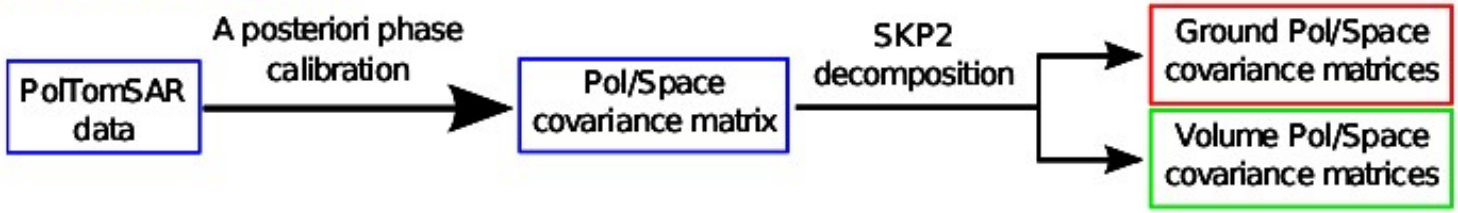

Ground topography estimation

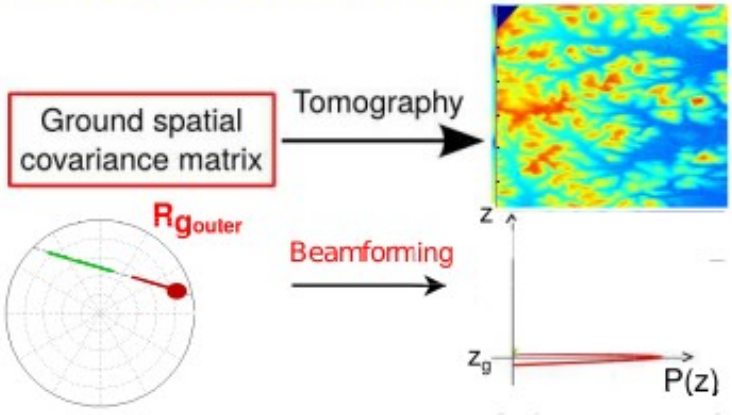

Tree top heigh estimation

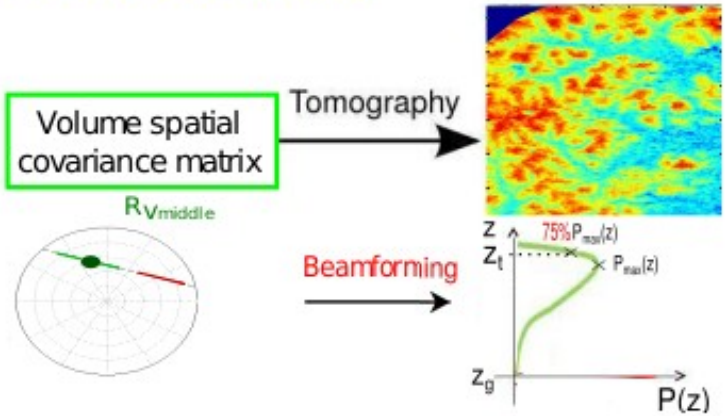

Vegetation height estimation

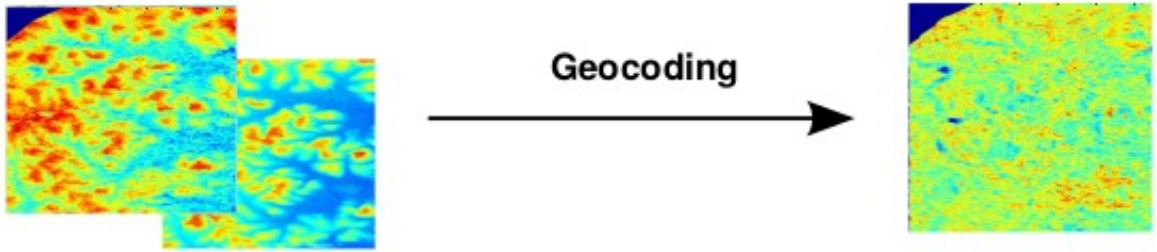

Performance over Paracou

Ground topography retrieval

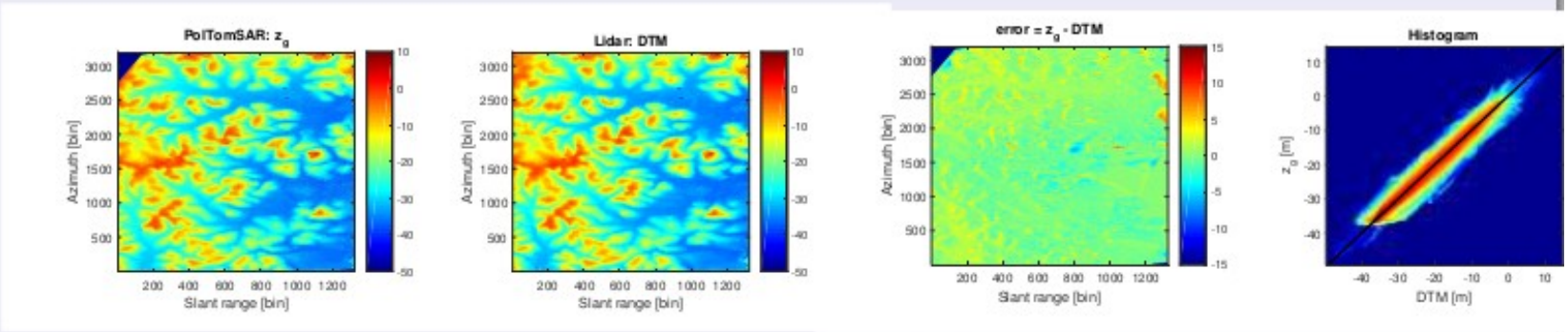

$$rmse = 2.3m \; ; \; r_p = 92\%$$

Canopy top height retrieval

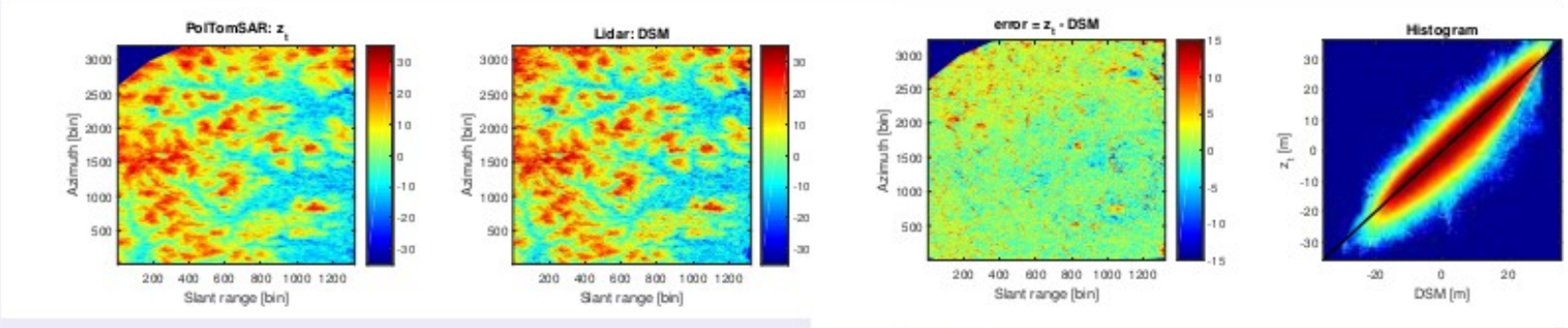

$$rmse = 4.1m \; ; \; r_p = 89\%$$

Performance of biomass estimators

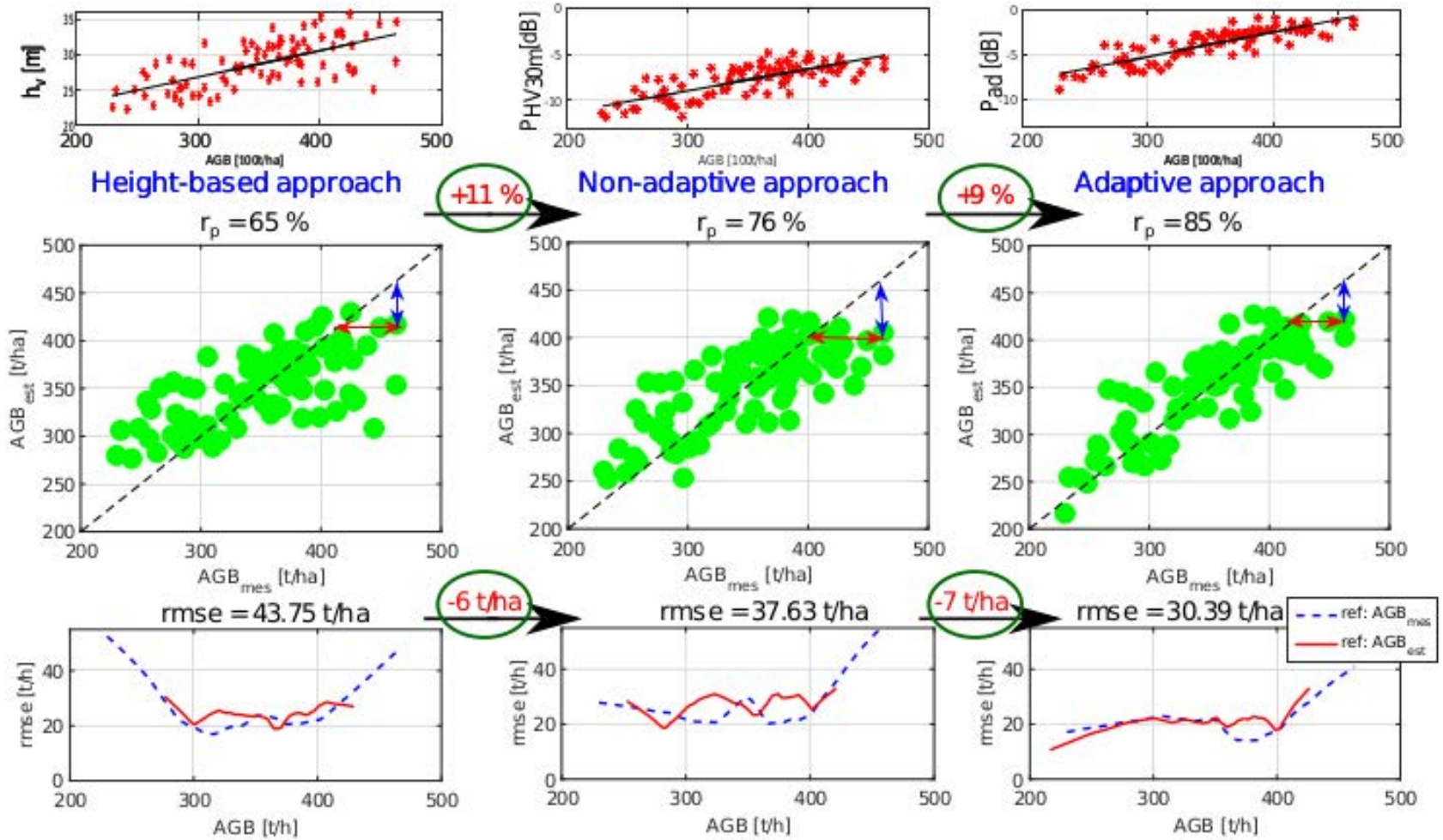

Assessment of Spaceborne SAR tomographic imaging of forests

Fighting against temporal decorrelation

Single pass systems:

- *Cartwheel*
- *Tandem-X*
- *Tandem-L*
- *SAOCOM*

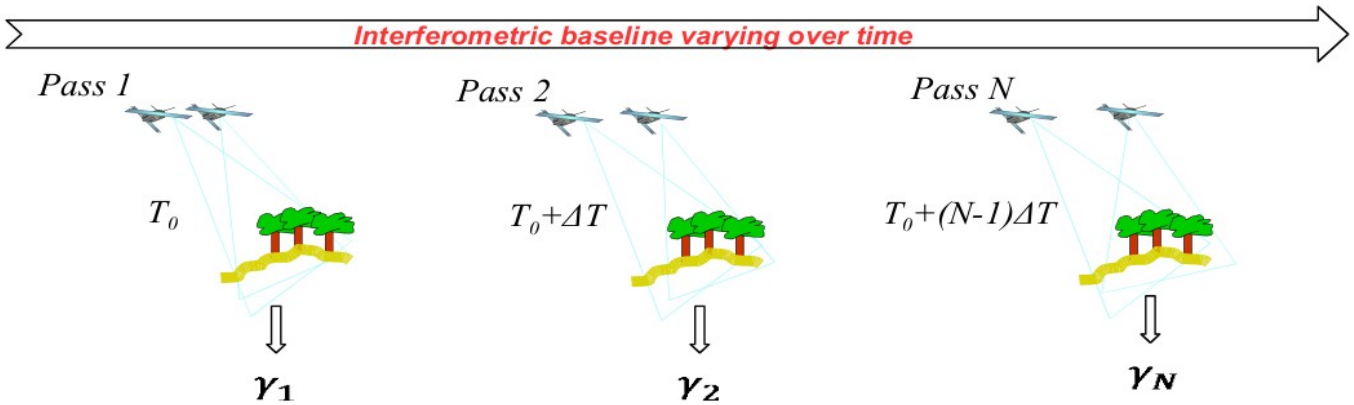

Processing:

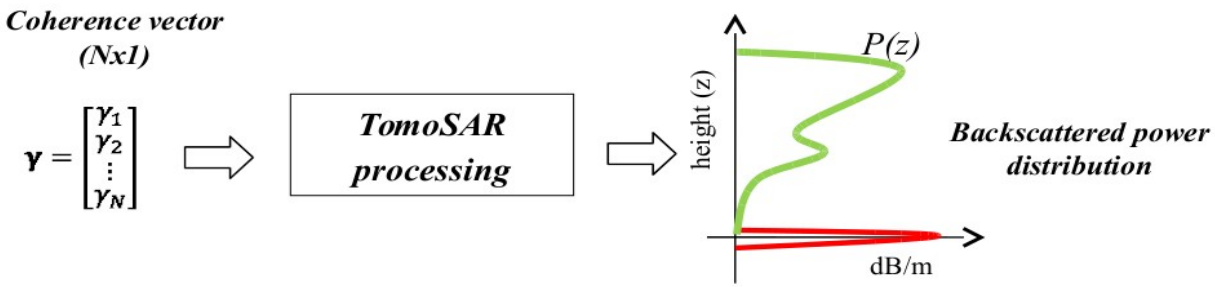

Interferometric pair are acquired nearly simultaneously
→ Intrinsically robust to temporal decorrelation:

3-D imaging of natural environments from space

Fighting against temporal decorrelation

P(z) retrieval from SLC data

$$\mathbf{R} = \begin{bmatrix} 1 & \gamma_{12} & \cdots & \gamma_{1N} \\ \gamma_{21} & 1 & & \\ \vdots & & \ddots & \vdots \\ \gamma_{N1} & & \cdots & 1 \end{bmatrix} \Rightarrow \boxed{\textit{TomoSAR processing}} \Rightarrow$$

- **R** is (semi-)positive definite => $P(z) \geq 0 \rightarrow$ **physically consistent !**
- Equivalent to coherent focusing if inversion is carried out using linear methods (Fourier)
- Assumption: **Frozen Forest = Stable Scatterers**

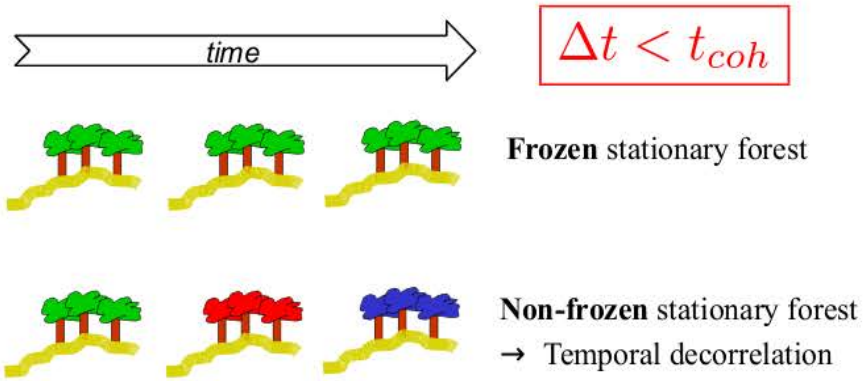

Physical source: motion and EM changes of scattering elements

P(z) retrieval from single-pass InSAR pairs

$$\boldsymbol{\gamma} = \begin{bmatrix} \gamma_1 \\ \gamma_2 \\ \vdots \\ \gamma_N \end{bmatrix} \Rightarrow \boxed{\textit{TomoSAR processing}} \Rightarrow$$

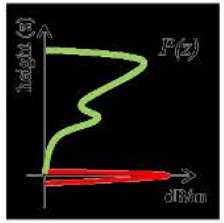

- **The solution is not guaranteed to be ≥ 0**

  ⇒ Countermeasures needed to enforce positive definitiveness
- Not equivalent to coherent focusing – convergence in expected value if proper weighting is applied
- Assumption: **Stationary Forest = Stable Structure**

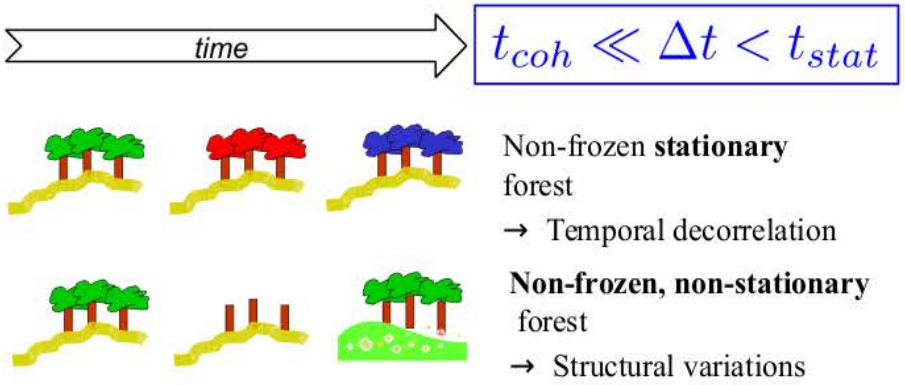

Physical source: seasonality, weather conditions, soil moisture, forest growth, …

Test site and data

Campaign	BioSAR 2008 - ESA
System	E-SAR - DLR
Site	Krycklan river catchment, Northern Sweden
Scene	Boreal forest Pine, Spruce, Birch, Mixed stand
Topography	Hilly
Tomographic Tracks	6 + 6 – Fully Polarimetric (South-West and North-East)
Carrier Frequency	P-Band and L-Band
Slant range resolution	1.5 m
Azimuth resolution	1.6 m
Vertical resolution (P-Band)	20 m (near range) to >80 m (far range)
Vertical	6 m (near range) to 25 m (far

L band SW data set

Forest height

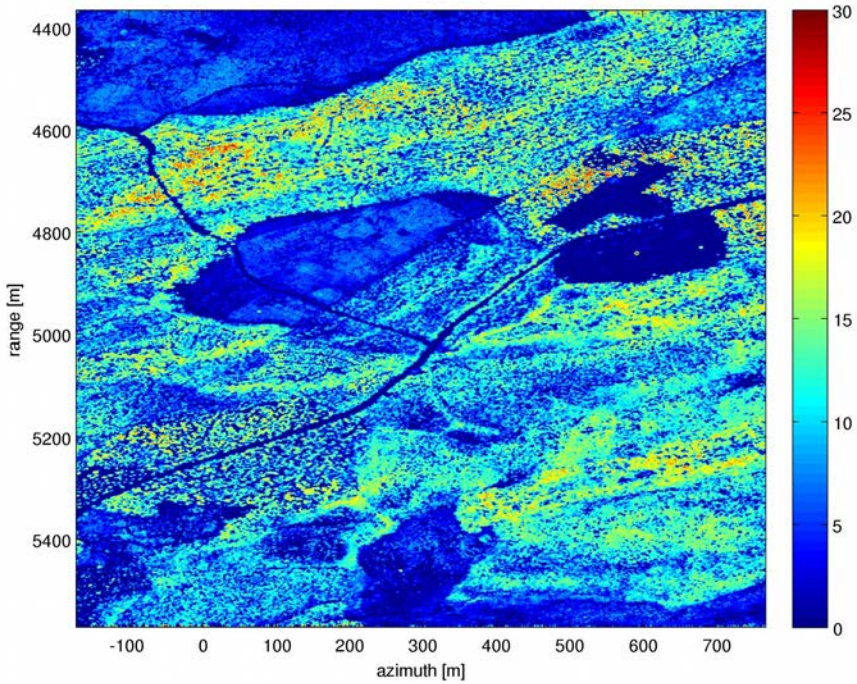

HH intensity

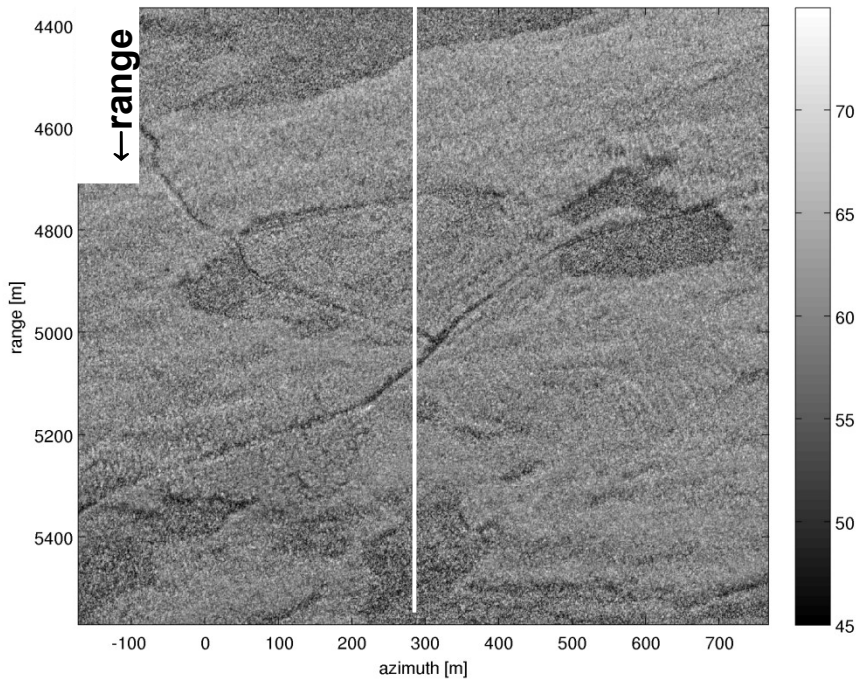

DEM

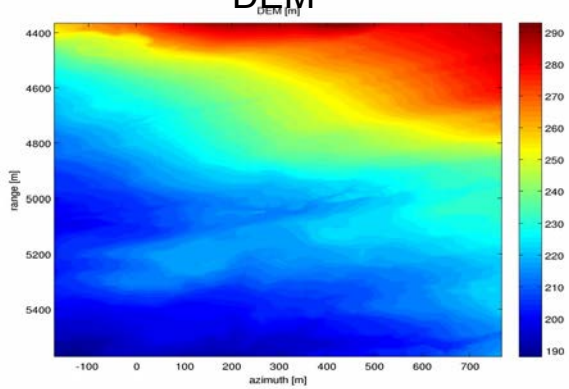

3-D imaging of natural environments from space

Range resolution reduction

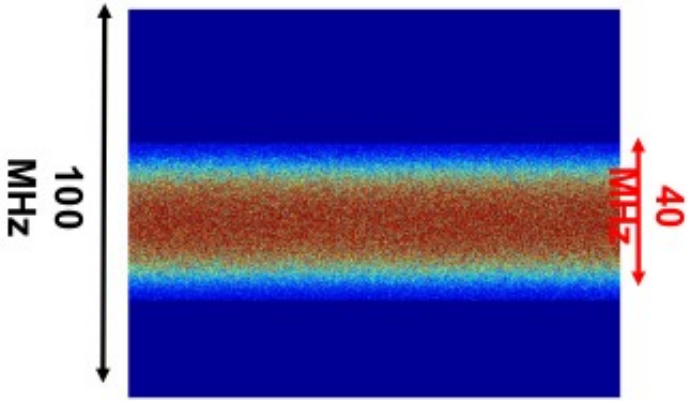

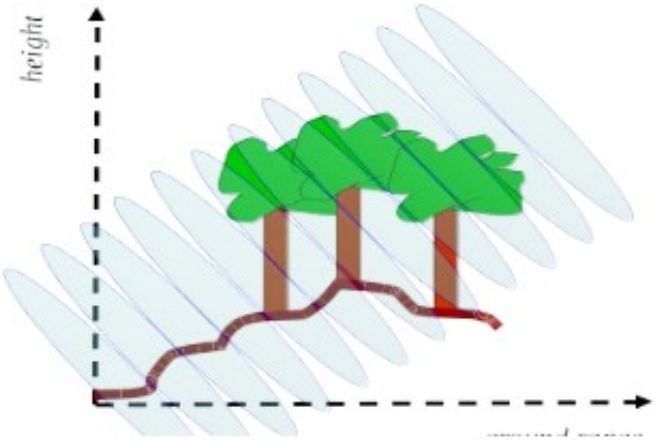

Loss of redundancy & information

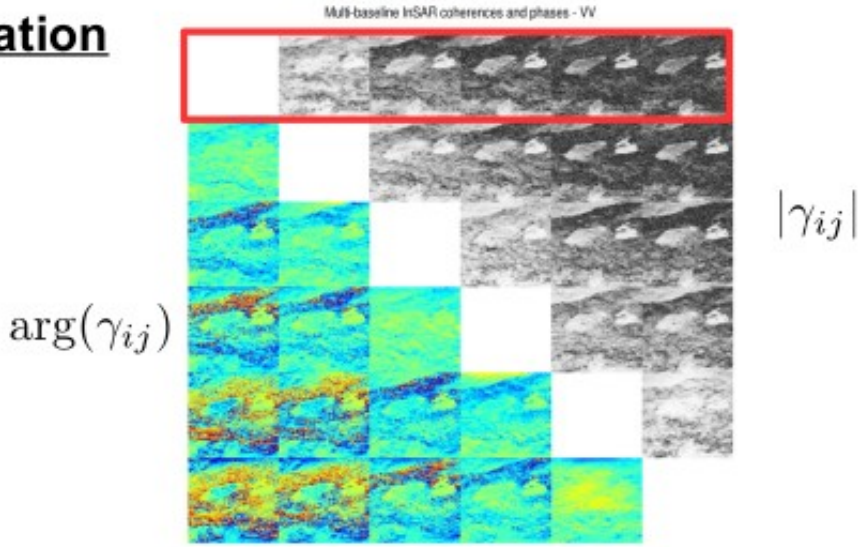

Full vs reduced resolution processing

B_f = 100 MHz

Multi-baseline InSAR coherences and phases - VV

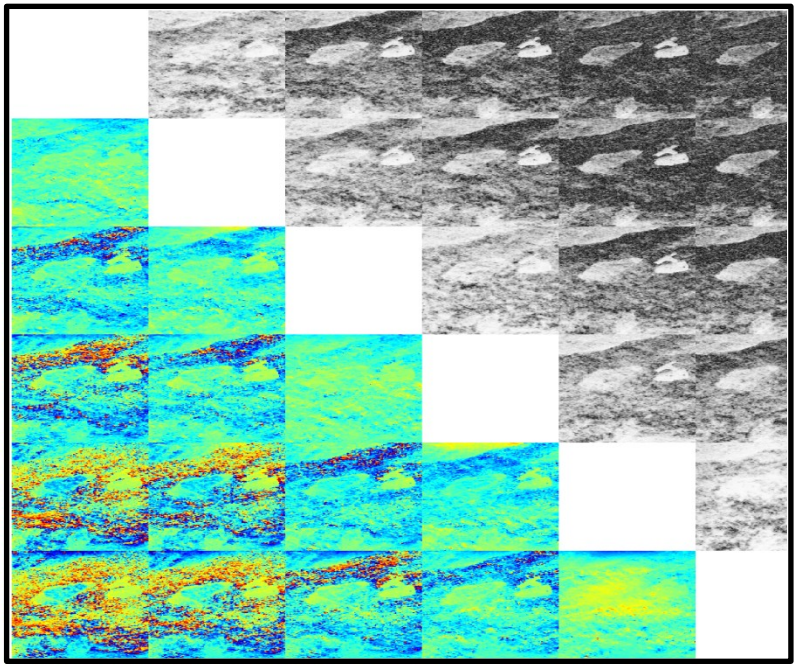

B_f = 40 MHz

Multi-baseline InSAR coherences and phases - VV

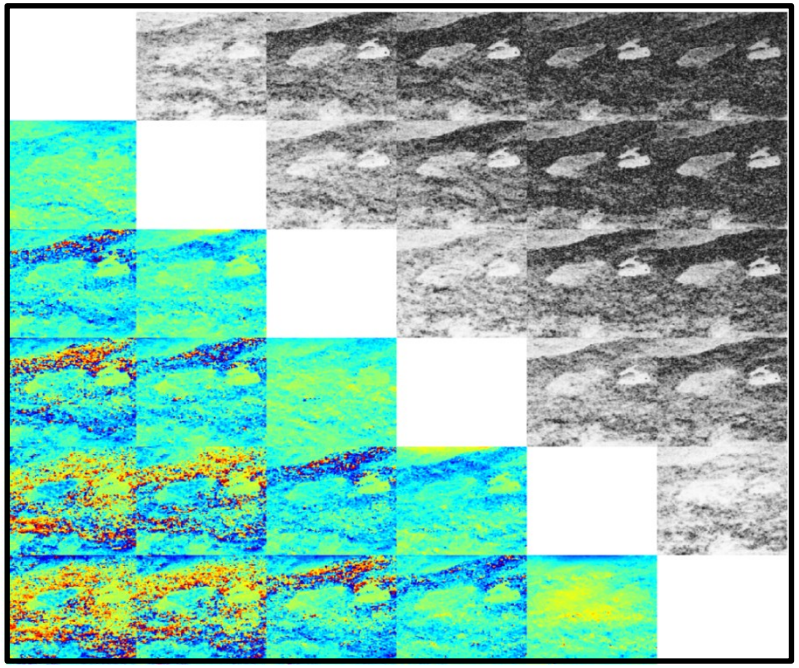

- Quasi regular baselines (almost Toeplitz)
- No noticeable temporal decorrelation
- Theoretical vertical resolution # 10m

No noticeable effects on coherence values even at near range

Full vs reduced resolution processing

B_f = 100 MHz

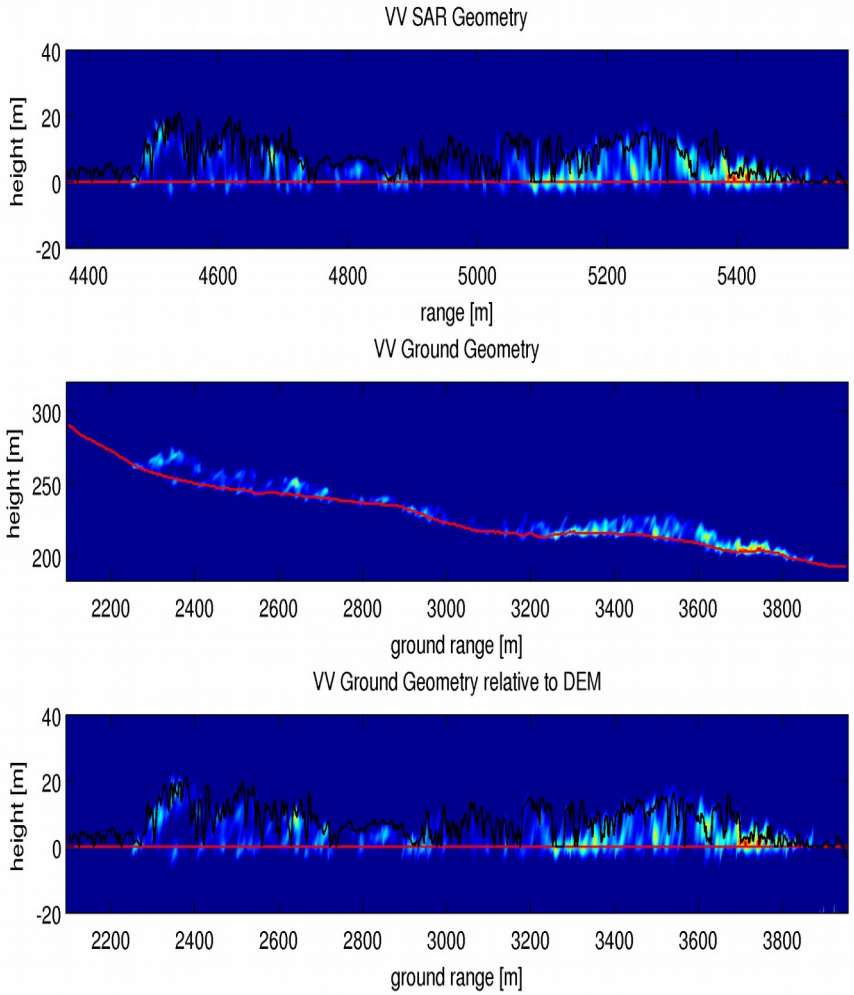

B_f = 40 MHz

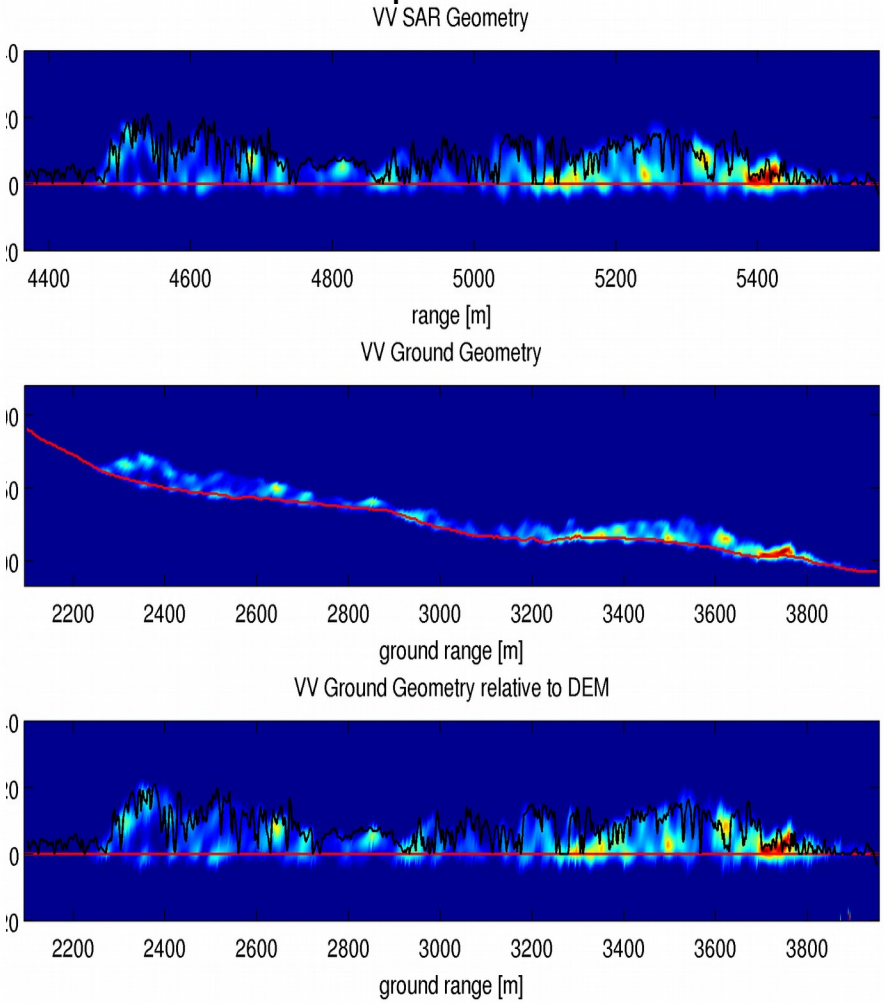

- Comparable performance for terrain topography and tree height

Full matrix vs coherence set processing

SAR: 2D Imaging

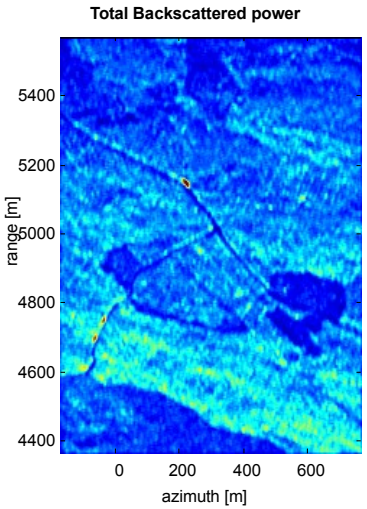

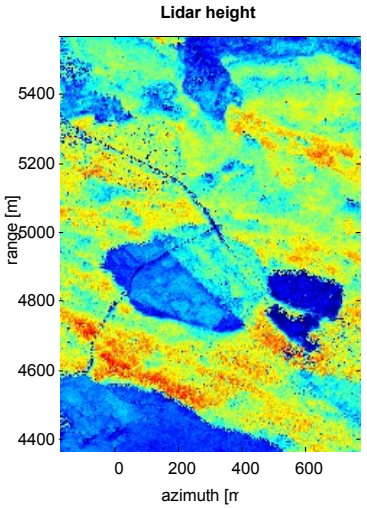

TomoSAR: 3D Imaging

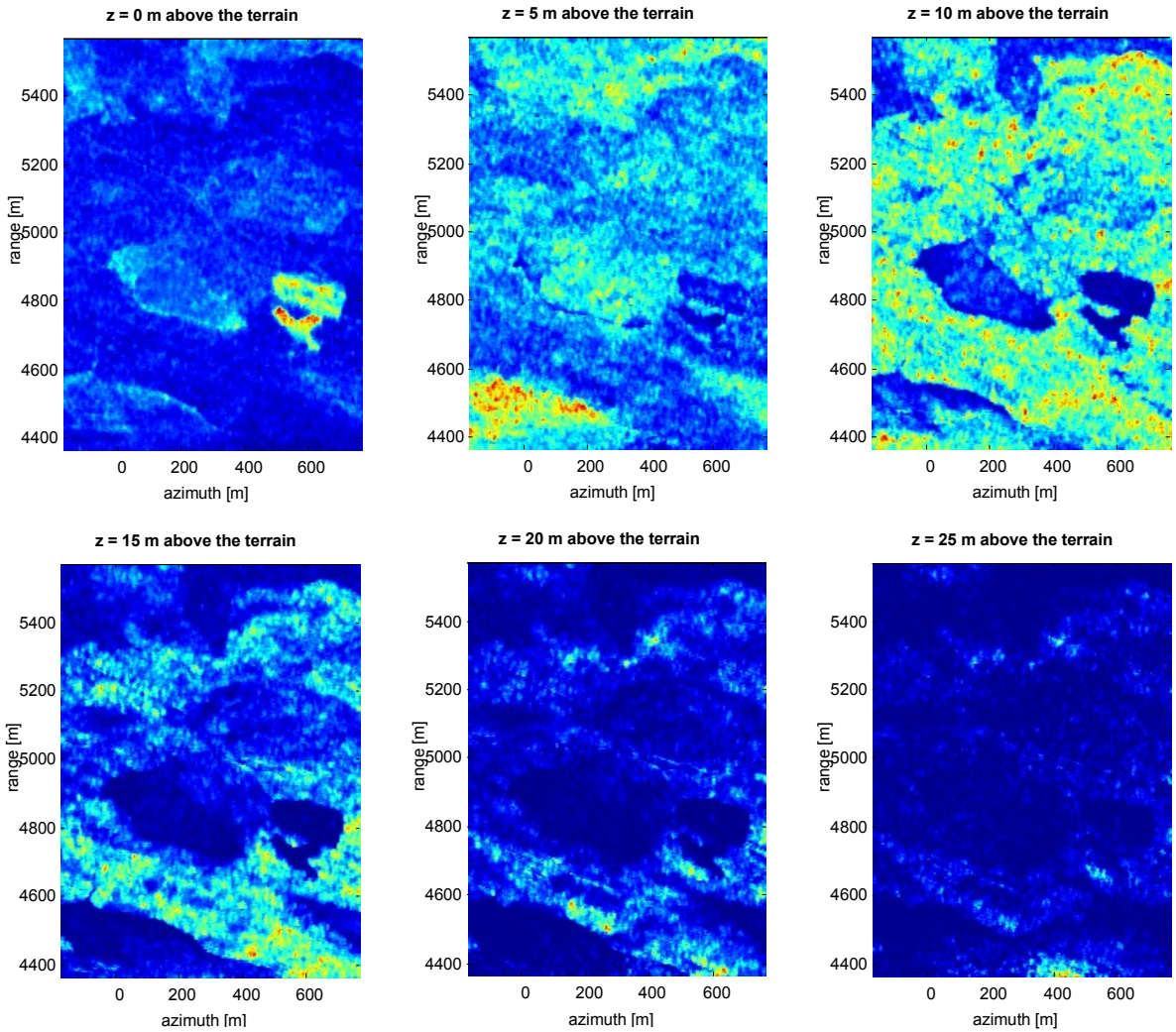

- Power distribution in height direction
- Full-resolution CAPON

Full matrix vs coherence set processing

SAOCOM: 2D Imaging

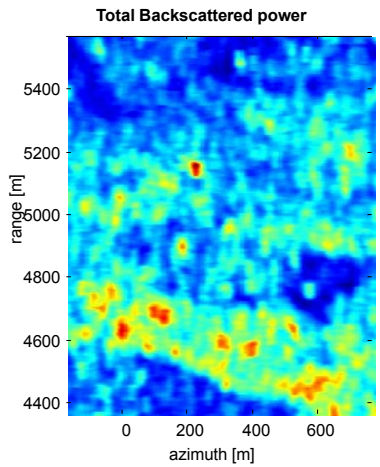

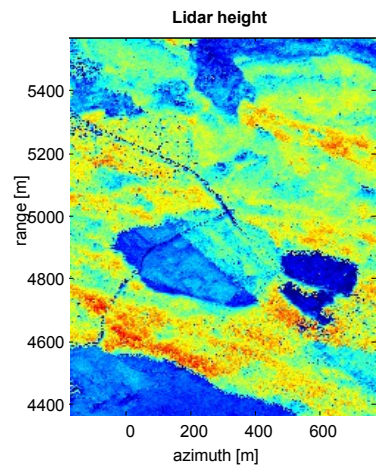

Spaceborne TomoSAR: 3D Imaging

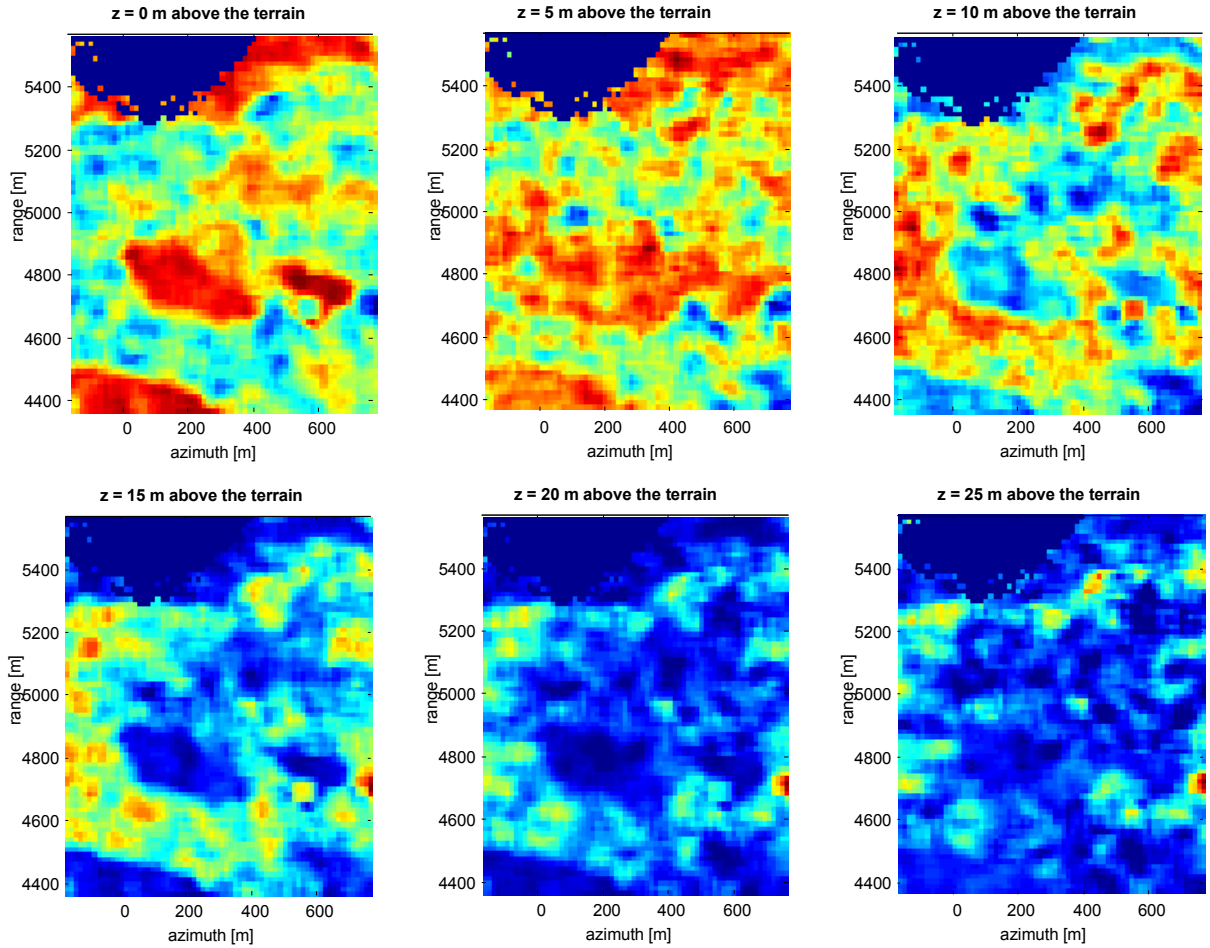

- Power distribution in height direction
- Spaceborne mode BEAMFORMER

Full matrix vs coherence set processing

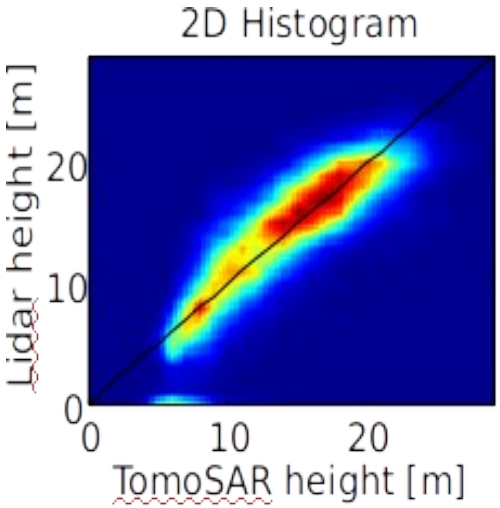

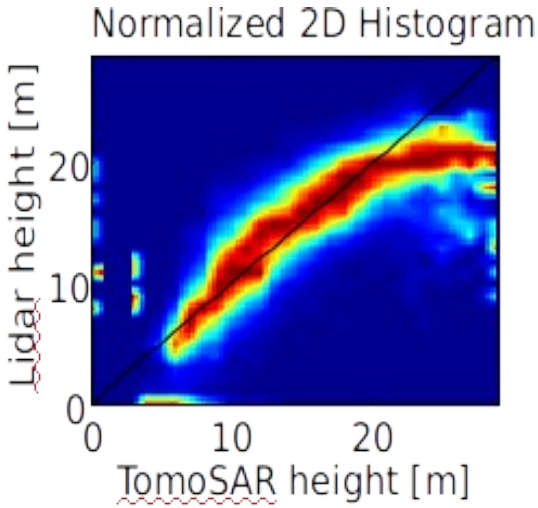

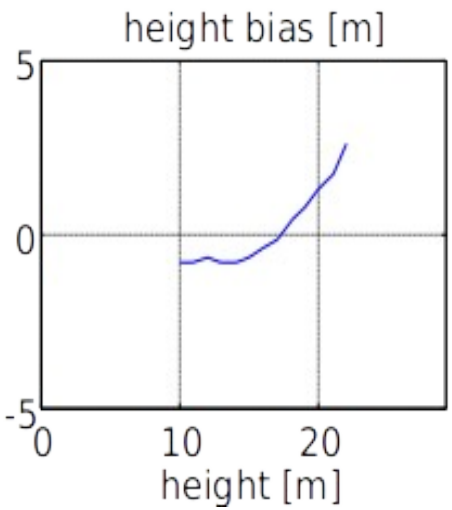

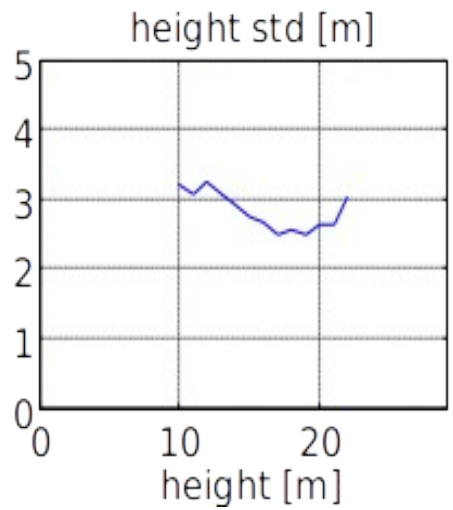

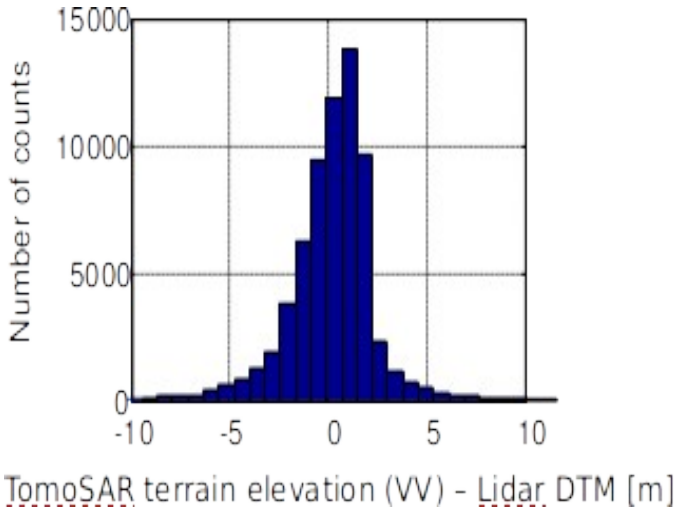

Limitations of the interpolation approach

$$|\gamma_{ij}| \qquad \gamma \xrightarrow{\text{interpolation}} \widehat{\mathbf{R}}$$

$\arg(\gamma_{ij})$

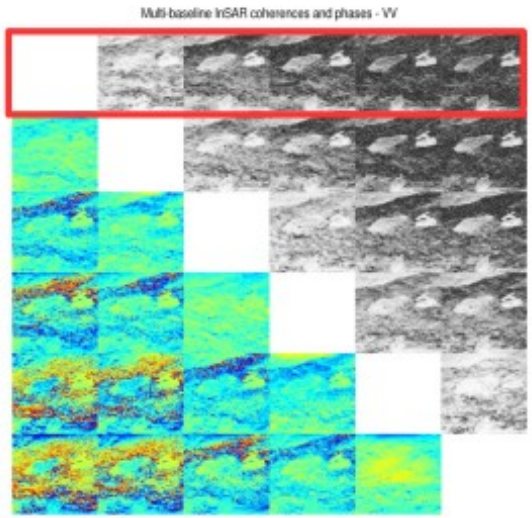

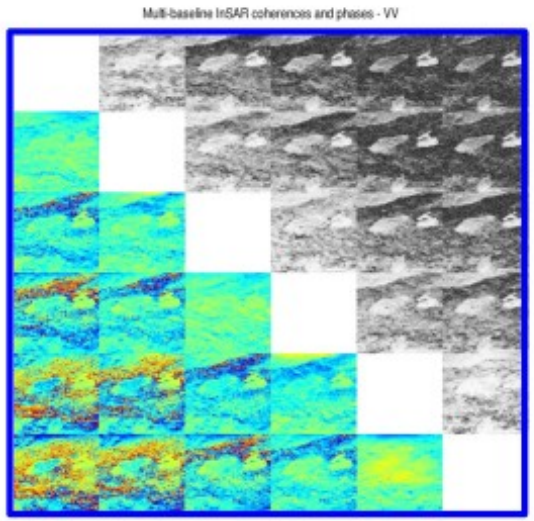

Principles of covariance matrix estimation through coherence interpolation

- For a negligible temporal decorrelation $\boxed{\gamma_{mn} = \gamma(k_{z_n} - k_{z_m}) = \gamma(\Delta k_{z_{mn}})}$

- **Regular** interpolation from a set of known values

$$\gamma(\Delta kz_{12}), \ldots, \gamma(\Delta kz_{1N}) \longrightarrow \widehat{\gamma}(\Delta \tilde{k}_{z_{mn}}) = \widehat{\gamma}\left((n-m)\Delta \tilde{k}_z\right)$$

- Covariance matrix (Toeplitz) reconstruction

$$\boxed{\widehat{\mathbf{R}}_{mn} = \hat{I}\,\widehat{\gamma}\left((n-m)\Delta \tilde{k}_z\right)}$$

Limitations of the interpolation approach

- **Regular** interpolation from a set of known values:

  - most sensible choice
  - enforces Toeplitz symetry
  - does not guarantee semi-definite positiveness:

$$I(z) = \mathbf{a}^H(z)\widehat{\mathbf{R}}\mathbf{a}(z) \text{ may be negative}$$

- Interpolation relies on very strong assumptions

  - small bandwidth
  - baseband behavior

- Problems may arise

  - with **irregular** original spatial **sampling**
  - with imperfectly known scene related **phase terms**

Limitations of the interpolation approach

Sample Covariance Matrix (SCM) vs Interp'd coherence vector

Airborne (High Res) case

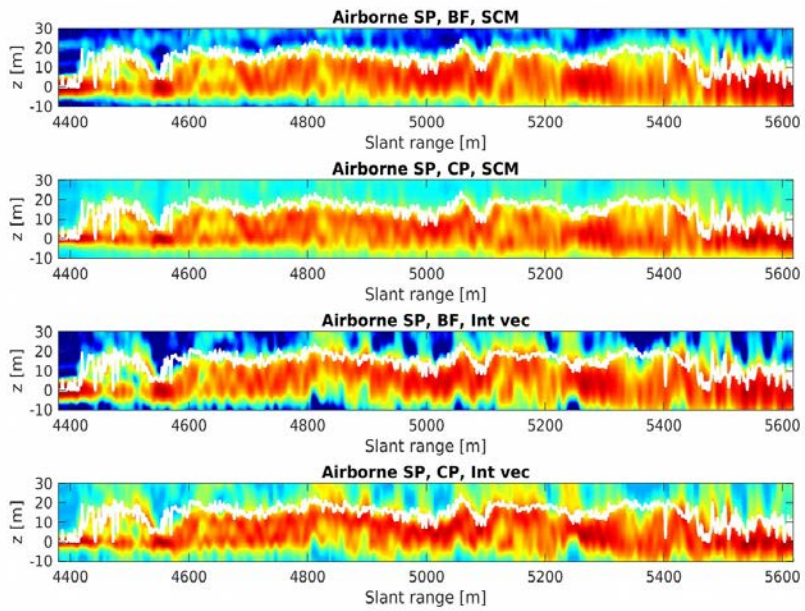

Spaceborne (Low Res) case

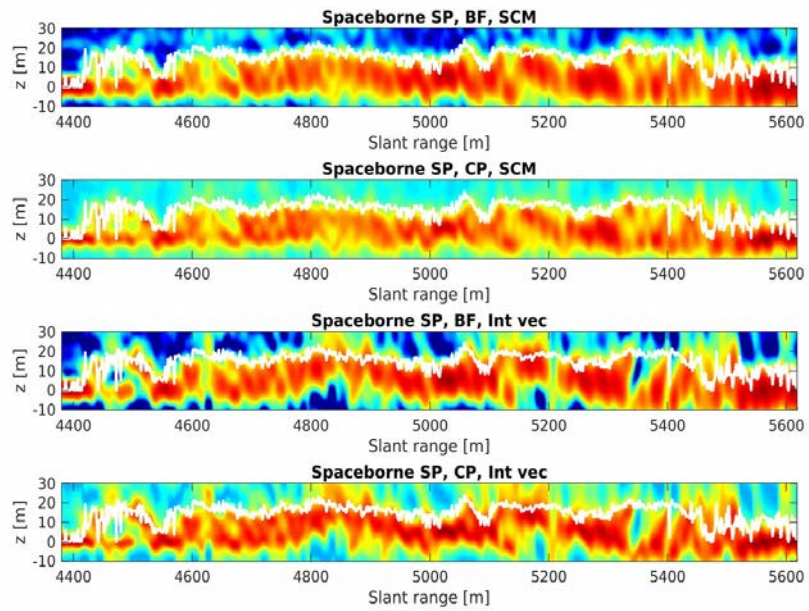

Airborne (High Res) ⟶ Spaceborne (Low Res)

SCM ⟶ Interpolated coherence vector

→ OK

Limitations of the interpolation approach

Non PSD intensity estimates (Spaceborne case)

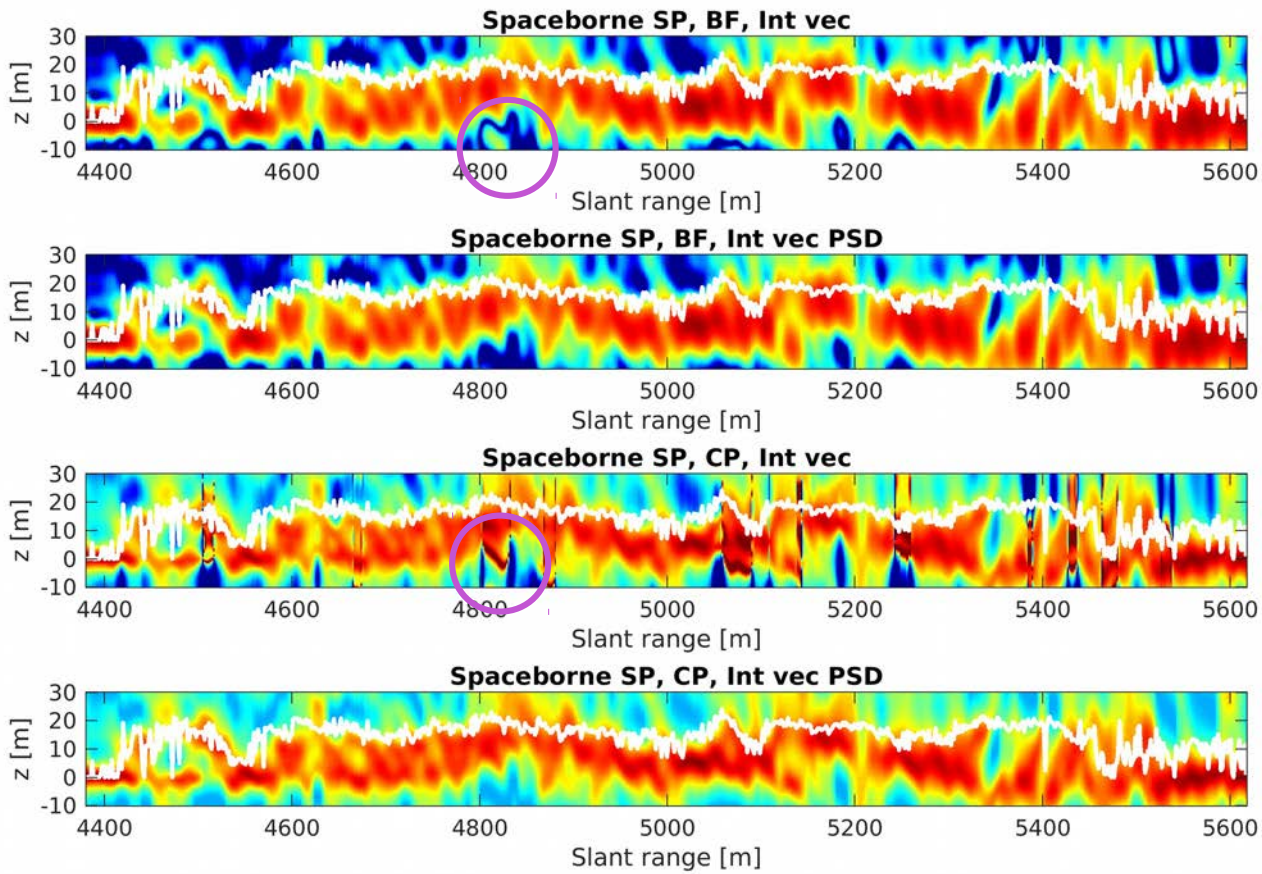

Enforced PSD

Enforced PSD

PSD has to be enforced at low resolution

Limitations of the interpolation approach

Irregular baseline sampling: 1 image missing

$$|\gamma_{ij}| \qquad \gamma \xrightarrow{\text{interpolation}} \hat{\mathbf{R}}$$

$\arg(\gamma_{ij})$

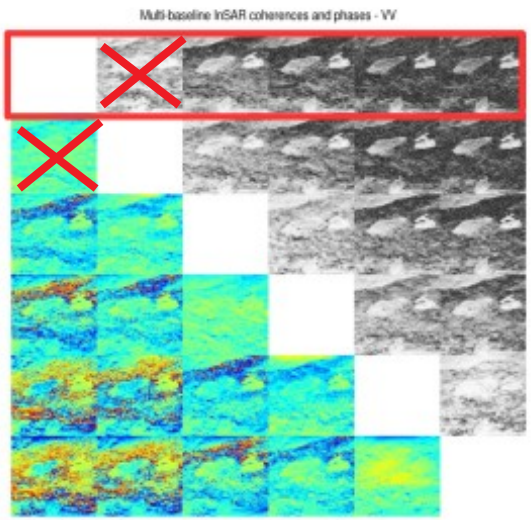

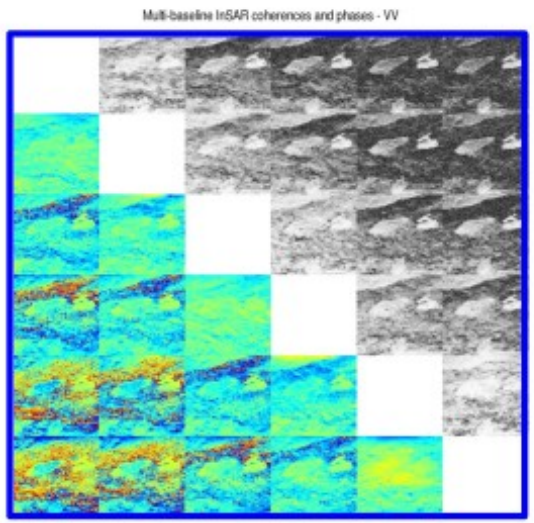

Unknown phase terms (imperfect DEM comp.)

- constant (small) shift in elevation: 0m to 15m

- unknown DEM (gentle topography):

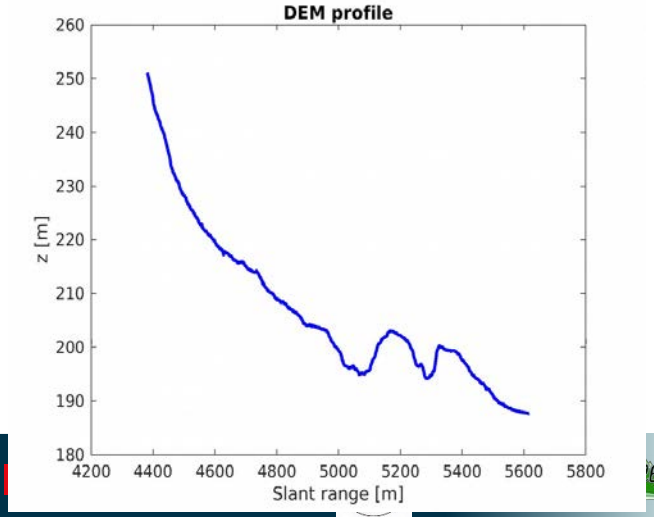

Limitations of the interpolation approach

Interpretation of coherence interpolation

- Naive linear interpolation $\gamma_1 = \gamma(k_{z_1}),\ \gamma_2 = \gamma(k_{z_2}) \longrightarrow \gamma_m = \dfrac{\gamma_1 + \gamma_2}{2}$

- Unknown elevation offset Δz

$$\tilde{\gamma}_i = \gamma_i \, \mathrm{e}^{j k_{z_i} \Delta z} \quad \Longrightarrow \quad \tilde{\gamma}_2 \tilde{\gamma}_1^* = \tilde{\gamma}_2 \tilde{\gamma} \, \mathrm{e}^{j \Delta\phi}, \text{ with } \Delta\phi = \Delta k_z \Delta z$$

- Interpolation may be affected (wrong) for large $\Delta\phi$ values

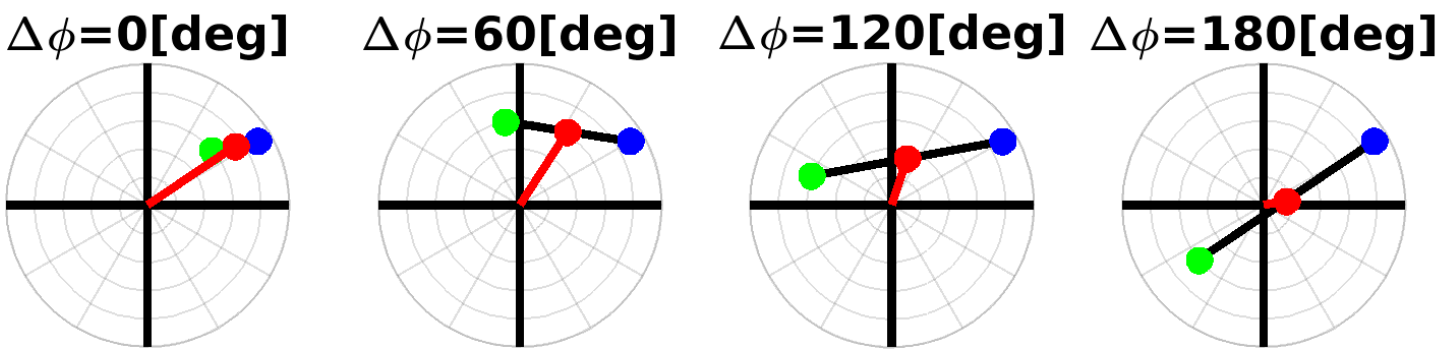

Limitations of the interpolation approach

Irregular sampling (1 image missing), unknown elevation shift Δz

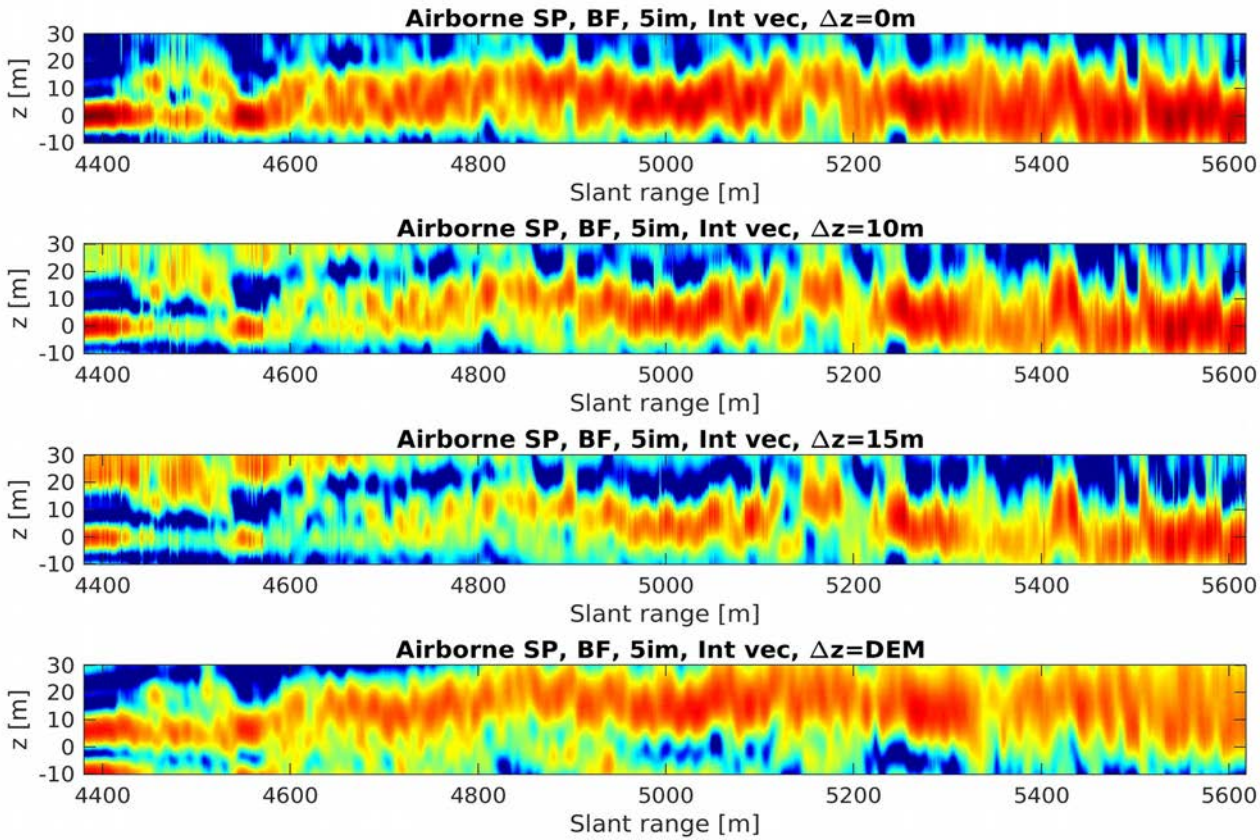

$\Delta z = 0m$

$\Delta z = 10m$

$\Delta z = 15m$

$\Delta z = \mathrm{DEM}$

Large Δϕ values

- large DEM errors: Δz
- large perp. Baselines: Δk_z (Near-range effect)

A robust solution: WV-based coherence synthesis

Characteristics of covariance matrix synthesis based on reflectivity estimation

$$\widehat{\mathbf{p}} = \arg\min_{\mathbf{p}\geq\mathbf{0}} \|\mathbf{v}_{\widehat{\mathbf{R}}} - \mathbf{p}^T \mathbf{A}^H(\mathbf{z})\|_2 \qquad \widetilde{\mathbf{R}} = \widetilde{\mathbf{A}}(\mathbf{z})\,\mathrm{diag}(\widehat{\mathbf{p}})\widetilde{\mathbf{A}}^H(\mathbf{z})$$

- No need to define a sampling strategy
- Naturally adapted to any reconstruction configuration (Toeplitz ...)
- Naturally PSD
- Increased robustness w.r.t. irregular sampling and unknown phase terms

- Discrete description: not well adapted to continuous reflectivity densities

$$\boxed{\mathbf{R} = \mathbf{A}(\mathbf{z})\,\mathrm{diag}(\mathbf{p})\mathbf{A}^H(\mathbf{z})} \equiv \boxed{\gamma(k_{z_{mn}}) = \frac{\sum_i p_i\, \mathrm{e}^{jk_{z_{mn}} z_i}}{\sum_i p_i}} \equiv \boxed{f(z) = \sum_i p_i \delta(z - z_i)}$$

- Sensible solution: use a set of (orthogonal) functions

$$f(z) = \sum_l w_i \upsilon_l(z) \quad \Longrightarrow \quad \mathbf{p} = \mathbf{\Psi}^T \mathbf{w}, \quad \mathbf{w} = \mathbf{\Psi}\mathbf{p}$$

A robust solution: WV-based coherence synthesis

Irregular sampling (1 image missing), unknown elevation shift Δz (Spaceborne case)

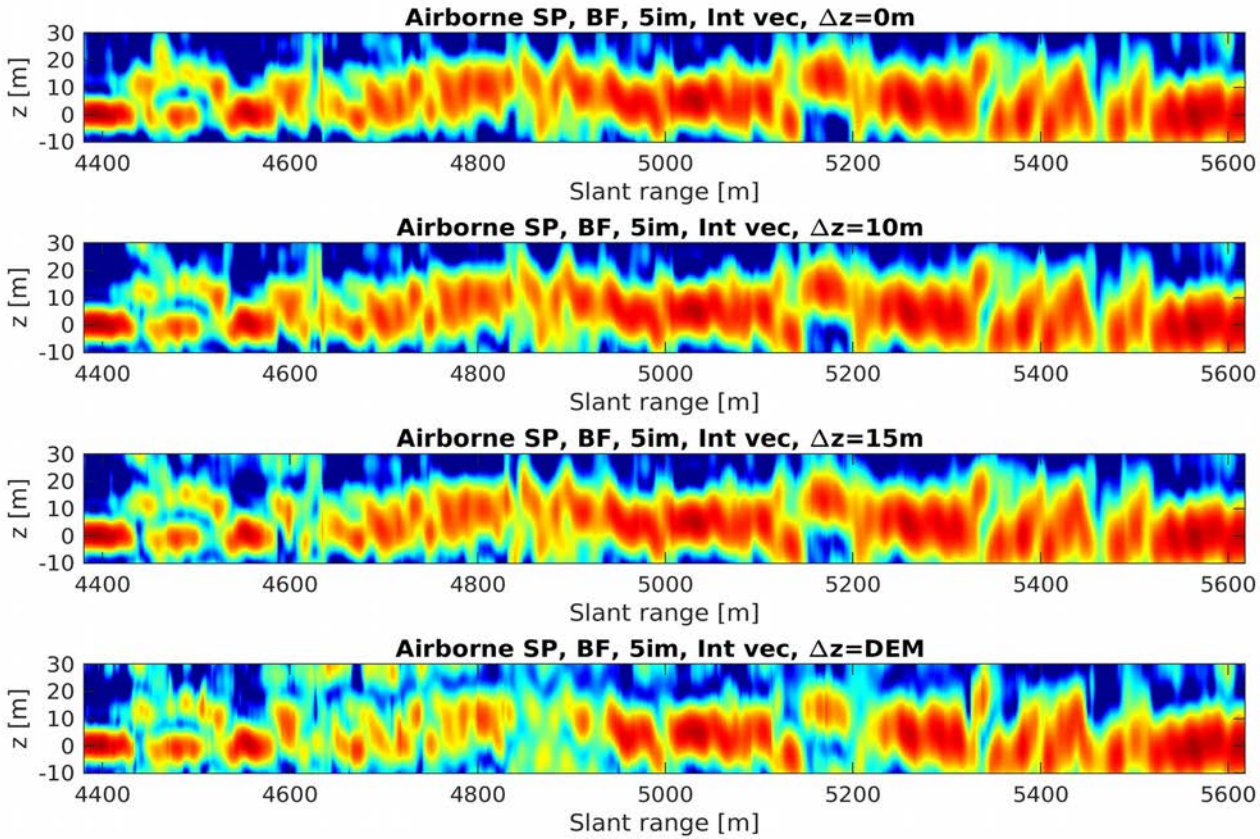

$\Delta z = 0m$

$\Delta z = 10m$

$\Delta z = 15m$

$\Delta z = \mathrm{DEM}$

- Robust to unknown elevation shifts
- Slight changes in the Δz=DEM case: modified search range (resolution), easily avoided

A robust solution: WV-based coherence synthesis

Performance w.r.t. resolution
(I(z) vs. p(z) and Airborne vs. Spaceborne case)

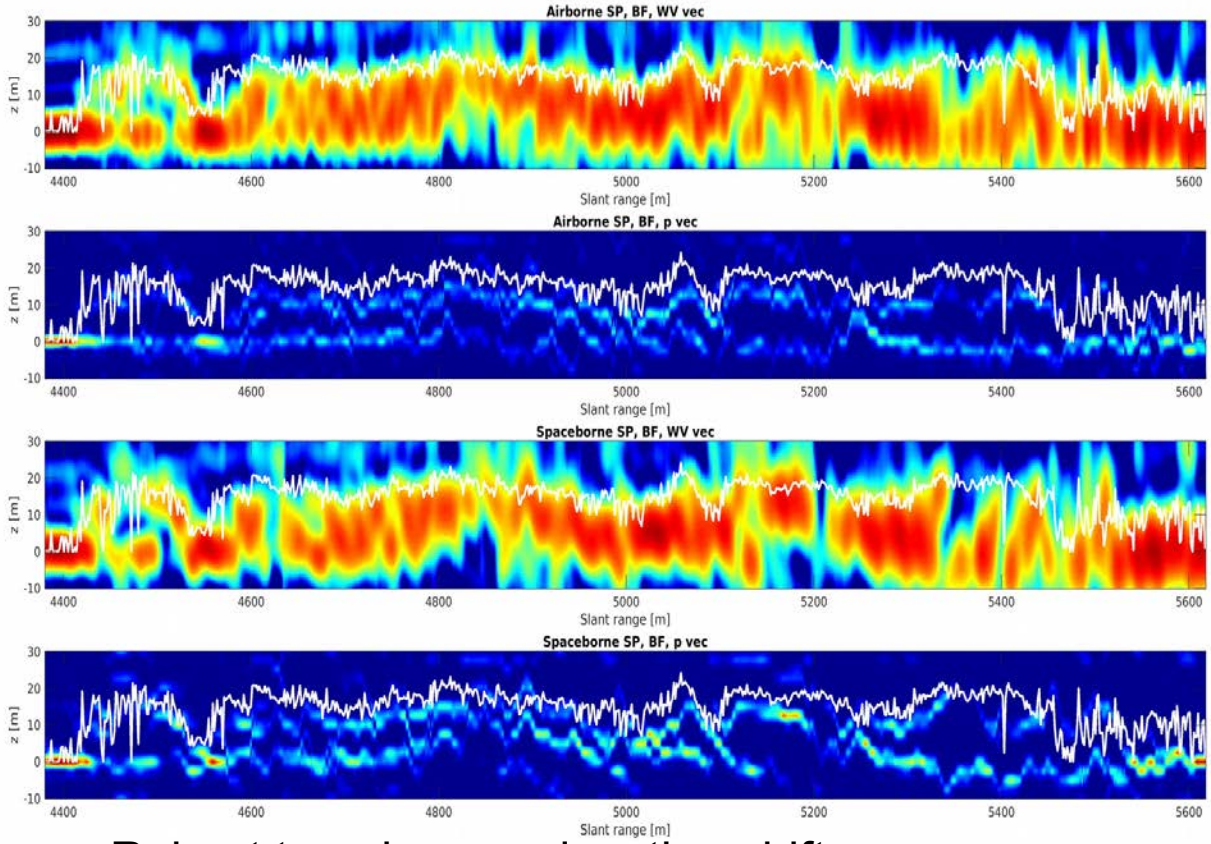

$I(z)$, Airborne

$p(z)$, Airborne

$I(z)$, Spaceborne

$p(z)$, Spaceborne

- Robust to unknown elevation shifts
- Spaceborne & Airborne p(z) extremely close
  → Deconvolution HR effect

$$\widetilde{\mathbf{R}} = \widetilde{\mathbf{A}}(\mathbf{z})\,\mathrm{diag}(\widehat{\mathbf{p}})\,\widetilde{\mathbf{A}}^H(\mathbf{z})$$

A robust solution: WV-based coherence synthesis

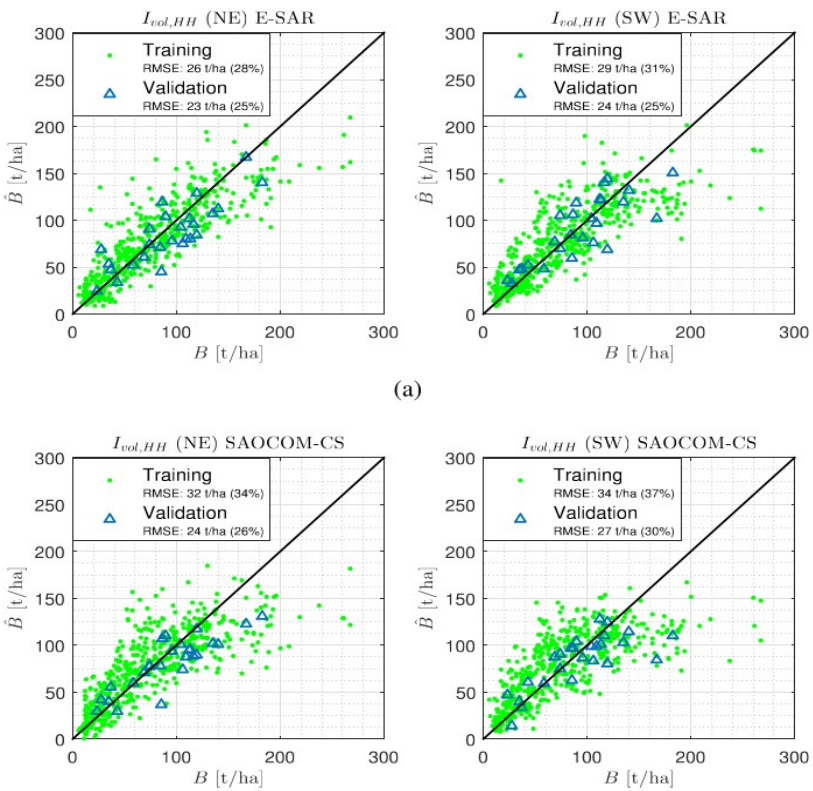

Radiometric accuracy assessment
Biomass estimation using SAR tomography

Blomberg et al. Forest Biomass Retrieval From L-Band SAR Using Tomographic Ground Backscatter Removal, GRSL 2018

$$\hat{B} = \exp(a_0 + a_1 I_v[dB]) \quad I_v = \int_{z=10m}^{z=30m} I(z)\mathrm{d}z$$

	Coh int 6 im Dz=0m	Coh int 5 im Dz=0m	Wv est 5 im Dz=0m	Coh int 5 im Dz=10m	Wv est 5 im Dz=10m	Coh int 5 im Dz=15m	Wv est 5 im Dz=15m
Airborne (HR)	**2.64 %**	14.03 %	**4.25 %**	8.74 %	**4.91 %**	25.84 %	**4.69 %**
Spaceborne (LR)	**9.89 %**	42.35 %	**9.75 %**	31.27 %	**11.23 %**	84.30 %	**11.58 %**